



**Escola de Camins**  
Escola Tècnica Superior d'Enginyeria de Camins, Canals i Ports  
UPC BARCELONATECH

# Catalytic decomposition of ammonia by a mechanochemical approach

Treball realitzat per:

**Laia Pascua Solé**

Dirigit per:

**Jordi Llorca Piqué**

**Xavier Vendrell Villafruela**

Màster en:

**Enginyeria Ambiental**

Barcelona, 18 de juny de 2021

Departament d'Enginyeria Ambiental

**TREBALL FINAL DE MÀSTER**

---

## Abstract

Over the life of the Earth, several changes in climate have occurred, but they were due to natural causes. The current climate change is man-made, as the cause is the amount of CO<sub>2</sub> emitted from the combustion of fossil fuels to obtain energy. Not only they have caused the global warming, but they have worsened the air quality, in general. It is the biggest challenge that current society will face and will continue to be for future generations. Actions to stop, or slow down, this change are being made from public organisms and individual citizens. Hydrogen rises as one of the best solutions to drive the change into a zero emissions society by 2050. However, its storage does present issues for automobile applications. It is suggested that ammonia could be an energy vector to produce hydrogen on board.

The decomposition of ammonia produces hydrogen and nitrogen, thus, becoming a clean fuel. This reaction happens spontaneously at more than 600 °C, temperatures not suitable for a vehicle. A catalyst is needed to decrease the temperature of the reaction, as it reduces the energy needed to decompose the ammonia. In this work, monometallic Ni and Ru catalyst, as well as bimetallic NiRu catalysts have been mainly prepared by ball milling. The bimetallic catalysts are of interest because they can represent a feasible option to substitute expensive Ru-based catalysts. In addition, they were prepared with different orders of addition. Afterwards, their performance regarding ammonia decomposition was calculated by determining the amount of ammonia converted. Bimetallic catalysts achieved higher conversion values than Ni catalysts but not compared to Ru catalysts. Moreover, it was found that the order did affect significantly to the ammonia conversion, exhibiting higher results when Ni was milled first for 5 min, and then Ru, altogether for 5 more minutes (Ni-Ru-b and Ni10-Ru5-b). Three of the bimetallic samples prepared were analysed by Raman spectroscopy. Even though some hypotheses could be made, no conclusions were extracted, regarding the reason why adding Ni first enhanced the performance of the catalyst.

The initial statement about ammonia as a feasible fuel has been proven through a discussion. It was found that it could be indeed, as competitive as hydrogen and electricity. All three options should be considered as future clean fuels.

The study of catalysts is complex because multiple parameters influence the ammonia conversion. Further studies need to be done to precisely find the catalysts that would allow ammonia to be a viable as a fuel.

# Index

Abstract.....	II
Index.....	III
List of Figures.....	VI
List of Tables .....	X
Acronyms .....	XII
<b>1. Introduction.....</b>	<b>15</b>
<b>1.1. Climate change .....</b>	<b>15</b>
1.1.1. Background .....	15
1.1.2. Current Climate Change.....	15
<b>1.2. Future projections.....</b>	<b>17</b>
<b>1.3. Europe.....</b>	<b>18</b>
1.3.1. The Strategy .....	18
1.3.2. Challenges .....	19
<b>1.4. Generation on board: ammonia.....</b>	<b>20</b>
<b>1.5. Air quality.....</b>	<b>22</b>
1.5.1. Classification of air pollutants.....	22
1.5.2. Effects of air pollutants .....	23
1.5.3. European policies .....	24
<b>2. Aims and objectives.....</b>	<b>29</b>
<b>3. State of art.....</b>	<b>30</b>
<b>3.1. Ammonia decomposition and the use of catalysts .....</b>	<b>30</b>
<b>3.2. Ceria .....</b>	<b>33</b>
<b>3.3. Incipient Wetness Impregnation (IWI) .....</b>	<b>34</b>
<b>3.4. Ball milling (BM).....</b>	<b>34</b>
<b>3.5. Fuel cells (FC).....</b>	<b>35</b>
<b>4. Methodology .....</b>	<b>38</b>
<b>4.1. Preparation of catalysts .....</b>	<b>38</b>
4.1.1. Preparation of the support (CeO <sub>2</sub> ).....	38

4.1.2.	Preparation of catalysts .....	38
4.1.2.1.	<i>Ball milling (BM)</i> .....	41
4.1.2.2.	<i>Incipient Wetness Impregnation (IWI)</i> .....	42
<b>4.2.</b>	<b>Reaction: ammonia decomposition</b> .....	42
4.2.1.	Phases of the process .....	44
4.2.1.1.	<i>Previous preparation</i> .....	44
4.2.1.2.	<i>Activation</i> .....	44
4.2.1.3.	<i>Reaction</i> .....	45
<b>4.3.</b>	<b>Characterisation techniques: Raman spectroscopy</b> .....	45
<b>5.</b>	<b>Results</b> .....	47
<b>5.1.</b>	<b>Ammonia decomposition analysis</b> .....	47
5.1.1.	Nickel catalysts .....	48
5.1.1.1.	<i>Ethanol nickel catalysts</i> .....	49
5.1.2.	Nickel and ruthenium catalysts .....	49
5.1.3.	Ruthenium catalysts .....	50
5.1.4.	Final catalysts .....	51
<b>5.2.</b>	<b>Characterisation: Raman spectroscopy</b> .....	52
<b>6.</b>	<b>Discussion</b> .....	58
<b>6.1.</b>	<b>Nickel catalyst</b> .....	59
<b>6.2.</b>	<b>Ruthenium catalyst</b> .....	62
<b>6.3.</b>	<b>Nickel and ruthenium catalyst</b> .....	62
6.3.1.	<b>Raman spectroscopy</b> .....	63
<b>7.</b>	<b>Fuel analysis: viability of NH<sub>3</sub> as a fuel</b> .....	68
<b>7.1.</b>	<b>Fossil fuels</b> .....	68
7.1.1.	Gasoline and diesel .....	68
7.1.2.	Natural gas .....	71
<b>7.2.</b>	<b>Electricity</b> .....	73
<b>7.3.</b>	<b>Hydrogen and ammonia from steam reforming</b> .....	77
7.3.1.	Hydrogen and ammonia from renewables .....	80

---

<b>7.4. Discussion and comparison</b> .....	82
7.4.1. Fuel prices .....	82
7.4.2. Car prices.....	84
7.4.3. Environmental impact .....	87
7.4.4. Storage and power .....	88
7.4.5. Criticism and conclusions .....	90
<b>8. Conclusions</b> .....	93
<b>9. Bibliography</b> .....	95
<b>10. Annex</b> .....	108
<b>10.1. Annex 1</b> .....	108
<b>10.2. Annex 2</b> .....	111
<b>10.3. Annex 3</b> .....	112
<b>10.4. Annex 4</b> .....	113
<b>10.5. Annex 5</b> .....	114
<b>10.6. Annex 6</b> .....	116
<b>10.7. Annex 7</b> .....	126
<b>10.8. Annex 8</b> .....	127
<b>10.9. Annex 9</b> .....	128
<b>10.10. Annex 10</b> .....	129

## List of Figures

Figure 1.1. Temperature change and concentration of CO <sub>2</sub> of the pasts 800000 years (NOAA, 2020). .....	15
Figure 1.2. Temperature anomaly from 1880 until 2020, relative to 1951-1980 average temperatures (NASA, 2020b).....	16
Figure 1.3. Representation of the emission of CO <sub>2</sub> (right axis and pink) and the atmospheric CO <sub>2</sub> (left axis and blue) from 1750 to 2020 (Lindsey, 2020). .....	16
Figure 1.4. Representation of the amount of GHG emitted, in 2016, globally by sector, expressed in Mt of CO <sub>2</sub> equivalent (Data extracted from: (Climate Watch, 2020)).....	17
Figure 1.5. Projections of different scenarios of the change in CO <sub>2</sub> emissions and the increase of temperature (Climate Action Tracker, 2020). .....	18
Figure 1.6. The “seven main strategic building blocks” defined by the European Commission (Data extracted from: (European Commission, 2018)). .....	19
Figure 1.7. Representation of the risk associated with different fuel tanks for vehicle applications (Dujim, Markert and Paulsen, 2005). .....	21
Figure 1.8. Evolution from 2000 to 2018 of the urban population exposed to pollution levels higher than the limits established by (a) Directive 2008/50/EC and (b) the WHO guidelines (EEA, 2019). .....	27
Figure 1.9. Map of the current LEZ in Europe (CLARS, 2021). .....	28
Figure 3.1. Representation of the activation energy of a reaction with (green) and without catalyst (black) (own elaboration). .....	30
Figure 3.2. Decomposition of NH <sub>3</sub> in a nickel catalyst step by step. The greyish blue spheres represent Ni, the blue arrows, N <sub>2</sub> , and the white arrows, H <sub>2</sub> . The asterisk represents an excited state of the molecule (Mukherjee et al., 2018). .....	31
Figure 3.3. Volcano type graph for the NH <sub>3</sub> decomposition. The TOF of the reaction and the logarithm of the reaction’s rate are plotted against the dissociative N <sub>2</sub> adsorption energy (Bell and Torrente-Murciano, 2016). .....	32
Figure 3.4. Fluorite type structure of ceria. Oxygen atoms are in green and cerium, in white (Sherman, 2019). .....	33
Figure 3.5. Scheme of ceria and Ni catalyst structure made by BM and IWI (Zhang et al., 2014). .....	35
Figure 3.6. Scheme of the parts of a FC and its functioning (own elaboration). .....	36
Figure 4.1. Image of (a) the set up to filtrate the cerium oxide (b) the residue obtained after filtration and (c) the final ceria, dried and calcined (own elaboration). .....	38
Figure 4.2. Image of (a) the planetary mill from Fritsch <sup>MR</sup> (Pulverisette 7 premium line) used and (b) the ZrO <sub>2</sub> cylinder and balls, with ceria (own elaboration). .....	42

Figure 4.3. Image of the complete system for the decomposition of ammonia. A: furnace; B: bypass; C: to mass spectrometer (not shown); D: mass flow of argon, hydrogen and nitrogen; E: flowmeter; F: mass flow of ammonia (own elaboration). .....	43
Figure 4.4. Process flow diagram of the system for the ammonia decomposition. The numbers are used to indicate which gas flows through the pipelines in the next sections (own elaboration). .....	44
Figure 4.5. Image of the Confocal Raman Microscope inVia™ Qontor® from Renishaw (own elaboration). .....	45
Figure 5.1. Ammonia conversion at different temperatures for Ni-D-10 (dry conditions and milled during 10 min), Ni-IWI (prepared with IWI), Ru-400-5 (milled at 400 rpm, during 5 min) and Ni-Ru-b (large concentration, addition of Ni first and milling Ni for 10 min and Ru for 5 min). ...	47
Figure 5.2. Ammonia conversion for Ni catalysts, at 450 °C (Ni-D-X indicates the dry samples and the milling time (X); Ni-W-Y, the addition of water (W) and their amount (Y) and Ni-E-Z, the addition of ethanol (E) and their amount (Z)). The error bars indicate the range of variation of some conversion values of the samples.....	48
Figure 5.3. Evolution over time of Ni-E-1 (ethanol, 1 mL) and Ni-E-0.5 (ethanol 0.5 mL), compared to Ni-D-10 (dry conditions, milled for 10 min), at 450 °C. The error bars indicate the range of variation of some conversion values of the samples. ....	49
Figure 5.4. Ammonia conversion for bimetallic catalysts at 450 °C (-b, and -s for 5% Ni and 2.5% Ni, respectively, and Ru-Ni indicates that the first addition to the milling was Ru; Ni-Ru, was Ni and NiRu, were both added at the same time).....	50
Figure 5.5. Ammonia conversion of Ru catalysts, at 450 °C a) at the same speed but different grinding time and b) at different speed but same grinding time (Ru-X-Y, where indicates X and Y indicate the speed and the duration of the milling). .....	51
Figure 5.6. Ammonia conversion, at 450 °C, for Ru-400-5 (milled at 400 rpm during 5 min), Ni-D-10 (dry conditions and milled during 10 min), Ni-Ru-b (5% Ni, addition of Ni first) and Ni10-Ru5-b (5% Ni, addition of Ni first and milling Ni for 10 min and Ru for 5 min). The error bars indicate the range of variation of some conversion values of the samples. ....	52
Figure 5.7. Raman spectra of ceria, Ni-D-10, Ru-400-10, and NiRu-b (1 and 2), before reaction. ....	54
Figure 5.8. Raman spectra of ceria, Ni-D-10, Ru-400-10, and Ru-Ni-b (1 and 2), before reaction. ....	55
Figure 5.9. Raman spectra of ceria, Ni-D-10, Ru-400-10, and Ni-Ru-b (1, 2 and 3), before reaction.....	56
Figure 5.10. Raman spectra of ceria, Ni-D-10, Ru-400-10, and NiRu-b, after reaction. ....	57
Figure 6.1. Image of Ni-W-0.5 and Ni-D-10 (own elaboration). .....	61

Figure 6.2. Raman spectra of the three bimetallic catalysts: NiRu-b, Ru-Ni-b and Ni-Ru-b. Some of the most significant peaks are marked, as well as the two different types of spectra, labelled as A and B. ....	64
Figure 7.1. Scheme of the distillation tower of the refining process of crude oil (EIA, 2020c). 68	
Figure 7.2. Composition of the exhaust gas from the combustion of gasoline and diesel in percentage (Data extracted from: (Sassykova et al., 2019)).....	70
Figure 7.3. Scheme of the production, transmission and distribution of the natural gas (EIA, 2020b). ....	72
Figure 7.4. Distribution of the global energy production per source (2019) (Data extracted from: (BP, 2020)).....	74
Figure 7.5. Distribution of the generation of electricity by power plant in Spain (2020)(Data extracted from: (REE, 2021a)). ....	75
Figure 7.6. Scheme of the steps to produce hydrogen and ammonia (Data extracted from: (Koroneos et al., 2004)).....	78
Figure 7.7. Haber-Bosch process scheme (Ash and Scarbrough, 2019). ....	78
Figure 7.8. Electrolytic cell scheme (Koroneos et al., 2004). ....	81
Figure 7.9. Comparison of the price for each fuel (€/kWh) (Data extracted from: (Boulamanti and Moya, 2017; Hydrogen Council, 2020; Shiozawa, 2020; Geoportal, 2021; REE, 2021b)). .....	83
Figure 7.10. Comparison of car prices (€) depending on their fuel (Data extracted from: (Fiat, 2021; Hyundai, 2021b, 2021a; Peugeot, 2021; Skoda, 2021)).....	85
Figure 7.11. Projected evolution of 4 years of TCO for different fuelled vehicles (BEUC, 2016). ....	86
Figure 7.12. Comparison of the environmental impact g CO <sub>2</sub> eq/MJ) for each fuel explained (Data extracted from: (Ngene et al., 2016; Bicer et al., 2017; Zijlema, 2018; EIA, 2020b; Prussi et al., 2020; Prussi, M., Yugo, M., De Prada, L., Padella, M. and Edwards, 2020; REE, 2020; Smith, Hill and Torrente-Murciano, 2020)).....	87
Figure 7.13. Representation of the energy density against the specific energy, for the different fuels explained (Data extracted from: (Nave, 2001; Cook, 2002; Kolb, 2017; U.S. DRIVE Partnership, 2017; Wilberforce et al., 2017; Shen et al., 2018; Ding et al., 2019; Edwards et al., 2020; Lazard, 2020)).....	89
Figure 7.14. Scheme of the comparison of weight and volume for diesel, hydrogen and an electric battery, to obtain an autonomy of 500 km (Wilberforce et al., 2017). ....	90
Figure 7.15. Scheme of the efficiencies of the different processes from WTW, for direct electrification, hydrogen and liquid fossil fuels (Transport & Environment, 2021). ....	92
Figure 10.1. (a) Scheme of the characteristic measurements of the reactor, (b) an image of the real reactor used and (c) the placement of the catalyst in the reactor (in white the glass wool fibre, in Black the SiC and in green the catalyst).....	112



---

Figure 10.2. Scheme of the transitions between electronic states that produce the Stokes and Anti-Stokes peaks (Jones et al., 2019).....	113
Figure 10.3. Raman spectrum of ceria with a table with the peaks specified. ....	116
Figure 10.4. Raman spectra of Ni-IWI fresh with a table with the peaks specified and an image of its surface. ....	116
Figure 10.5. Raman spectrum of Ni-IWI after reaction with a table with the peaks specified. ....	117
Figure 10.6. Raman spectrum of Ru-IWI fresh with a table with the peaks specified. ....	117
Figure 10.7. Raman spectrum of Ru-IWI after reaction with a table with the peaks specified. ....	118
Figure 10.8. Raman spectrum of Ni-D-10 fresh with a table with the peaks specified.....	118
Figure 10.9. Raman spectrum of Ni-D-10 after reaction with a table with the peaks specified. ....	119
Figure 10.10. Raman spectrum of Ru-400-10 fresh with a table with the peaks specified.....	119
Figure 10.11. Raman spectrum of Ru-400-100 after reaction with a table with the peaks specified. ....	120
Figure 10.12. Raman spectra of NiRu-b with a table with the peaks specified. ....	120
Figure 10.13. Raman spectrum of NiRu-b after reaction with a table with the peaks specified. ....	121
Figure 10.14. Raman spectra of Ru-Ni-b fresh with a table with the peaks specified and an image of its surface. ....	121
Figure 10.15. Raman spectrum of Ru-Ni-b after reaction with a table with the peaks specified. ....	122
Figure 10.16. Raman spectra of Ni-Ru-b with a table with the peaks specified. ....	123
Figure 10.17. Raman spectra of Ni-Ru-b after reaction with a table with the peaks specified. ....	124
Figure 10.18. Raman spectra of ceria, Ni-D-10, Ru-400-10, and Ru-Ni-b, after reaction.....	124
Figure 10.19. Raman spectra of ceria, Ni-D-10, Ru-400-10, and Ni-Ru-b, after reaction.....	125
Figure 10.20. Screenshot of a tweet from the account @elonmusk, of 11 <sup>th</sup> June 2020 (Musk, 2020). ....	129

## List of Tables

Table 1.1. Values of specific energy, energy density and price to produce 10 kWh in Spain (2020) for different fuels (Data extracted from: (Kolb, 2017; Shen et al., 2018; Ding et al., 2019; Edwards et al., 2020; Hydrogen Council, 2020; Lazard, 2020; Geoportal, 2021; REE, 2021b)).	20
Table 1.2. Classification of the most common air pollutants and their source (Data extracted from: (IPCC, 1990; Seinfeld and Pandis, 1998; Daly and Zannetti, 2007; Conselleria d’Agricultura, Desenvolupament Rural, 2015; EEA, 2016; Registro Estatal de Emisiones y Fuentes Contaminantes, 2019; EPA, 2019; Directive (EU) 2015/2193)).	23
Table 1.3. Limits for the pollutants decided by Europe and WHO (Data extracted from: (Directive 2008/50/EC; World Health Organisation, 2018)).	25
Table 3.1. Types of fuel cells and its characteristics (Data extracted from: (Edwards et al., 2020)).	36
Table 4.1. Characteristics of the batches of CeO <sub>2</sub> prepared.	38
Table 4.2. Table of the samples prepared with the details of their preparation.	40
Table 4.3. Base parameters for BM.	41
Table 4.4. Identification of the catalysts analysed and repeated in this study. The cells marked in green indicate those samples that were analysed by the methodology explained and in red the ones that not.	46
Table 5.1. Legend of the symbols used to identify the species and their characteristic Raman shift values.	53
Table 7.1. Summary of the characteristics and the impacts associated with gasoline and diesel (Data extracted from: (Nave, 2001; Cook, 2002; Kolb, 2017; Masnadi, El-Houjeiri and Schunack, 2018; OCU, 2018; Zijlema, 2018; Edwards et al., 2020; Hoekstra, 2020; Lazard, 2020)).	71
Table 7.2. Summary of the characteristics of the CNG and the LNG (Data extracted from: (Nave, 2001; Cook, 2002; Zijlema, 2018; Prussi et al., 2020; Skoda, 2021)).	73
Table 7.3. Summary of the characteristics of the electricity (Data extracted from: (Shen et al., 2018; Ding et al., 2019; REE, 2020; Peugeot, 2021; REE, 2021b)).	77
Table 7.4. Summary of the characteristics of green and grey hydrogen and ammonia (Data extracted from: (Bicer et al., 2017; Boulamanti and Moya, 2017; U.S. DRIVE Partnership, 2017; Wilberforce et al., 2017; Hydrogen Council, 2020; NH <sub>3</sub> hydrofuel, 2020; Shiozawa, 2020; Smith, Hill and Torrente-Murciano, 2020)).	82
Table 10.1. Reduction level objective for each European State Member for SO <sub>2</sub> , NO <sub>x</sub> , NMVOC, NH <sub>3</sub> and PM <sub>2.5</sub> (Directive (EU) 2016/2284).	108
Table 10.2. EU emission standards for passenger cars (Dieselnet, 2019).	111
Table 10.3. Data of the ammonia conversion for the catalysts analysed.	114
Table 10.4. Ni-based catalysts for ammonia decomposition.	126

---

Table 10.5. Ru-based catalysts for ammonia decomposition.....	127
Table 10.6. Bimetallic catalysts for ammonia decomposition. ....	128

## Acronyms

**AC:** Alternating Current.

**BAT:** Best Available Techniques.

**BM:** Ball milling.

**BREFs:** BAT References.

**CHP:** Combined Heat and Power.

**CNG:** Compressed Natural Gas.

**DC:** Direct Current.

**FC:** Fuel Cell.

**GHG:** Green House Gases.

**GHSV:** Gas Hourly Space Velocity.

**HP:** Horsepower.

**IED:** Industrial Emissions Directive.

**IPCC:** Intergovernmental Panel on Climate Change.

**IWI:** Incipient Wetness Impregnation.

**JEC:** JRC (Joint Research Centre), EUCAR (European Council for Automotive R&D) and Concauwe.

**LCA:** Life-Cycle Assessment.

**LEZ:** Low Emissions Zone.

**LNG:** Liquid Natural Gas.

**MCPD:** Medium Combustion Plant Directive.

**MOVES:** Programa de Incentivos a la **M**ovilidad **E**ficiente y **S**ostenible.

**NECD:** National Emission Ceilings Directive.

**NEDC:** New European Driving Cycle.

**NMVOC:** Non-Methane Volatile Organic Compounds.

**PAH:** Polycyclic Aromatic Hydrocarbon.

**PEMFC:** Proton-Exchange Membrane Fuel Cell.

**PM:** Particulate Matter.

**PM<sub>10</sub>:** Particulate Matter under 10 µm diameter.

**PM<sub>2.5</sub>:** Particulate Matter under 2.5 µm diameter.

**PNIEC:** Plan Nacional Integrado de Energía y Clima.

**TAR:** Third Assessment Report.

**TOF:** Turn Over Frequency.

**VOC:** Volatile Organic Compounds.

**WHO:** World Health Organization.

**WLTP:** Worldwide harmonised Light-duty vehicles Test Procedure.

**WTT:** Well-To-Tank.

**ZEZ:** Zero Emissions Zone

## **Chemical nomenclature**

**Al<sub>2</sub>O<sub>3</sub>:** Aluminium(III) oxide or alumina.

**Ar:** Argon.

**As:** Arsenic.

**BaP:** Benzo(a)pyrene.

**C<sub>2</sub>H<sub>6</sub>:** Ethane.

**C<sub>3</sub>H<sub>8</sub>:** Propane.

**C<sub>6</sub>H<sub>6</sub>:** Benzene.

**Cd:** Cadmium.

**CeO<sub>2</sub>:** Cerium(IV) oxide or ceria.

**CH<sub>4</sub>:** Methane.

**CNT:** Carbon nanotube.

**CO:** Carbon monoxide.

**CO<sub>2</sub>:** Carbon dioxide.

**H<sup>+</sup>**: Proton.

**H<sub>2</sub>**: Hydrogen.

**H<sub>2</sub>S**: Hydrogen sulphide.

**HCHO**: Formaldehyde.

**KOH**: Potassium hydroxide.

**Li**: Lithium.

**N<sub>2</sub>**: Nitrogen.

**NH<sub>3</sub>**: Ammonia.

**Ni(NO<sub>3</sub>)<sub>2</sub>·6H<sub>2</sub>O**: Nickel(II) nitrate hexahydrate.

**Ni(OH)<sub>2</sub>**: Nickel(II) hydroxide.

**Ni**: Nickel.

**NO<sub>2</sub>**: Nitrous oxide.

**NO<sub>x</sub>**: Nitrogen oxides.

**O<sub>2</sub>**: Oxygen.

**O<sub>3</sub>**: Ozone.

**OH**: Hydroxyl.

**Pb**: Lead.

**Pt**: Platinum.

**Ru**: Ruthenium.

**RuCl<sub>3</sub>**: Ruthenium(III) chloride.

**S**: Sulphur.

**SiC**: Silicon carbide.

**SO<sub>2</sub>**: Sulphur dioxide

# 1. Introduction

## 1.1. Climate change

### 1.1.1. Background

Over the life of the Earth, numerous changes in its climate have occurred naturally. Figure 1.1 shows how the temperature is not stable through the years, proving that climate is something dynamic and somewhat presents a periodicity. This pattern can be explained by changes in the orbit of the Earth, which happen, approximately, every 100000 years. Other events may cause a change in the climate such as a variation in the Sun's intensity, which may increase the amount of energy that arrives into the Earth; or a season with high volcanic activity, resulting in the introduction of the so called greenhouse gases (GHG) into the atmosphere (Australian Academy of Science, 2020).

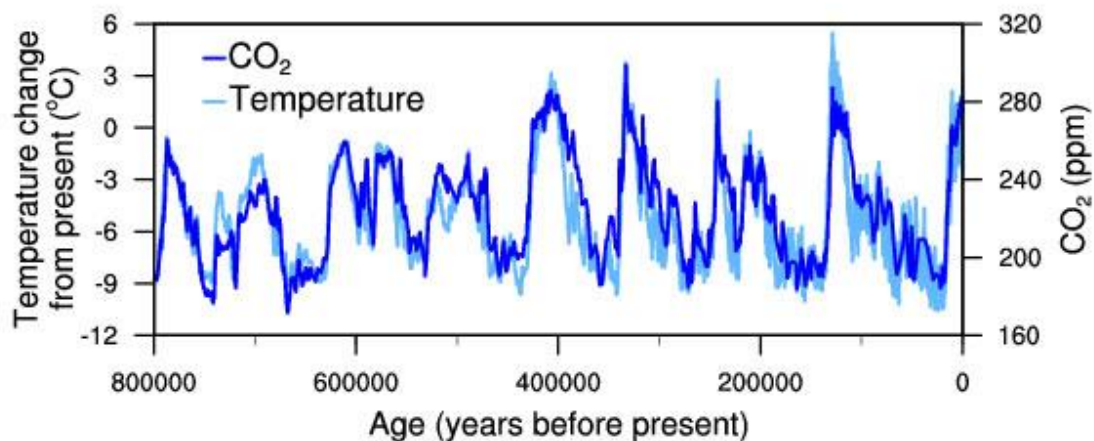


Figure 1.1. Temperature change and concentration of CO<sub>2</sub> of the pasts 800000 years (NOAA, 2020).

Figure 1.1 also shows that this variation of temperature is influenced by the concentration of CO<sub>2</sub>, which is a GHG. Thus, this is an evidence that the change in temperature is driven by the greenhouse effect. CO<sub>2</sub> is found in the atmosphere naturally as well as other GHG like water vapor, CH<sub>4</sub> and N<sub>2</sub>O. They have high permanence times in the atmosphere (except for the water vapor) and they can block the heat that the Earth produces as a result of the incident solar energy. Therefore, as the amount of greenhouse gases increases, more heat is retained and the temperature rises (NASA, 2020c).

### 1.1.2. Current Climate Change

Nowadays, it is well known and proved that the Earth is going through a climate change, specifically it is becoming warmer, which is called global warming. However, some other changes have been reported, such as an increase of temperature and acidity of the oceans, the melting of glaciers or an increment in frequency and intensity of meteorological events (NASA, 2020a). All

these positively feed back into an increase in temperature. The reason behind this behaviour is because there is an interconnection between the different systems that form the climate system, as it is defined by the IPCC in its 2001 report, TAR 01, (Baede *et al.*, 2001):

*“The climate system, is an interactive system consisting of five major components: the atmosphere, the hydrosphere, the cryosphere, the land surface and the biosphere, forced or influenced by various external forcing mechanisms, the most important of which is the Sun. Also, the direct effect of human activities on the climate system is considered an external forcing.”*

Analysing the data reported for the current situation, as shown in Figure 1.2 and Figure 1.3, there is an exponential tendency for both temperature and concentration of CO<sub>2</sub>. This pattern has not been seen before in Figure 1.1. The rate at which they increase cannot be explained only by natural causes, human actions must be considered, such as the massive use of fossil fuels.

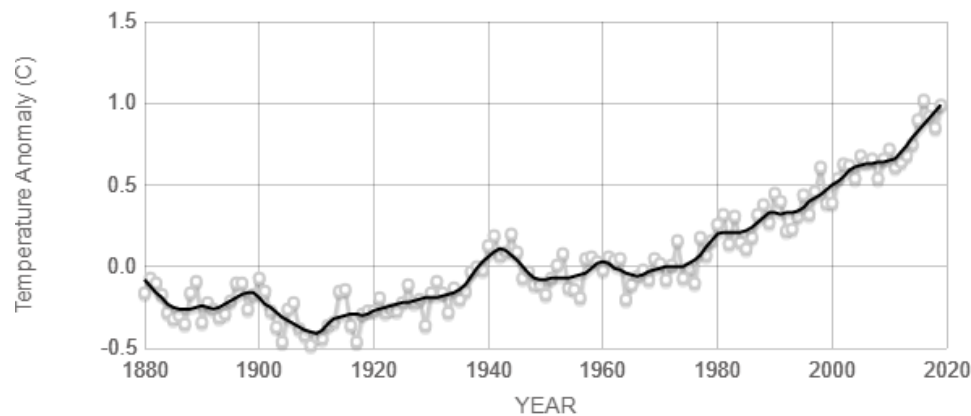


Figure 1.2. Temperature anomaly from 1880 until 2020, relative to 1951-1980 average temperatures (NASA, 2020b).

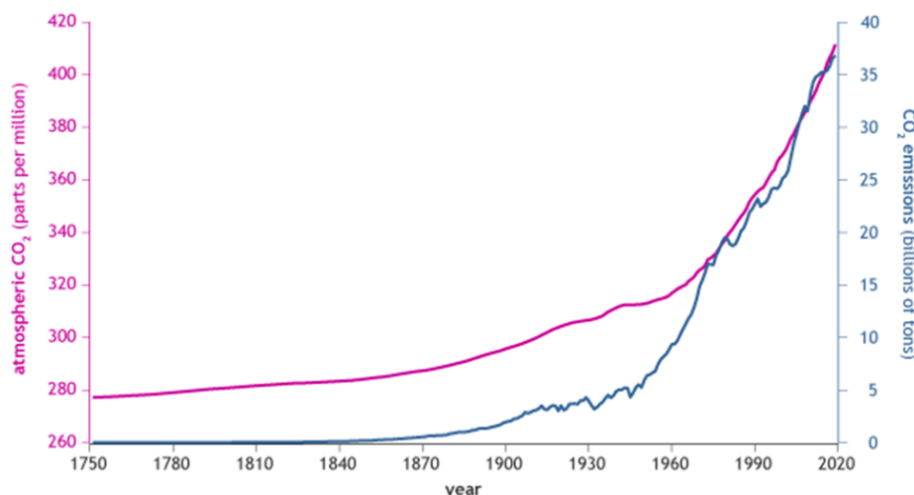


Figure 1.3. Representation of the emission of CO<sub>2</sub> (right axis and pink) and the atmospheric CO<sub>2</sub> (left axis and blue) from 1750 to 2020 (Lindsey, 2020).

Since pre-industrial era, fossil fuels have become the main source of energy. The economic growth started, and the population grew proportionally. That lead into more use of this kinds of



fuels, which when combust produce GHG. From that time, the concentration of CO<sub>2</sub>, being the mainly product generated, has been increasing, from 280 ppm to more than 400 ppm, as seen in Figure 1.3. This is extremely likely to be the main reason for the abrupt change in the climate of the Earth (Pachauri and Meyer, 2014).

To evidence that the current society is fuel-based, Figure 1.4 shows the quantity of GHG emitted globally and by sectors. Almost 75% of them comes from the energy production, being the generation of electricity the 42% and the transportation, the 22% of this sector (World Resources Institute, 2020).

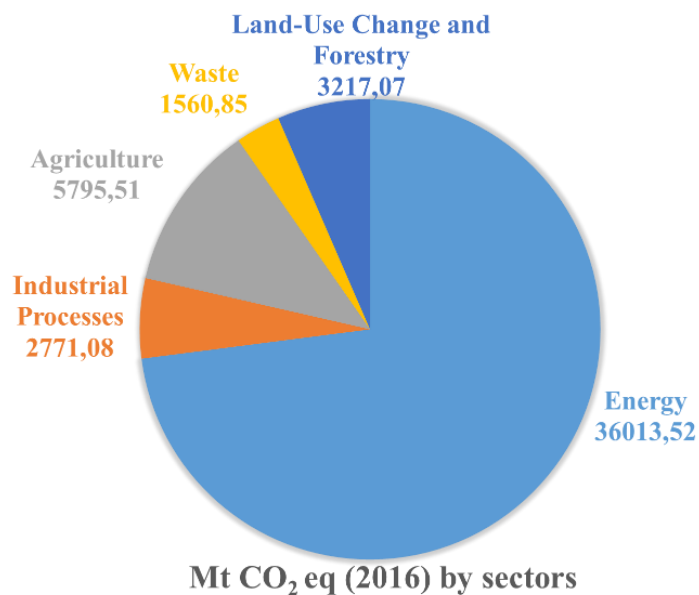


Figure 1.4. Representation of the amount of GHG emitted, in 2016, globally by sector, expressed in Mt of CO<sub>2</sub> equivalent (Data extracted from: (Climate Watch, 2020)).

## 1.2. Future projections

If no changes are made, temperature could increase 4.1°C-4.8°C by 2100, with respect from the pre-industrial values (see Figure 1.5) (Climate Action Tracker, 2020). However, some policies have been made, such as the Paris Agreement, which, internationally, aimed to not have a rise in temperature more than a 1.5°C-2°C; even though, not all the countries ratified the policy. Because its optional nature, countries can propose the changes they consider more suitable for them to reduce GHG emissions, without having a mandatory objective. This kind of agreement has led to some improvements, mainly because of the aim of decarbonisation from Europe (EU Science Hub, 2020). However, this is not enough, as seen in Figure 1.5, which displays that this continuous behaviour will result in an increment above the Paris Agreement (Climate Action Tracker, 2020; United Nations Framework Convention on Climate Change, 2020).

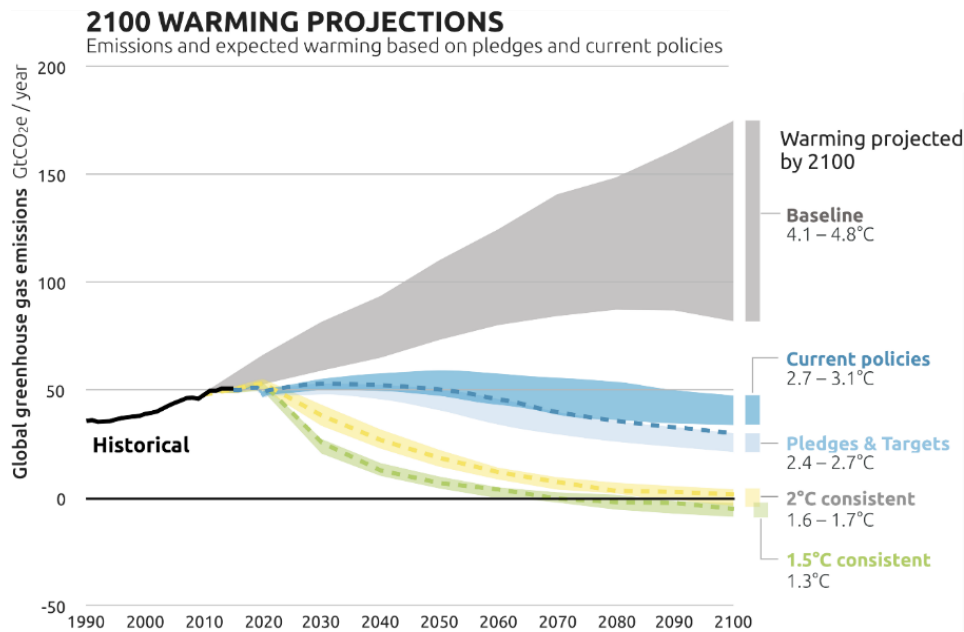


Figure 1.5. Projections of different scenarios of the change in CO<sub>2</sub> emissions and the increase of temperature (Climate Action Tracker, 2020).

### 1.3. Europe

#### 1.3.1. The Strategy

Since the Paris Agreement, Europe has set the goal of emitting zero GHG into the atmosphere by 2050. As most of the emissions come from the energetic sector (similar to Figure 1.4), the strategy is focused on transitioning from a fossil fuel to a clean energy production (European Commission, 2018; EU Science Hub, 2020). Specifically, Europe supports a hydrogen-oriented economy as a solution for decarbonisation.

Hydrogen presents the best characteristics to not contribute to the current climate change and supply the demanded energy. Even though hydrogen is not an energy source, as an energy carrier is able to generate electricity by powering a fuel cell and to combust to produce heat. For both processes, the only product is water vapor; thus, no GHG are emitted (Llorca, 2010; Edwards *et al.*, 2020).

In order to achieve a hydrogen-oriented economy and zero GHG emissions by 2050, the European Commission defined “seven main strategic building blocks” (European Commission, 2018) to address the topic, presented in Figure 1.6.

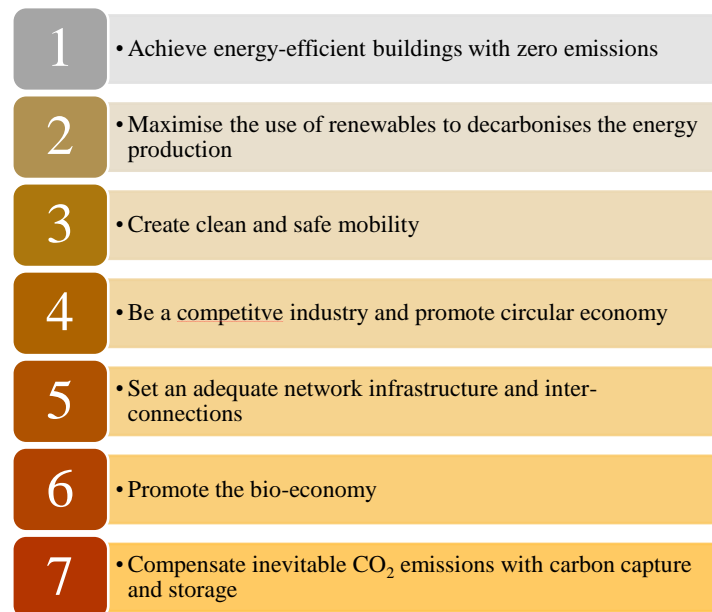


Figure 1.6. The “seven main strategic building blocks” defined by the European Commission (Data extracted from: (European Commission, 2018)).

By 2050, the global energy demand will increase double or triple than the current one. At the moment, renewables by themselves cannot supply this demand. Since their nature depends on the meteorological conditions, at a certain moment an excess of energy can be generated. Hydrogen can also store this energy. Thus, the use of renewables could be maximised. Moreover, hydrogen, if locally produced, could be used in transport; offering the opportunity to have a clean network of transportation due to the technology of fuel cells (Edwards *et al.*, 2020).

Although the production of hydrogen already exists, the main source is methane by steam reforming. In order to reduce GHG emissions, other processes must be used, like water electrolysis. Despite of having an efficiency of 70-75%, this method is much more expensive than steam reforming. Besides, the energy needed to generate the gas must be from renewable sources to not contribute further in emitting GHG (Edwards *et al.*, 2020).

### 1.3.2. Challenges

The “seven strategic building blocks” presented in Figure 1.6, pretend to establish a path in order to overcome the three main technological challenges that the fuel cells and hydrogen represent: the cost and durability of fuel cells, the cost of production and delivery of sustainable hydrogen, and smaller and more efficient storage for stationary and mobile applications (European Commission, 2018; Edwards *et al.*, 2020).

Firstly, fuel cells are an efficient system to obtain electricity with products that do not pollute and do not contribute to the climate change. Besides, their efficiency is much higher than the internal combustion engines (Edwards *et al.*, 2020). Nevertheless, they are very delicate systems that can be easily polluted if the fuel used is not pure enough and contains elements such as CO, NH<sub>3</sub>, H<sub>2</sub>S

or halogen compounds. Another issue is the high cost due to precious metals that they contain (Zamel and Ā, 2008; Jacques, 2011).

Regarding the hydrogen distribution, it is noteworthy that is used in small-scale, only for industries near the source. Its reason is the low density of the hydrogen, that implies a higher velocity to transport the same mass, compared to other gases. Furthermore, because it is a small particle, it diffuses into the pipe material, generating metal hydrides and cracking the pipe, hence, there is leakage (Llorca, 2010; Edwards *et al.*, 2020).

The same problem of leakage, explained for the distribution, can be applied as well for its storage. In addition, as seen in Table 1.1, hydrogen has the highest specific energy among the most currently used fuels. Despite that, its energy density is one of the lowest. To illustrate it, for 1dm<sup>3</sup> (or 1L) of hydrogen at 200 bars only can generate 0.53 kWh, while diesel (a conventional fossil fuel) produces 10.6 kWh. Therefore, a much bigger volume of hydrogen is required in order to achieve the same energy production as standard fossil fuels (Prigent, 1997; Kolb, 2017; Lazard, 2020).

*Table 1.1. Values of specific energy, energy density and price to produce 10 kWh in Spain (2020) for different fuels (Data extracted from: (Kolb, 2017; Shen *et al.*, 2018; Ding *et al.*, 2019; Edwards *et al.*, 2020; Hydrogen Council, 2020; Lazard, 2020; Geoportat, 2021; REE, 2021b)).*

Fuel	Specific Energy (kWh/kg)	Energy density (kWh/dm <sup>3</sup> )	Price (€/10kWh)
Hydrogen (200 bar)*	1.4	1.0	0.403
CNG (200 bar)	13.9	2.3	0.701
LNG	13.9	5.6	0.503
Petrol	12.8	9.5	1.367
Diesel	12.6	10.6	1.065
Electricity**	0.9-1.2	0.47	0.404

\*The data from the hydrogen is considering the production via steam reforming, and that the hydrogen it is already stored to be used in a vehicle.

\*\*The values of specific energy and energy density are related to the average Li-ion battery from electric cars.

#### 1.4. Generation on board: ammonia

Nevertheless, a solution to the storage of hydrogen, for mobile applications, could be the generation of it on board. The choice for the source of hydrogen must be in liquid state under normal conditions, in order to be able to compete against the fossil fuels (Llorca, 2010). By this way, the energy density can be higher than its gas form. In addition, the reaction must produce large amounts of hydrogen, which can be achieved with alcohols, like methanol or ethanol, synthetic fuels or ammonia.

In this work, the hydrogen source chosen is ammonia. This molecule has one of the highest percentage in mass of hydrogen (17.6%) (Llorca, 2010). Moreover, regarding its decomposition, approximately 75% of the products are hydrogen (Prigent, 1997). What is more, ammonia has 35% more energy density than liquid hydrogen (ARPA-E, 2017). Thus, so far, ammonia presents the features to be a good source of hydrogen.

A part from those advantages, ammonia distribution already exists and its network has all the safety measures needed to assure minimum leakage (Dujim, Markert and Paulsen, 2005). In terms of transport, safe storages must be developed. Even though, studies have shown that the risk associated with leaking of ammonia tanks are similar to the ones with fossil fuels. As shown in Figure 1.7, ammonia is the safest amongst the fossil fuels until 15 meters from the tank. Further, the risk related to the gasoline drops abruptly, while the tendency of ammonia keeps decreasing at a slower rate, until 30 meters, approximately. Even though the risk associated to ammonia tanks is low, is not zero, so it could be toxic. That is why, this issue has to be taken into account in order to further minimise this risk (Dujim, Markert and Paulsen, 2005; ARPA-E, 2017).

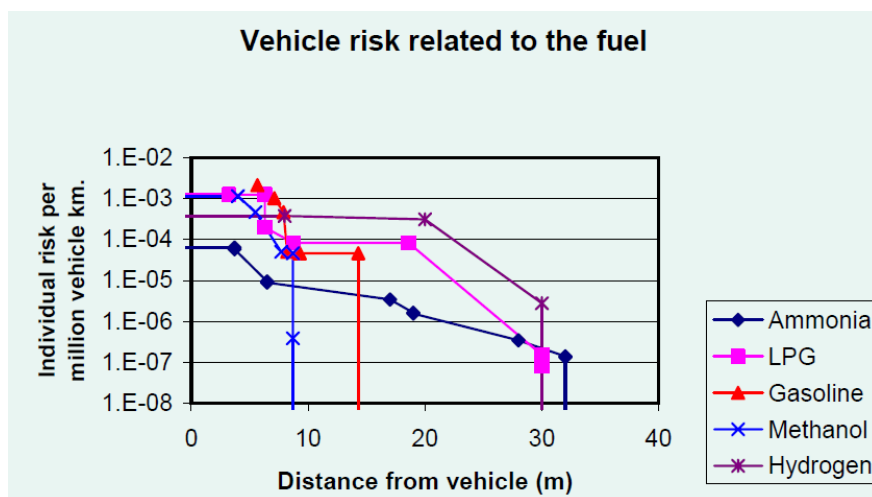


Figure 1.7. Representation of the risk associated with different fuel tanks for vehicle applications (Dujim, Markert and Paulsen, 2005).

Nowadays, a downside of using ammonia as a source of hydrogen, it is its origin. Globally, 100 Mtonne/year ammonia are produced, and 95% come from fossil fuels. As a result, 420 Mtonne/year of carbon dioxide are emitted (Wilkinson, Nayak-luke and Ban, 2018), which represent, approximately, 1% of the global CO<sub>2</sub> emissions (Service, 2018).

Ammonia (NH<sub>3</sub>) is produced from N<sub>2</sub> and H<sub>2</sub>. The first molecule comes from the air, but hydrogen is obtained by steam reforming from natural gas, mainly. Then, once hydrogen is generated, ammonia is synthesised by Haber-Bosch<sup>1</sup> process. In the process CO<sub>2</sub> is emitted. Furthermore,

<sup>1</sup> It is an artificial process to fixate atmospheric nitrogen to generate ammonia by reacting with hydrogen and in presence of a catalyst (Wilkinson, Nayak-luke and Ban, 2018)

the energy provided comes from fossil fuel sources (See **Hydrogen and ammonia from steam reforming**) (Service, 2018; Zhang *et al.*, 2020). In addition, models predict a rise of the demand of ammonia; therefore, if no change in the source is done, the emissions of carbon dioxide will increase (Wilkinson, Nayak-luke and Ban, 2018).

New ways of transforming this process into emitting zero carbon dioxide are being explored. By using renewable energies like wind or the sun, the excess energy generated can be used to perform water electrolysis, and therefore, generate hydrogen. The product can be used in the ammonia synthesis. Even though it is an efficient process, the issue with this method is the slowness at which hydrogen is produced (Wilkinson, Nayak-luke and Ban, 2018; Zhang *et al.*, 2020).

Studies have shown that the production of ammonia from renewable energy is possible and economically competitive (Wilkinson, Nayak-luke and Ban, 2018). On one hand, by using the hydrogen produced by electrolysis from renewables energies, it is enough for stationary uses. On the other hand, for mobile applications, ammonia, obtained from green sources, is a better option than hydrogen as it has been exposed previously.

## 1.5. Air quality

Nowadays, the climate change issue is daily talked and concerned. However, the combustion of fossil fuels not only is associated with the emission of CO<sub>2</sub>, but other components. Those are pollutants, and although most of them are not GHG, they have negative effects on the ecosystem and on the human health, at relatively small concentrations.

Then, air pollution happens when elements that do not belong to the intrinsic composition of the atmosphere appear, or their natural concentration increases. Episodes of contamination usually have a duration of a few weeks and happen locally. It is noteworthy that those can be produced in a different place where they are causing an episode of contamination. The reason is due to the dispersive character of the atmosphere. As it is in a continuous movement, it tends to even its composition.

### 1.5.1. Classification of air pollutants

Pollutants can come from natural emissions like volcano eruptions, natural forest fires or biological processes. However, humans are responsible for producing them from the combustion of fossil fuels to obtain energy or from their industrial processes. In short or long term, these can cause health problems, which eventually can cause death, or can be potentially harmful for the environment. Table 1.2 exhibits the most common pollutants, classified by the type and origin (Daly and Zannetti, 2007; Ley 34/2007, de 15 de noviembre). They can be classified by their spatial scale: if locally, there are pollutants, if their effects are global, they are GHG. All those presented in Table 1.2 are pollutants, except for the O<sub>3</sub> and the CH<sub>4</sub> that are also GHG. In addition,

they can be further sorted out in primary or secondary pollutants. The former is directly emitted into the atmosphere while the latter is formed by the primaries which act as precursors. (Daly and Zannetti, 2007).

*Table 1.2. Classification of the most common air pollutants and their source (Data extracted from: (IPCC, 1990; Seinfeld and Pandis, 1998; Daly and Zannetti, 2007; Conselleria d'Agricultura, Desenvolupament Rural, 2015; EEA, 2016; Registro Estatal de Emisiones y Fuentes Contaminantes, 2019; EPA, 2019; Directive (EU) 2015/2193)).*

Type of air pollutant	Pollutant	Source
Primary	PM	<b>Natural:</b> volcanoes, forest fire, sea, dust
		<b>Anthropogenic:</b> fossil fuel combustion
	SO <sub>2</sub>	<b>Natural:</b> volcanoes, biological processes
		<b>Anthropogenic:</b> fossil fuel combustion. Industrial processes
	NO <sub>x</sub>	<b>Natural:</b> forest fire, biological processes
		<b>Anthropogenic:</b> fossil fuel combustion, industrial processes, fertilization
	NH <sub>3</sub>	<b>Natural:</b> biological processes
		<b>Anthropogenic:</b> agriculture and livestock, fossil fuel combustion
	VOC	<b>Natural:</b> vegetation
		<b>Anthropogenic:</b> industrial processes, fossil fuels
	CH <sub>4</sub>	<b>Natural:</b> decomposition of organic matter, vegetation, ruminant animals
		<b>Anthropogenic:</b> fossil fuel combustion, extraction and refining, livestock, landfill
Heavy metals	<b>Natural:</b> soil erosion, volcanoes	
	<b>Anthropogenic:</b> industrial processes, mining, waste incineration	
CO	<b>Natural:</b> volcanoes, methane oxidation	
	<b>Anthropogenic:</b> fossil fuel combustion, forest fire, industrial processes	
Secondary	PM	From NO <sub>x</sub> and VOC
	O <sub>3</sub>	From NO <sub>x</sub> and VOC (photochemical reaction)

### 1.5.2. Effects of air pollutants

Regarding the health issues that an overexposure to these pollutants may cause, there is a wide range of illnesses. In general, these compounds tend to affect the airways by irritation. More specifically, organic compounds like CH<sub>4</sub> and VOC have a high carcinogenic risk, and immediate effects could be nausea, dizziness or, for extremely high concentrations, they can cause death. CO can decrease the transport of oxygen in the blood, which produces, instantaneously, trouble breathing; and a prolonged exposure can lead to death by asphyxia. Neurologic effects can be caused by NO<sub>x</sub> (Directive (EU) 2015/2193; EEA, 2016; EPA, 2019; EEA, 2020b).

Generally, ozone, (NO<sub>x</sub> and VOC) and SO<sub>2</sub> are the compounds that can be harmful for the environment. An episode with high ozone concentrations is called photochemical smog, which is produced when there is an extra emission of VOC and NO<sub>x</sub>, with solar radiation. This inhibits the

---

photosynthesis and their reproductive capacity (EPA, 2006; European Commission, 2014a). An increase of the emissions of SO<sub>2</sub> and NO<sub>x</sub> can lead to interactions with the water in the atmosphere and acidifying the precipitation. The acid water destabilises soils, which generated a lixiviation of their nutrients. The soil will impoverish and the lixivate will end up in mass water where it will cause eutrophication (Ministerio para la Transición Ecológica, 2016). Vegetation is exposed to their loss of nutrients, as well. These changes will disturb the ecosystem and the animal that live within.

### 1.5.3. European policies

Air quality is necessary to assure a healthy environment. According to European studies (European Commission, 2019), more than 400000 people die prematurely because of pollution, and 6.5 million people develop sicknesses due to the harmful air quality. Regarding the ecosystems, currently approximately two thirds of Europe's environment are endangered by the air pollution. (European Commission, 2019; EEA, 2020a).

In order to prevent any harm to humans or ecosystems, regulations need to be made. This would allow controlling the emissions of pollutants and assuring that the concentrations would not cause any damage. Table 1.3 shows the values marked by the WHO, as well as the Directive 2008/50/EC<sup>2</sup> (Directive 2008/50/EC; World Health Organisation, 2018).

---

<sup>2</sup>Directive 2008/50/EC of the European Parliament and of the Council of 21 May 2008 on ambient air quality and cleaner air for Europe (Directive 2008/50/EC).



Table 1.3. Limits for the pollutants decided by Europe and WHO (Data extracted from: (Directive 2008/50/EC; World Health Organisation, 2018)).

Pollutant	European limits		WHO limits
	Health	Vegetation	
PM <sub>2.5</sub>	25 µg · m <sup>-3</sup> (a calendar year) 20 µg · m <sup>-3</sup> (exposure concentration obligation)	-	25 µg · m <sup>-3</sup> (a day) 10 µg · m <sup>-3</sup> (a calendar year)
PM <sub>10</sub>	50 µg · m <sup>-3</sup> (a day) 40 µg · m <sup>-3</sup> (a calendar year)	-	50 µg · m <sup>-3</sup> (a day) 20 µg · m <sup>-3</sup> (a calendar year)
SO <sub>2</sub>	350 µg · m <sup>-3</sup> (an hour) 125 µg · m <sup>-3</sup> ( a day)	20 µg · m <sup>-3</sup> (a calendar year)	500 µg · m <sup>-3</sup> (10 minutes) 20 µg · m <sup>-3</sup> (a day)
NO <sub>2</sub>	200 µg · m <sup>-3</sup> (an hour) 40 µg · m <sup>-3</sup> (a year)	30 µg · m <sup>-3</sup> (a calendar year)	200 µg · m <sup>-3</sup> (an hour) 40 µg · m <sup>-3</sup> (a calendar year)
BaP	1 ng · m <sup>-3</sup> (target vaue a year)	-	0.12 ng · m <sup>-3</sup> (a calendar year)
C <sub>6</sub> H <sub>6</sub>	5 µg · m <sup>-3</sup> (a calendar year)	-	1.7 µg · m <sup>-3</sup> (a calendar year)
Pb	0..5 µg · m <sup>-3</sup> (a calendar year)	-	0.5 µg · m <sup>-3</sup> (a calendar year)
As	6 ng · m <sup>-3</sup> (a calendar year)	-	6.6 ng · m <sup>-3</sup> (a calendar year)
Cd	5 ng · m <sup>-3</sup> (a calendar year)	-	5 ng · m <sup>-3</sup> (a calendar year)
Ni	20 ng · m <sup>-3</sup> (a calendar year)	-	25 ng · m <sup>-3</sup> (a calendar year)
CO	10 mg · m <sup>-3</sup> (a daily 8-hour mean)	-	30 mg · m <sup>-3</sup> (an hour) 10 mg · m <sup>-3</sup> (a daily 8-hour mean)
O <sub>3</sub>	120 µg · m <sup>-3</sup> (target value, a daily 8-hour mean)	10000 µg · hour <sup>-1</sup> · m <sup>-3</sup> (from April to September)	100 µg · m <sup>-3</sup> (a daily 8-hour mean)

The legal framework for European air is constituted by Ambient Air Quality Directives and the National Emission reduction Commitments Directive (NECD)<sup>3</sup>. The former includes the Directive 2008/50/EC which sets the limit values for each pollutant, as well as air quality objectives (see Table 1.3) (Directive 2008/50/EC). A part, also it considers the Directive 2004/107/EC<sup>4</sup> (Directive 1004/107/EC), about heavy metals and hydrocarbons; the Directive 2015/1480/EC<sup>5</sup> (Directive (EU) 2015/1480/EC), which normalises the methodology for gathering and analyse data; and the Commission Implementing Decision 2011/850/EU<sup>6</sup> (European Commission, 2011) determining the communication of information regarding air quality data.

<sup>3</sup> Directive (EU) 2016/2284 of the European Parliament and of the Council of 14 December 2016 on the reduction of national emissions of certain atmospheric pollutants, amending Directive 2003/35/EC and repealing Directive 2001/81/EC (Directive (EU) 2016/2284).

<sup>4</sup> Directive 2004/107/EC of the European Parliament and of the Council relating to arsenic, cadmium, mercury, nickel and polycyclic aromatic hydrocarbons in ambient air (Directive 2004/107/EC).

<sup>5</sup> Directive 2015/1480/EC of 28 August 2015 amending several annexes to Directives 2004/107/EC and 2008/50/EC of the European Parliament and of the Council laying down the rules concerning reference methods, data validation and location of sampling points for the assessment of ambient air quality (Directive (EU) 2015/1480/EC).

<sup>6</sup> Commission Implementing Decision of 12 December 2011 laying down rules for Directives 2004/107/EC and 2008/50/EC of the European Parliament and of the Council as regards the reciprocal exchange of

The NECD (Directive (EU) 2016/2284) establishes the commitments of the Member States to reduce the emission levels of SO<sub>2</sub>, NO<sub>x</sub>, NMVOC, NH<sub>3</sub> and PM<sub>2.5</sub>. In addition, it requires the Members to present control programmes, and monitor their emissions. By that, WHO guideline requirements could potentially be met. In the **Annex 1** are the reduction objectives for each Member State (Directive (EU) 2016/2284).

Moreover, there are other European Directives that regulate the emissions produced by big industries. The Directive (EU) 2015/2193<sup>7</sup> (Directive (EU) 2015/2193) on medium combustion plants (MCPD) controls and sets limit values for SO<sub>2</sub>, NO<sub>x</sub> and PM for plants between 1 MW and 50 MW that combust fossil fuels (Directive (EU) 2015/2193). In order to achieve such values while considering costs and efficiencies, industries must use the Best Available Techniques (BAT), included in the Directive 2010/75/EU<sup>8</sup> (Directive 2010/75/EU) on industrial emissions (IED).

To further increase the mechanisms to achieve the air pollution goals, the European Commission created the Clean Air Policy Package, in 2013. This programme revisited all the policies related to air quality and emissions. With that, it was concluded that the first step was to write a new proposal for NECD and MCPD to be able to reach levels lower than what is determined by WHO (European Commission, 2013).

By applying these policies and writing new proposals, there is a reduction of European emissions. For PM, the reduction is about 63%; for SO<sub>2</sub>, 80%; for NO<sub>x</sub>, 65%; and for NH<sub>3</sub>, 25% (European Commission, 2019). However, this is not enough, and Europe has still concentrations higher than WHO and even, than the limits set in Directive 2008/50/EC; in addition, they are not in the line of their reduction commitments. In Figure 1.8 is presented the evolution of the emissions in Europe. In fact, it is represented the population exposed to concentrations above European (a) and WHO (b) limits. It can be seen that there is a decrease in most of the pollutants, which shows the positive effect of all the regulations that have been applied. Thus, analysing the evolution regarding the European Directive, the percentage of exposed population is relatively low, and by 2030 it could further decrease. However, for WHO values, the decreasing rate is slower than expected, and by 2030 such goals could not be achieved (EEA, 2019).

---

information and reporting on ambient air quality (notified under document C(2011) 9068) (Directive 2011/850/EU).

<sup>7</sup> Directive (EU) 2015/2193 of the European Parliament and of the Council of 25 November 2015 on the limitation of emissions of certain pollutants into the air from medium combustion plants (Directive (EU) 2015/2193).

<sup>8</sup> Directive 2010/75/EU of the European Parliament and of the Council of 24 November 2010 on industrial emissions (integrated pollution prevention and control) (Directive 2010/75/EU).

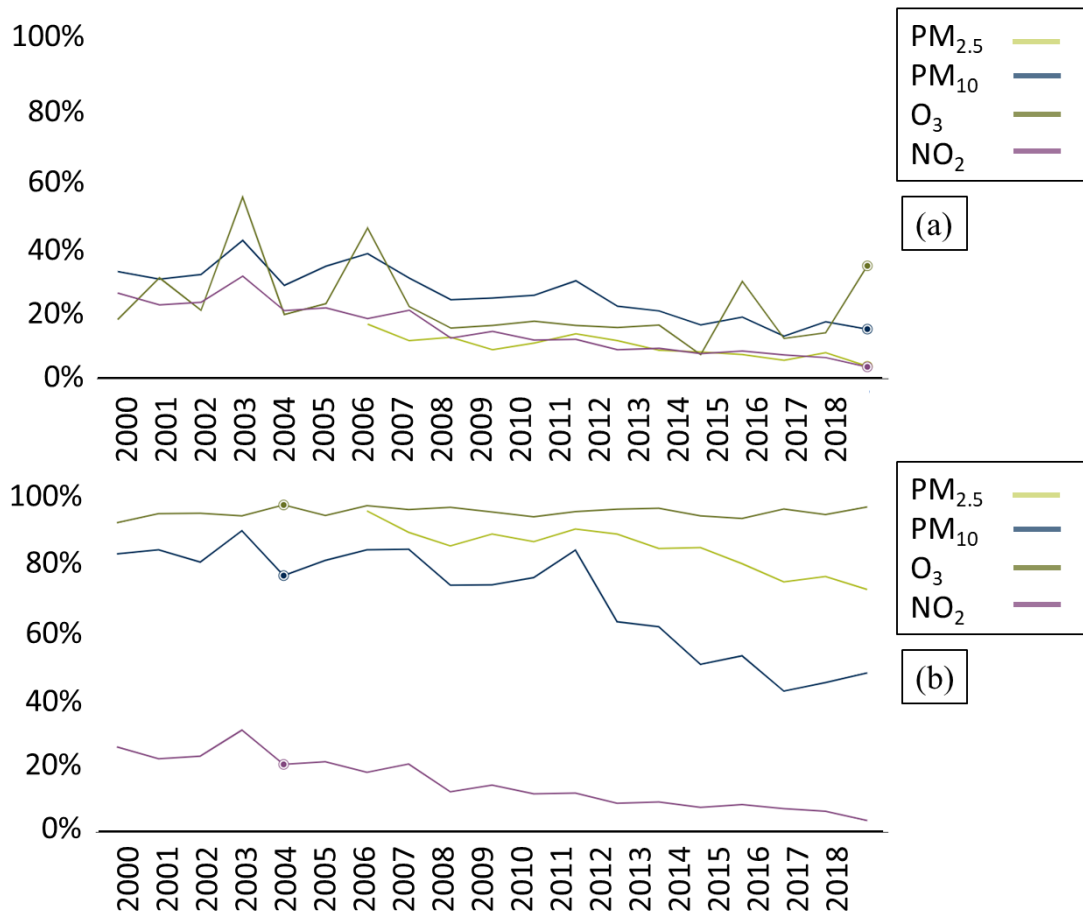


Figure 1.8. Evolution from 2000 to 2018 of the urban population exposed to pollution levels higher than the limits established by (a) Directive 2008/50/EC and (b) the WHO guidelines (EEA, 2019).

Some other mechanisms have to be applied if WHO limit values want to be achieved. In fact, since the beginning of the 2000s, European cities have been defining Low Emissions Zones (LEZ), where the traffic is limited to a certain type of cars. In the map shown in Figure 1.9 are represented the more than 250 cities that have a LEZ (Transport & Environment, 2019). In these areas, certain cars are permitted depending on their classification under the European Emissions Standards (see classification in **Annex 3**) and cities choose which vehicles can circulate there. Most of the current LEZ only allow Euro 5 and Euro 6 cars, which are the most recent and stricter classification (Council Directive 91/441/EEC; Council Directive 93/59/EEC; Directive 94/12/EC, Directive 96/69/EC; Directive 98/69/EC; Directive 2002/80/EC; European Commission, 2007; Urban Access Regulations, 2021). With this measure it can be assured that the pollution in these areas reaches levels that are not harmful for their residents. The highest decrease of emission in pollutants has been in Madrid, for the  $\text{NO}_2$ , which decreased 32%, respectively to values without LEZ. Moreover, other European cities have seen improvements in their air quality. Nevertheless, the measures have to become stricter, and with 67% of Europeans supporting these areas, there must be a transition from LEZ to Zero Emissions Zone (ZEZ) (Transport & Environment, 2019).



Figure 1.9. Map of the current LEZ in Europe (CLARS, 2021).

---

## 2. Aims and objectives

Environmental engineering's research focuses on finding solutions to protect the environment and the humans. It proposes solutions that could potentially reduce or avoid possible contamination of the air, water or soil. On that account, the aim of this work will be to contribute into this research by studying cleaner fuels, as alternatives to the fossil fuels. Specifically, **the main objective of this work is to analyse the performance of bimetallic catalysts under the ammonia decomposition reaction and find more feasible solutions than the current ones, which are too expensive to be competitive.**

Hence, secondary objectives set to be achieved by the end of this work are:

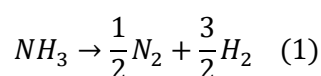
- **Produce a bimetallic catalyst (Ni and Ru) with efficiencies within a difference of 5%, when compared to Ru and Ni monometallic catalysts, for temperatures higher than 450 °C.** By analysing different parameters, concentrations and methods, there could be an optimal combination that could decrease the activation energy of the decomposition of ammonia and allow to reach values similar to Ru catalysts.
- **Compare the final results to existing literature.** The efficiencies obtained in this work need to be compared to analyse whether the final samples perform better than the already known catalysts.
- **Demonstrate that ammonia could be considered a feasible option.** By an exhaustive comparison between fossil and clean fuels, it will be discussed if ammonia could represent a sustainable alternative.

### 3. State of art

In this chapter, some concepts will be explained in order to understand the basis of this work and the results obtained. The following aspects will be described: the ammonia decomposition and the use of catalysts, ceria as a support, the ball milling (BM) and incipient wetness impregnation (IWI) method and fuel cells (FC).

#### 3.1. Ammonia decomposition and the use of catalysts

The decomposition of  $NH_3$  (Eq. 1) is an endothermic reaction, which means that energy has to be given for the reaction to happen. In this case, at a temperature of 673 K and 1 atm, 99.1% of  $NH_3$  conversion is reached (Yin *et al.*, 2004a).



At this temperature, the decomposition of  $NH_3$  on site to obtain  $H_2$  is not viable. For that reason, a catalyst is needed. It is defined as a substance that increases the rate of a reaction, without being consumed nor changing the overall standard Gibbs energy. As it is shown in Figure 3.1, introducing a catalyst in a reaction allows the reactants to generate intermediate products, which have a lower activation energy than the final product. This is still the same final product of the reaction without the catalyst, but it is achieved through a different path (IUPAC, 2019).

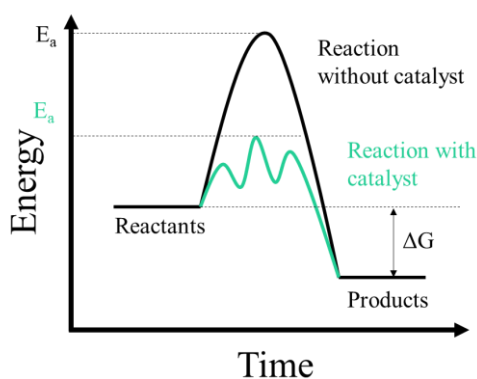


Figure 3.1. Representation of the activation energy of a reaction with (green) and without catalyst (black) (own elaboration).

There are two types of catalyst: heterogeneous and homogeneous. The main difference is that the catalyst is in a different state from the reactants, being the homogeneous catalyst the one with components of the same phase. In this work only the heterogeneous catalyst will be used. Catalysts are made from some components, which may vary for different reactants because they must be “just right” for the reactant, as it is stated by the Sabatier Principal. That means that it has to have enough binding energy in order for the reactant to be adsorb into its surface and desorb when the reaction is all done (Lamb, Dolan and Kennedy, 2018).

The reaction in the Eq. 1, with the presence of a catalyst, undergoes the same process explained. As it can be seen in Figure 3.2,  $\text{NH}_3$  is adsorbed into the surface of the catalyst, in this case, Ni. These particles become active sites, where the reaction is more likely to happen; due to better transfer of electrons. Once there, the molecule suffers consecutive cleavages of the N-H bond, allowing the hydrogen, in white in the Figure 3.2, to recombine to form  $\text{H}_2$ . When all the bonds are broken,  $\text{N}_2$  is formed, in blue in the Figure 3.2, and desorbs from the catalytic surface. Then, the active site is free to accept another molecule (García-bordejé *et al.*, 2014; Bell and Torrente-Murciano, 2016a).

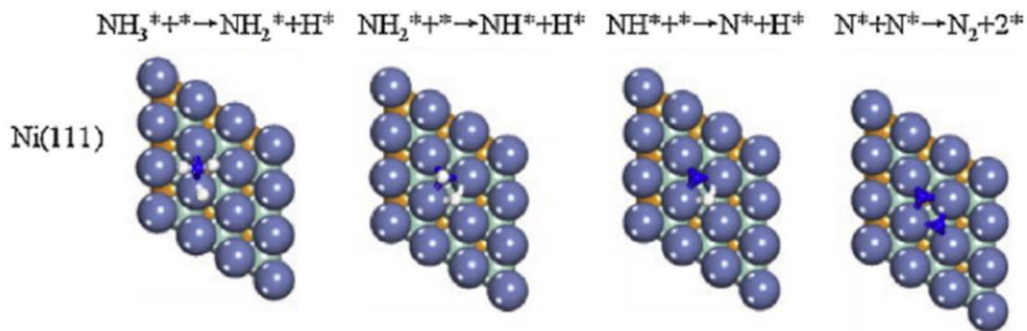


Figure 3.2. Decomposition of  $\text{NH}_3$  in a nickel catalyst step by step. The greyish blue spheres represent Ni, the blue arrows,  $\text{N}_2$ , and the white arrows,  $\text{H}_2$ . The asterisk represents an excited state of the molecule (Mukherjee *et al.*, 2018).

There are different ways to characterise the activity of the catalyst, as it can be described as the equations 2, 3 and 4. The TOF or turn over frequency value (Eq. 2) compares the amount of active sites of a catalyst with the  $\text{NH}_3$  decomposition rate. Thus, it indicates the rate at which the active sites are able to decompose the  $\text{NH}_3$ . The catalyst activity (Eq. 3) describes the amount of  $\text{NH}_3$  decomposed after passing through or over the catalyst. The conversion (Eq. 4) is a measure of the efficiency of the catalyst, as meaning 100% that all the  $\text{NH}_3$  in the reaction is decomposed (Lamb, Dolan and Kennedy, 2018).

$$\text{TOF} = \frac{\text{mols of product generated} \cdot \text{time}^{-1}}{\text{mols of active sites}} \quad (2)$$

$$\text{Catalyst activity} = \frac{\text{mols } \text{NH}_3 \text{ decomposed}}{\text{time} \cdot \text{grams of catalyst}} \quad (3)$$

$$\text{Conversion} = 100 \cdot \frac{\text{NH}_3 \text{ outlet concentration}}{\text{NH}_3 \text{ inlet concentration}} \quad (4)$$

Catalysts tend to contain metallic elements. The choice is not trivial and depends on the reactants, as it has been said previously. For the  $\text{NH}_3$  decomposition, Ru is the element which allows to have the most efficient reaction rate, as it can be seen in Figure 3.3. This type of graphic, called volcano type graph, represents the reaction rate versus a property of the reaction such as the enthalpy of

the reaction or desorption energy from one of the reactants. The shape of the plot, a volcano, has a maximum, which can be understood as the optimal catalyst for a certain reaction. In Figure 3.3 there is an example of volcano type graph. In the x-axis the dissociative  $N_2$  adsorption energy is represented. In the y-axis is plotted the TOF of the reaction and the reaction rate. It can be seen that Ru, has the highest rate reaction with relatively low dissociative adsorption energy. Furthermore, for a 99% conversion of the  $NH_3$  into  $H_2$ , Ru has a high TOF (Lamb, Dolan and Kennedy, 2018).

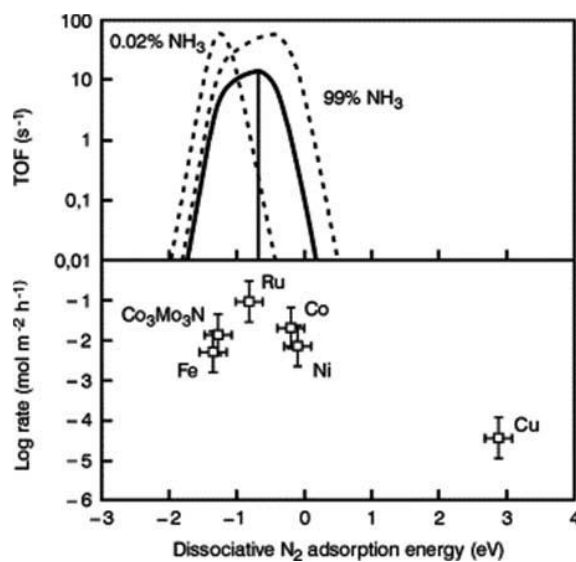


Figure 3.3. Volcano type graph for the  $NH_3$  decomposition. The TOF of the reaction and the logarithm of the reaction's rate are plotted against the dissociative  $N_2$  adsorption energy (Bell and Torrente-Murciano, 2016).

Although Ru is the best catalyst for ammonia decomposition, it is expensive. For that reason, bimetallic systems appear as a second good option. Instead of using a pure Ru catalyst, mixing it with other metals can generate an active catalyst, comparable with the pure one. In this work, the combination of Ru and Ni will be explored.

There can be catalysts that are only formed by large metal particles, called unsupported catalyst. The total surface area, where the molecules adsorb, has an important role in the activity rate of the reaction. Without a support, the metallic particles tend to be larger and the active surface is lower, decreasing the efficiency of the reaction (Bell and Torrente-Murciano, 2016).

The aim of a supported catalyst is to increase the active surface. The supports tend to be porous, which allows the particles to be dispersed and remain small in size. Thus, the structure of the support and the catalyst particles, and their size, determine the number of active sites a catalyst can have.

Nevertheless, the support not only acts as a surface to disperse the catalyst, but it can also interact with it and consequently affecting the activity rate of the reaction. In  $NH_3$  decomposition, it has been reported that supports with high conductivity, allow a transfer of electrons toward the



metallic particles, hence, increasing the recombinative desorption of  $N_2$  in the surface (Yin *et al.*, 2004a; García-bordejé *et al.*, 2014; Bell and Torrente-Murciano, 2016a). Moreover, to further increase its activity, the support should be basic (Yin *et al.*, 2004a).

There is another element that, although it is not always necessary, could further improve the performance of the catalyst: the promoters. They can help the metallic particles disperse into the support, as well as prevent the catalyst from being inhibited. Promoters, such as alkali, alkaline earth or rare earth metals, tend to be the choice for the ammonia reaction. They help decrease the metallic particle size and enhance the activity of the catalyst by donating electrons into the reaction (Yin *et al.*, 2004a; García-bordejé *et al.*, 2014).

### 3.2. Ceria

The support chosen in this work is ceria. This material presents certain characteristics that improve the performance of the reaction. The formula for ceria is  $CeO_2$ , which means that cerium has a valence of +IV. This gives a fluorite type structure, with space group  $Fm\bar{3}m$ , shown in Figure 3.4. Moreover, this structure is really stable under changes of temperature.

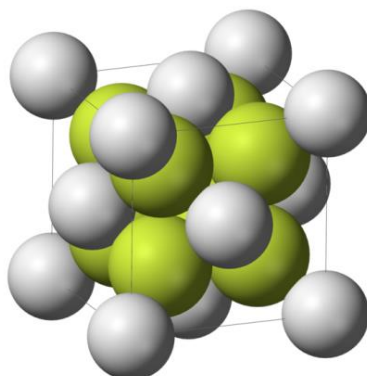


Figure 3.4. Fluorite type structure of ceria. Oxygen atoms are in green and cerium, in white (Sherman, 2019).

However, the reality is that ceria is never 100% stoichiometric; that means that there are cerium atoms, with valence of +III. These characteristics generate  $O_2$  vacancies because  $Ce^{+3}$  needs less oxygens than  $Ce^{+4}$ . The defects in this material make it an electron donor, therefore the ceria is considered to be electropositive. This extra contribution increases the efficiency of the reaction; more specifically increases the rate at which the  $N_2$  can be desorbed (Mogensen, Sammes and Tompsett, 2000). Furthermore, another process occurs with the presence of  $H_2$ ; called the hydrogen spillover. When  $H_2$  is in contact with ceria, in its surface, it is able to break its bond and  $H_2$  reduces cerium which generates more vacancies, and hence more electrons can be given (Karim *et al.*, 2017).

Nevertheless, high conductivity is needed in order to deliver the electrons into the reaction. Ceria presents good electron conductivity. The mechanism by which the electrons move is by the

generation of polarons. They are created when an electron is trapped at a given site and the positive charges around it relocate themselves in order to neutralise the change in the local charge. Because of temperature, the polaron (the electron plus the distortion associated) is able to migrate (Mogensen, Sammes and Tompsett, 2000).

Apart from this intrinsic characteristic that improves the efficiency, ceria presents an irregular surface that allows the metallic particles to have a better dispersion, smaller size and, hence, a larger active surface, overall.

### 3.3. Incipient Wetness Impregnation (IWI)

One of the most used methods to prepare catalyst is by IWI. By adsorption, a solution with the active precursor and the smallest amount of dissolvent is applied into the dried support. If a big amount of solution is applied, it can create a film that blocks the pores of the support and the particles cannot be dispersed. When small amounts are applied, it is needed to be dried between applications to prevent the generation of this film. Once the active precursor is all applied, the catalyst needs to be calcined (Regalbuto, 2016).

In Figure 3.5, it is shown a scheme of a catalyst prepared with IWI. The result is a relatively ordered disposition of the active precursor, allowing the particles to have its lowest energy (Zhang *et al.*, 2014).

### 3.4. Ball milling (BM)

Traditionally, conventional methods, such as IWI, had being used to produce catalysts. Recently, BM is gaining attention due to its better performance in the generation of catalysts.

This method consists in putting the powders, and optionally some liquid, in a container along with balls, which are the grinding media. The vessel is set in the machine, where it will be spun with respect its own axis and external centre, like a planetary movement. The combination of movements create enough centripetal force to generate the mechanical activation, in order, not only to grind the powders but to synthesis and to optimise their structure (Sadykov *et al.*, 2019).

Studies have shown the advantages of the BM versus IWI, exemplified in the Figure 3.5. It can be seen that the same catalyst is generated, Ni/CeO<sub>2</sub>, but the result is different. Previously, the characteristics of catalyst have been explained. A good support needs to be porous as well as allow to disperse the Ni particles, in this case. Referring to the Figure 3.5, it can be seen how the catalyst prepared with BM is more porous and Ni particles are better dispersed than the one prepared with IWI. Furthermore, metallic particles need to be smaller in order to have more active surface; with BM it can be achieved (Zhang *et al.*, 2014; House *et al.*, 2015). In addition, they

show higher stability and a higher material reactivity due to mechanical activation (Sadykov *et al.*, 2019).

The device used for BM allows controlling certain parameters that will affect the catalyst generated. These are: the rotation speed of the cylinder, number of balls used in the process, the diameter and material of the balls and the time of the duration of the milling process (Zhang *et al.*, 2014).

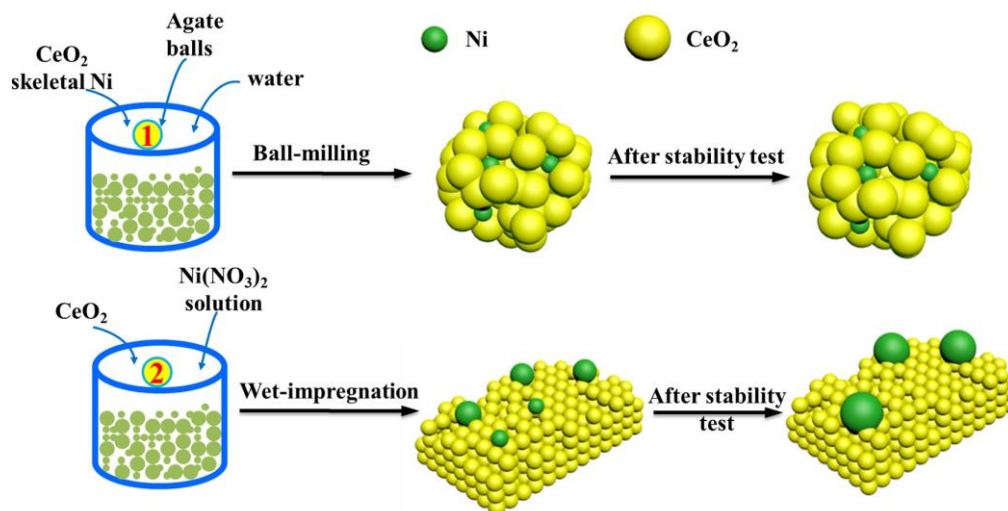
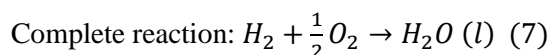
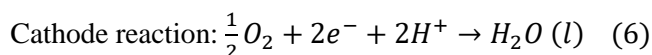
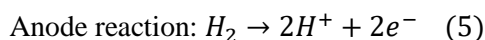


Figure 3.5. Scheme of ceria and Ni catalyst structure made by BM and WI (Zhang *et al.*, 2014).

### 3.5. Fuel cells (FC)

A fuel cell is a device that is able to convert chemical energy into electricity, through a continuous source of fuel and an oxidizing agent,  $O_2$  for example. The mechanism that drives such a process is a pair of redox reactions (Sadykov *et al.*, 2019). They convert  $H_2$ , or some fuel with high concentration of this element, into water and energy (electricity and heat) (Eq. 5, 6 and 7) (Cook, 2002)



In general, FC are composed by three elements: an anode, a cathode and an electrolyte. The process is described in Figure 3.6. The fuel, or  $H_2$ , undergoes an oxidation at the anode (Eq. 5). That generates protons ( $H^+$ ) and electrons. Protons go through the electrolyte, to the cathode. Meanwhile, the electrons generated at the anode have gone through an external circuit to produce electricity and power the device connected to the FC. At the cathode (Eq. 6),  $H^+$  suffer a reduction,

where they combine with  $O_2$  and the electrons from the circuit, to form water (Cook, 2002; Sadykov *et al.*, 2019).

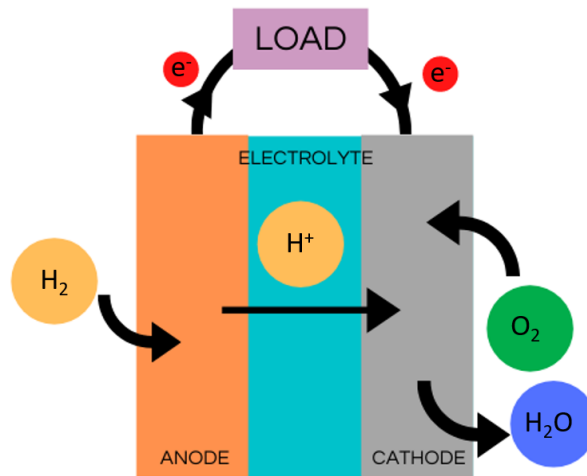


Figure 3.6. Scheme of the parts of a FC and its functioning (own elaboration).

The energy extracted from the cell can be calculated with the reactions, supposing ideal conditions. The enthalpy of the water formation, at standard conditions, is  $-285.83$  kJ; which is defined as an exothermic process. It releases energy, which mainly is transformed into electricity. Nevertheless, some is lost in the form of heat. Describing the loss of energy with the entropy, the output energy can be calculated with the enthalpy of formation minus the entropy factor. Therefore, the result is that  $237.13$  kJ/mol is extracted from the reaction and transformed into electricity (Nave, 2001; Cook, 2002).

The reality is far from this value, although it is still more efficient than the fossil fuel engines. Temperature has an important role in determining the efficiency of a FC; as it increases, more heat is released, and less electricity is generated. Currently, a FC has an efficiency of 40-60%, compared to the 25% of a fossil fuel engine. Moreover, if the heat released is used in other applications, such as the heating of a car, the efficiency increases up to 85% (Nave, 2001; Cook, 2002).

Table 3.1. Types of fuel cells and its characteristics (Data extracted from: (Edwards *et al.*, 2020)).

Fuel cell type	Operating temperature (°C)	Electrical power range (kW)	Electrical Efficiency (%)	Applications
Proton Exchange membrane (PEM)	60-110	0.01-250	40-55	Mobile, portable, low power generation
Alkaline	70-130	0.1-50	50-70	Space, military, mobile
Direct methanol	60-120	0.001-100	40	Portable, mobile
Phosphoric acid	175-210	50-1000	40-45	Medium to large scale power and CHP*
Molten carbonate	550-650	200-100000	50-60	Large scale power generation
Solid oxide	500-1000	0.5-2000	40-72	Medium to large scale power and CHP, vehicle, auxiliary power units, off-grid power

The component that characterises FC is the electrolyte. In Table 3.1 are some examples of different types. In this work the PEMFC will be considered because is the most widespread type and fully commercial. They operate at a range of temperatures of 60-110 °C, which compared to the temperature at which the ammonia decomposes is much lower. For that reason, a catalyst that can reduce this temperature within the range of operation of the fuel cell is needed.

Although PEMFC are the most commonly used type, there is an issue that needs to be considered. Usually, the cathode and anode of the cell has Pt particles to enhance the reaction. With CO, Pt creates a strong bond that prevents H<sub>2</sub> from reaching the active sites of the anode, and even the cathode, therefore reducing the efficiency of the reaction. This problem is concerning due to the fact that it happens when the temperature is low (Zamel and  $\tilde{A}$ , 2008). Moreover, not only CO can be damaging for the PEMFC, but other compounds as well, such as HCHO, NH<sub>3</sub>, H<sub>2</sub>S or halogen compounds (Jacques, 2011).

For that reason, it is needed a source of H<sub>2</sub> that does not generate these pollutants. Because the decomposition of NH<sub>3</sub> only has N<sub>2</sub> and H<sub>2</sub> as products, this source does not poison the PEMFC.

## 4. Methodology

### 4.1. Preparation of catalysts

#### 4.1.1. Preparation of the support (CeO<sub>2</sub>)

Ceria (CeO<sub>2</sub>) is the support for the catalysts analysed in this work. Over the time of this research, three batches of 20 g each were prepared by the following method. The characteristics of each preparation are exposed in Table 4.1.

Table 4.1. Characteristics of the batches of CeO<sub>2</sub> prepared.

Batch	Final weight (g)	Ce(NO <sub>3</sub> ) <sub>3</sub> ·6H <sub>2</sub> O (g)	NH <sub>3</sub> (mL)	Deionised water (L)	T oven (°C)	T calcination (°C)	Time calcination (h)
CeO-1	19,43	51,07	100	1,5	90	450	4
CeO-2	19,67	50,87	90	1,9	90	450	4
CeO-3	18,56	50,84	115	2,0	90	450	4

A dissolution of cerium nitrate hexahydrate (Ce(NO<sub>3</sub>)<sub>3</sub>·6H<sub>2</sub>O) 0.113M was prepared (50.44 g Ce(NO<sub>3</sub>)<sub>3</sub>·6H<sub>2</sub>O and 1.2 L deionised water). While agitating that mixture, a solution of 26% (wt.) ammonium hydroxide (NH<sub>4</sub>OH) was poured, slowly and in a controlled manner. The final solution had a pH within the range 9-10. Then, to obtain the solid residue, the mixture was filtered. The ensemble used is depicted in Figure 4.1(a). Afterwards, due to the basicity of the product and the leftover solution, deionised water was poured until the leftover solution reached a pH of 7. Usually, the amount of deionised water needed to achieve neutrality is between 1.5 L and 2.0 L. The product was a wet yellow solid as seen in Figure 4.1(b). It was dried at 90 °C, for 24 hours. Then, it was calcined in a furnace at 450 °C for 4 hours (Figure 4.1(c)).

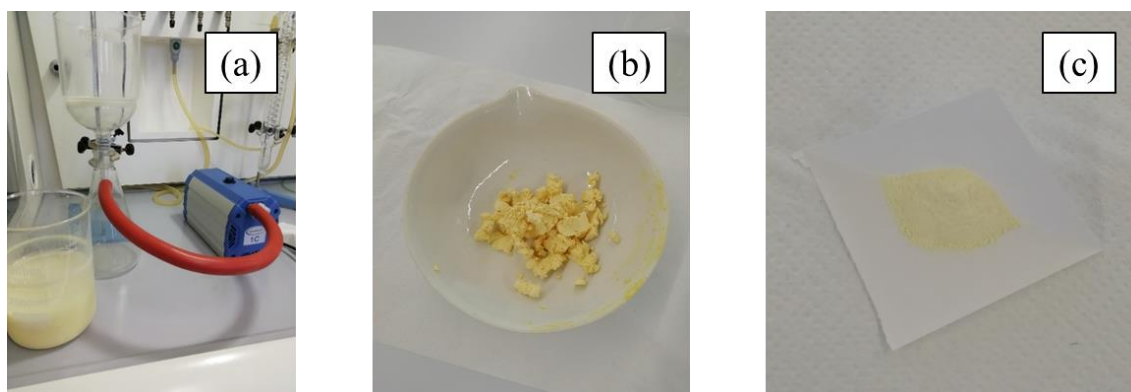


Figure 4.1. Image of (a) the set up to filtrate the cerium oxide (b) the residue obtained after filtration and (c) the final ceria, dried and calcined (own elaboration).

#### 4.1.2. Preparation of catalysts

All catalysts presented in this work have been prepared generally with BM, but some have been synthesised with IWI. Both techniques have been theoretically explained in the **State of Art**. The different samples prepared are presented in Table 4.2, with all the specifications on quantities,

time and parameters in order to prepare samples of 2 g, three combinations of metals were selected to be in the catalyst, supported by CeO<sub>2</sub>: Ni, Ru and both together (bimetallic).

For the Ni samples (Ni/CeO<sub>2</sub>), in yellow in Table 4.2, the content of Ni is 5% (wt.). Therefore, it was needed 95% CeO<sub>2</sub>, which is 1.90 g. Using Ni(NO<sub>3</sub>)<sub>2</sub>·6H<sub>2</sub>O, as precursor, the amount needed was 0.4952 g Ni(NO<sub>3</sub>)<sub>2</sub>·6H<sub>2</sub>O:

$$2g \text{ catalyst} \cdot \frac{5g \text{ Ni}}{100g \text{ catalyst}} \cdot \frac{1 \text{ mol Ni}}{58.69g \text{ Ni}} \cdot \frac{290.69g \text{ Ni(NO}_3)_2 \cdot 6\text{H}_2\text{O}}{1 \text{ mol Ni(NO}_3)_2 \cdot 6\text{H}_2\text{O}}$$

$$= 0.4952g \text{ Ni(NO}_3)_2 \cdot 6\text{H}_2\text{O} \quad (8)$$

For Ru catalyst (Ru/CeO<sub>2</sub>), in blue in Table 4.2, the content of Ru is 1% (wt.). Thus, it was needed 99% CeO<sub>2</sub>, which was 1.98 g. Using RuCl<sub>3</sub>, as precursor, the amount needed was 0.0411 g RuCl<sub>3</sub>:

$$2g \text{ catalyst} \cdot \frac{1g \text{ Ru}}{100g \text{ catalyst}} \cdot \frac{1 \text{ mol Ru}}{101.07g \text{ Ru}} \cdot \frac{207.42g \text{ RuCl}_3}{1 \text{ mol RuCl}_3} = 0.0411g \text{ RuCl}_3 \quad (9)$$

The last composition was for Ni and Ru catalyst (NiRu/CeO<sub>2</sub>), in orange in Table 4.2, with a content of (i) Ni of 5% (wt.) and of Ru of 1% (wt.) and (ii) Ni of 2.5% (wt.) and of Ru of 0.5% (wt.). With the former percentages (i), there was 94% CeO<sub>2</sub>, which was 1.88 g. The same amounts obtained in (1) and (2) were used for this preparation. For the latter (ii), CeO<sub>2</sub> represented the 97%, which was 1.94 g, and for Ni and Ru precursors, 0.2476 g and 0.0205 g, respectively:

$$2g \text{ catalyst} \cdot \frac{2.5g \text{ Ni}}{100g \text{ catalyst}} \cdot \frac{1 \text{ mol Ni}}{58.69g \text{ Ni}} \cdot \frac{290.69g \text{ Ni(NO}_3)_2 \cdot 6\text{H}_2\text{O}}{1 \text{ mol Ni(NO}_3)_2 \cdot 6\text{H}_2\text{O}}$$

$$= 0.2476g \text{ Ni(NO}_3)_2 \cdot 6\text{H}_2\text{O} \quad (10)$$

$$2g \text{ catalyst} \cdot \frac{0.5g \text{ Ru}}{100g \text{ catalyst}} \cdot \frac{1 \text{ mol Ru}}{101.07g \text{ Ru}} \cdot \frac{207.42g \text{ RuCl}_3}{1 \text{ mol RuCl}_3} = 0.0205g \text{ RuCl}_3 \quad (11)$$

It is noteworthy that some of the BM samples were prepared under dry conditions, and some had been prepared under wet condition, water or ethanol. In such case, three different volumes were used: 0.1 mL, 0.5 mL and 1 mL. After the BM, they were dried in the oven, overnight, at temperatures between 90 °C and 100 °C.

Table 4.2. Table of the samples prepared with the details of their preparation.

Name	Catalyst (g)	Method	Liquid (mL)	Liquid	CeO <sub>2</sub> batch	CeO <sub>2</sub> (%)	CeO <sub>2</sub> (g)	Ni (%)	Ni(NO <sub>3</sub> ) <sub>2</sub> ·6H <sub>2</sub> O(g)	Ru (%)	RuCl <sub>3</sub> (g)	Grinding speed (rpm)	Grinding time (min)	Ratio balls/catalyst	Diameter balls (mm)
Ni-D-10'	2	BM	-	-	CeO-1	95	1,9028	5	0,4953	-	-	400	10	10	10
Ni-W-0.5	2	BM	0,5	water (W)	CeO-1	95	1,9081	5	0,5101	-	-	400	10	10	10
Ni-IWI	2	IWI	1	water (W)	CeO-1	95	1,9088	5	0,4953	-	-	-	-	-	-
Ni-W-0.1	2	BM	0,1	water (W)	CeO-1	95	1,9062	5	0,495	-	-	400	10	10	10
Ni-W-1	2	BM	1	water (W)	CeO-1	95	1,9086	5	0,4988	-	-	400	10	10	10
Ni-E-0.1	2	BM	0,1	ethanol (E)	CeO-1	95	1,904	5	0,4961	-	-	400	10	10	10
Ni-E-1	2	BM	1	ethanol (E)	CeO-1	95	1,9104	5	0,4961	-	-	400	10	10	10
Ni-E-0.5	2	BM	0,5	ethanol (E)	CeO-1	95	1,9065	5	0,4969	-	-	400	10	10	10
Ni-D-20'	2	BM	-	-	CeO-2	95	1,9001	5	0,4982	-	-	400	20	10	10
Ru-Ni-s	2	BM	-	-	CeO-1	97	1,946	-	-	0,5	0,0205	400	10	10	10
								2,5	0,2481	-	-	400	20	10	10
Ni-Ru-s	2	BM	-	-	CeO-2	97	1,9414	2,5	0,2522	-	-	400	20	10	10
								-	-	0,5	0,0206		10		
NiRu-s	2	BM	-	-	CeO-2	97	1,9445	2,5	0,2504	0,5	0,0244	400	10	10	10
NiRu-b	2	BM	-	-	CeO-2	94	1,8823	5	0,4966	1	0,0414	400	10	10	10
Ru-Ni-b	2	BM	-	-	CeO-2	94	1,8801	-	-	1	0,0429	400	10	10	10
								5	0,4972	-	-		20		
Ni-Ru-b	2	BM	-	-	CeO-2	94	1,8814	5	0,4987	-	-	400	20	10	10
								-	-	1	0,0413		10		
Ni(10)-Ru(5)-b	2	BM	-	-	CeO-3	94	1,8854	5	0,4977	-	-	400	10	10	10
								-	-	1	0,0418		5		
Ru-400-10	2	BM	-	-	CeO-2	99	1,9816	-	-	1	0,0416	400	10	10	10
Ru-400-30	2	BM	-	-	CeO-2	99	1,9815	-	-	1	0,0423	400	30	10	10
Ru-400-5	2	BM	-	-	CeO-2	99	1,9804	-	-	1	0,0415	400	5	10	10
Ru-100-5	2	BM	-	-	CeO-3	99	1,9822	-	-	1	0,0415	100	5	10	10
Ru-800-5	2	BM	-	-	CeO-3	99	1,9805	-	-	1	0,0411	800	5	10	10
Ru-IWI	2	IWI	1	water (W)	CeO-3	99	1,9803	-	-	1	0,0414	-	-	-	-



#### 4.1.2.1. Ball milling (BM)

To synthesise the catalysts by BM, a planetary mill from Fritsch<sup>MR</sup> (Pulverisette 7 premium line) was used (Figure 4.2(a)). In Table 4.2 the different parameters that can be selected are presented (rotation speed, amount and diameter of grinding balls, material of balls and cylinder and time of duration). From previous studies on Ni/CeO<sub>2</sub> catalysts (Marin, 2020), it had been demonstrated that the optimal combination that produces the most efficient catalyst is the presented in Table 4.3. Those had been considered as a base parameter.

Table 4.3. Base parameters for BM.

Ratio balls/catalyst	10
Time grinding (min)	10
Rotation speed (rpm)	400

Both the cylinder and the balls were made of zirconium oxide (ZrO<sub>2</sub>). This choice was driven by its high mechanical strength (at room temperature); therefore, that assured that the sample could not be contaminated by fractured particles of the cylinder. Moreover, following the instructions of the device, larger balls (10 mm – 20 mm diameter) can cause high mechanical stress. The cylinder and the balls can be seen in Figure 4.2.(b).

The Ni/CeO<sub>2</sub> samples prepared by BM under dry conditions are marked with a D, and the ones prepared under wet conditions are marked with W for water, and E for ethanol. The formers used the parameters found in Table 4.3, thus the number next to their letters indicate the amount of liquid used. For the dry catalysts, their number indicates the grinding time chosen. For example, Ni-W-0.5 indicated a BM sample prepared at 400 rpm, during 10 min, with 0.5 mL water and Ni-D-20 was under dry conditions, grinded for 20 minutes and at 400 rpm.

Ru/CeO<sub>2</sub> samples were prepared under different speed and grinding time. The first number indicated speed (100, 400 o 800 rpm) and the second, the grinding time (5, 10, 30 min). So, Ru-800-5 was prepared at 800 rpm during 5 min.

Bimetallic samples were characterised by the order of addition and the concentration used. The latter was indicated by an -s if the catalysts had 0.5% Ru and 2.5% Ni, whereas a -b meant 1% Ru and 5% Ni. The order was denoted by placing the first element added, as the first element to read. So, Ni-Ru-b was prepared by adding 5% Ni first, for 10 min and then 1% Ru, together for 10 min more. Another bimetallic catalyst was named differently to exhibit different grinding times. Therefore, Ni10-Ru5-b was prepared similarly as Ni-Ru-b, but Ni was grinded for 5 min alone, and then Ru was added and grinded all together for 5 min more.

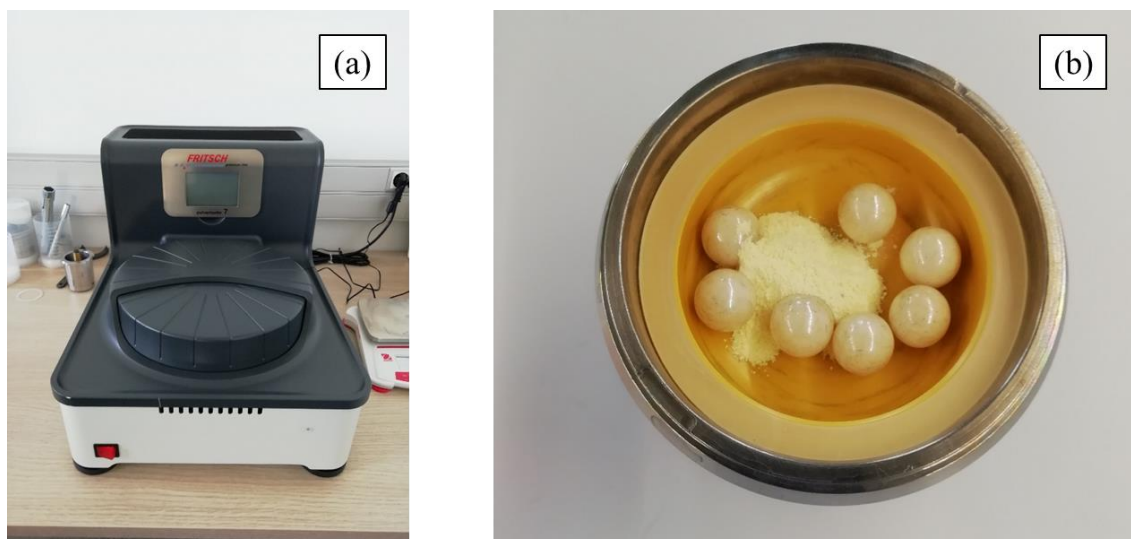


Figure 4.2. Image of (a) the planetary mill from Fritsch<sup>MR</sup> (Pulverisette 7 premium line) used and (b) the ZrO<sub>2</sub> cylinder and balls, with ceria (own elaboration).

#### 4.1.2.2. Incipient Wetness Impregnation (IWI)

The samples Ni-IWI and Ru-IWI (see Table 4.2) were the only ones prepared by IWI method, which had the same concentration as the other Ni and Ru catalysts (5% and 1%, respectively). With the same amount of Ni(NO<sub>3</sub>)<sub>2</sub>·6H<sub>2</sub>O from (Eq. 8), a solution was prepared with less than 1 mL of deionised water. To further dissolve the compound into the liquid, a magnetic agitator was used. Then, 1.90 g CeO<sub>2</sub> was deposited into a melting pot and the solution previously made was poured slowly, while incorporating it by mixing it with CeO<sub>2</sub>, until homogeneous. This process was repeated until the ensemble presented a more wet appearance. When that happened, it was dried into the oven for about 10 to 15 minutes, at less than 100 °C. All these steps were repeated until the solution had been all poured. At the end, the sample was calcined: first it was subjected to 100 °C, for 12 hours, and then at 450 °C, for 4 hours. The same process was applied to Ru-IWI, with the same amount of RuCl<sub>3</sub> as (Eq. 9).

Both catalysts, as well as Ni-D-10, were the reference samples for this study.

## 4.2. Reaction: ammonia decomposition

To characterise the performance of different catalyst, ammonia was decomposed at different temperatures, with the catalysts prepared, and the products generated were analysed. In Figure 4.3, the system used and its components are shown.

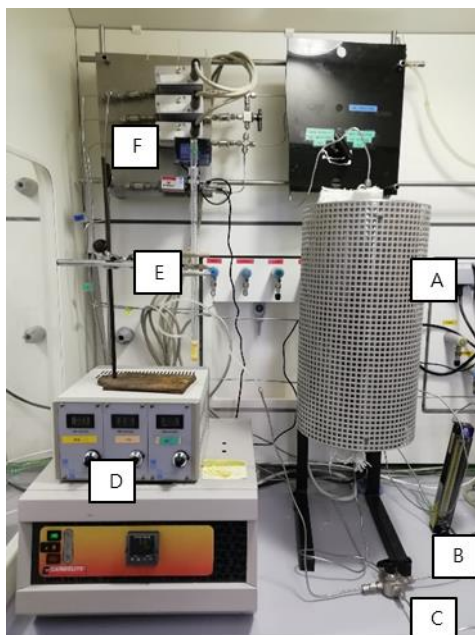


*Figure 4.3. Image of the complete system for the decomposition of ammonia. A: furnace; B: bypass; C: to mass spectrometer (not shown); D: mass flow of argon, hydrogen and nitrogen; E: flowmeter; F: mass flow of ammonia (own elaboration).*

The different elements of the system in Figure 4.3 are labelled from A to F. A represents the Carbolite™ vertical and tubular furnace, with an Eurotherm™ 3216 external controller. Inside the furnace is placed a Swagelok® tubular reactor of 50.5 cm length and ¼” external diameter and a thickness of 0.035” (see **Annex 3**, Figure 10.1 (a) and (b)).

The letter C indicates the line connected to the OmniStar™ mass spectrometer. This device determined the composition of a sample by vaporizing and then ionising it. The charged particles were accelerated by an electric field and then deflected by a magnetic one. The amount of deflection depended on the mass and the charge of the ion, so the mass spectrometer analysed the coefficient between these two parameters. Because its uniqueness, it can be associated with an element or compound. Through the software Quadrera®, the results in percentages were displayed; the error associated is about ±5%. Prior to any experiment, a calibration should be performed to assure the error would not be higher than 5%. Basically, knowing the composition of the gases that were sent to the spectrometer, the result should align with them.

The letter B and E indicates the bypass line and the flowmeter, respectively. The letter D and F represent the different mass flows that regulate the flows of the gases used: N<sub>2</sub> (D), H<sub>2</sub> (D), Ar (D) and NH<sub>3</sub> (F).

The full scheme of the system used for the ammonia decomposition is shown in Figure 4.4. All the elements above described are represented there, as well as the mass spectrometer.

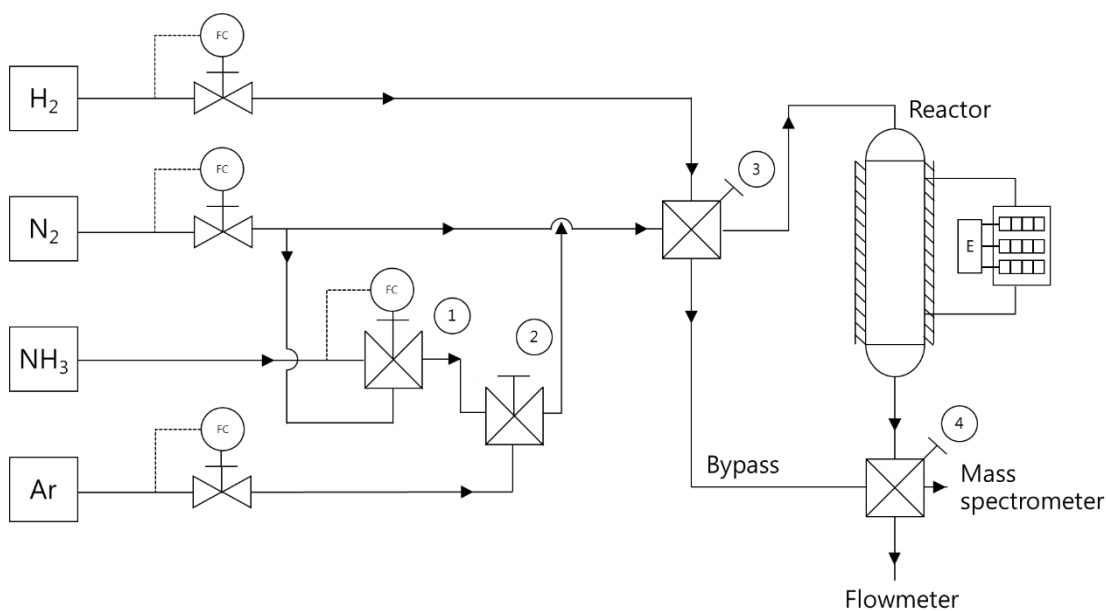


Figure 4.4. Process flow diagram of the system for the ammonia decomposition. The numbers are used to indicate which gas flows through the pipelines in the next sections (own elaboration).

#### 4.2.1. Phases of the process

The experiment can be divided in three phases: the preparation of the reactor and the system, the activation of the catalyst and the reaction at different temperature.

##### 4.2.1.1. *Previous preparation*

Prior to the reaction, the catalyst and the reactor must be prepared. All the samples prepared had 0.1 g of catalyst. Moreover, to have 45 cm<sup>3</sup> occupying the middle, the catalyst was mixed with SiC (see **Annex 3**, Figure 10.1(c)). Then, it was placed in the middle of the reactor and secured in that position by glass wool fibres on each side. This was to ensure that the temperature of the furnace was the same as the catalyst received as well as good mass transfer.

Once the reactor was prepared, it was assembled in the pipeline inside the furnace (Figure 4.3). Before starting the process, the flows of the different gases should be measured to check if there was any leakage on the system or some problems with the sources of the gases.

##### 4.2.1.2. *Activation*

The first step to decompose ammonia was to activate the catalyst. The active sites needed to be in a metallic form and that was achieved by reducing the Ni and Ru compounds. During an hour at 300° C, the catalyst underwent the activation with a flow of 80 mL·min<sup>-1</sup> of H<sub>2</sub> (10%) and N<sub>2</sub> (90%).

Referred to Figure 4.4, the mass flows for the NH<sub>3</sub> and the Ar were closed, hence, through the valves 1 and 2 did not flow any gas. The valve 3 allowed H<sub>2</sub> and N<sub>2</sub> to flow through the reactor. The valve 4 redirected the gases from the reactor to the flowmeter.

#### 4.2.1.3. Reaction

Once the catalyst was activated, the decomposition of  $\text{NH}_3$  can be performed. The reaction was done from 350 to 600 °C, with a 50 °C step, for about 30-45 minutes at each temperature. The reactants were  $\text{NH}_3$  and Ar, with a flow of  $25 \text{ mL} \cdot \text{min}^{-1}$  (ratio of  $\text{Ar}:\text{NH}_3 = 1.2:1$ ) and a gas hourly space velocity (GHSV) of  $3333 \text{ h}^{-1}$ .

Referencing Figure 4.4, through the valve 1, flowed  $\text{NH}_3$ , which was directed to the valve 2. The flow of Ar and  $\text{NH}_3$  reached the valve 3 and went into the reactor. The valve 4 redirected the products of the reaction into the mass spectrometer, where the composition was analysed. The information obtained was used to calculate the ammonia conversion at the different temperatures, by:

$$\% \text{NH}_3 \text{ conversion } (T) = 100 \cdot \frac{(\text{NH}_3 \text{out } (T) - \text{NH}_3 \text{in})}{\text{NH}_3 \text{in}} \quad (12)$$

### 4.3. Characterisation techniques: Raman spectroscopy

Some of the samples analysed were characterised by Raman spectroscopy (further explained its mechanisms in **Annex 6**). The aim was to determine the chemical composition, as well as particular variations of the bimetallic samples (NiRu-b, Ru-Ni-b and Ni-Ru-b) before (fresh) and after the reaction. Apart Ni-IWI, Ru-IWI, Ni-D-10, Ru-400-10 were analysed too, to allow a base reference for the study of the bimetallic catalysts. The measurements were performed on the Confocal Raman Microscope inVia™ Qontor® from Renishaw (see Figure 4.5). It is equipped with an optical microscope Leica DM2700M, with magnifications of 5X, 10X, 20X and 50X. Through this last one, the laser ( $532.1 \pm 0.3 \text{ nm}$ ) is focused on a spot of the sample to study, at 5% of its power (total nominal power of 100 mW), during exposition times of 0.5 s for 12 to 36 repetitions (depending on the signal-to-noise ratio).



Figure 4.5. Image of the Confocal Raman Microscope inVia™ Qontor® from Renishaw (own elaboration).

It is worth to note that not all the catalysts presented in Table 4.2 were analysed in terms of decomposing ammonia, nor in Raman spectroscopy (as already mentioned). Thus, in Table 4.4, there is specified which of the samples were analysed as the described methods. Moreover, the repeated catalysts are highlighted and the period of time between their replications. The reason for these was to assure the reproducibility of the experiments.

*Table 4.4. Identification of the catalysts analysed and repeated in this study. The cells marked in green indicate those samples that were analysed by the methodology explained and in red the ones that not.*

Name	Ammonia decomposition	Repetitions of ammonia decomposition	Time between repetitions (months)	Raman spectroscopy
Ni-D-10			4 months	
Ni-W-0.5			4 months	
Ni-IWI			-	
Ni-W-0.1			-	
Ni-W-1			4 months	
Ni-E-0.1			-	
Ni-E-1			2 months	
Ni-E-0.5			2 months	
Ni-D-20			-	
Ru-Ni-s			-	
Ni-Ru-s			-	
NiRu-s			-	
NiRu-b			-	
Ru-Ni-b			-	
Ni-Ru-b			-	
Ni(10)-Ru(5)-b			-	
Ru-400-10			-	
Ru-400-30			-	
Ru-400-5			-	
Ru-100-5			-	
Ru-800-5			-	
Ru-IWI			-	

## 5. Results

### 5.1. Ammonia decomposition analysis

The catalysts presented in Table 4.4 were analysed by applying the methodology explained (see **Methodology**). Firstly, the decomposition of ammonia was analysed. In **Annex 5** are displayed the data of the conversion values of ammonia of all the catalyst analysed (see Table 10.3). Some of the most representative are depicted in Figure 5.1, where the typical conversion curve was exhibited by this samples presented, but also by all the catalysts analysed. The tipping point ranged from 350 °C (Ru-400-5) to 450 °C (Ni-D-10). That allowed to reach full ammonia conversion, for all the samples studied, at a temperature of 550° C, whereas the reaction, without catalyst or only with the support, was far less efficient at the same temperature (see **Annex 5**).

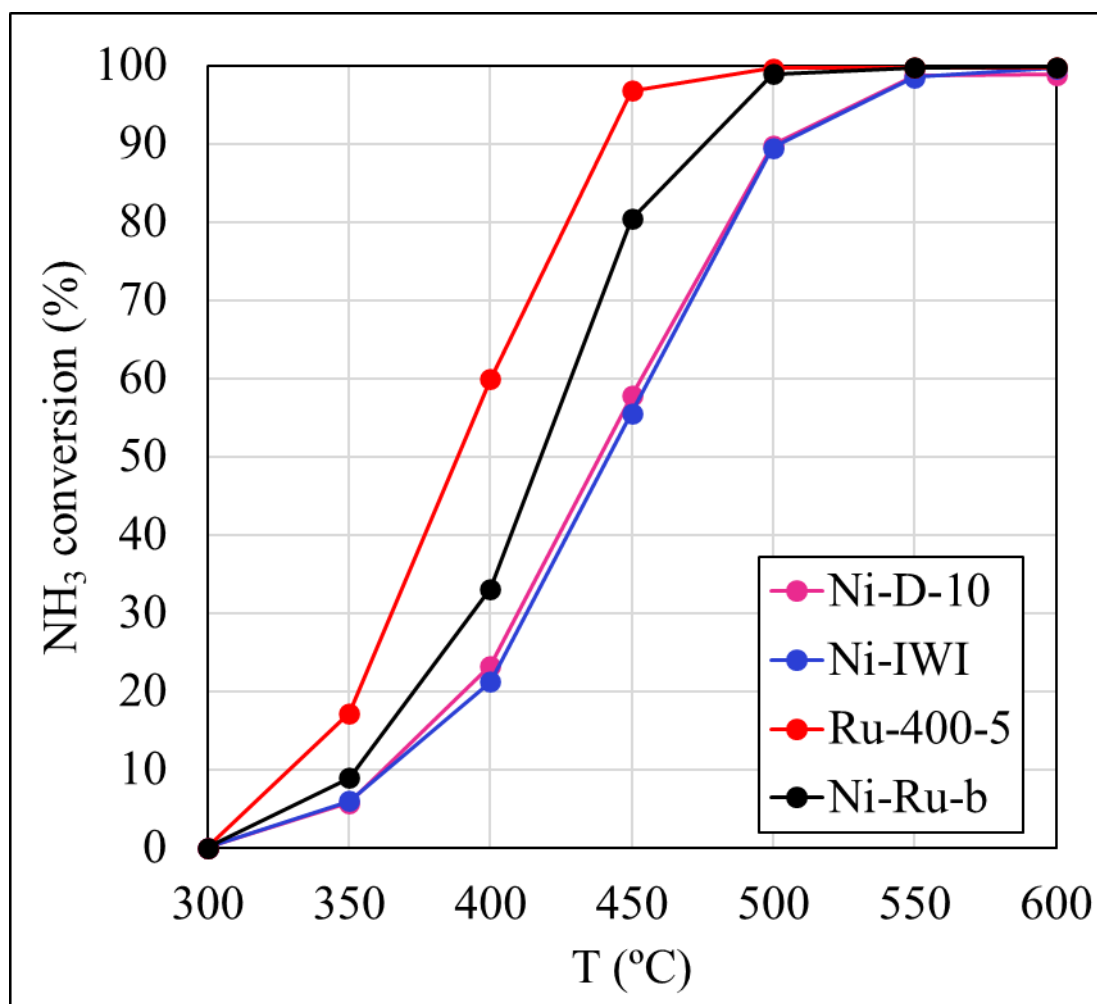


Figure 5.1. Ammonia conversion at different temperatures for Ni-D-10 (dry conditions and milled during 10 min), Ni-IWI (prepared with IWI), Ru-400-5 (milled at 400 rpm, during 5 min) and Ni-Ru-b (5% Ni, addition of Ni first and milling Ni for 10 min, and Ru for 5 min).

In order to facilitate the compression of the following results on ammonia decomposition, they will be depicted at a reference temperature of 450° C because it is where the samples presented

significantly different values. Then, for some of the bimetallic catalysts a Raman spectroscopy was performed.

### 5.1.1. Nickel catalysts

The first sets of measurements corresponded to Ni samples. The aim was to find the optimal conditions to then, be applied to the bimetallic catalysts. In Figure 5.2, the final measurements of Ni catalysts are shown at the representative temperature of 450 °C.

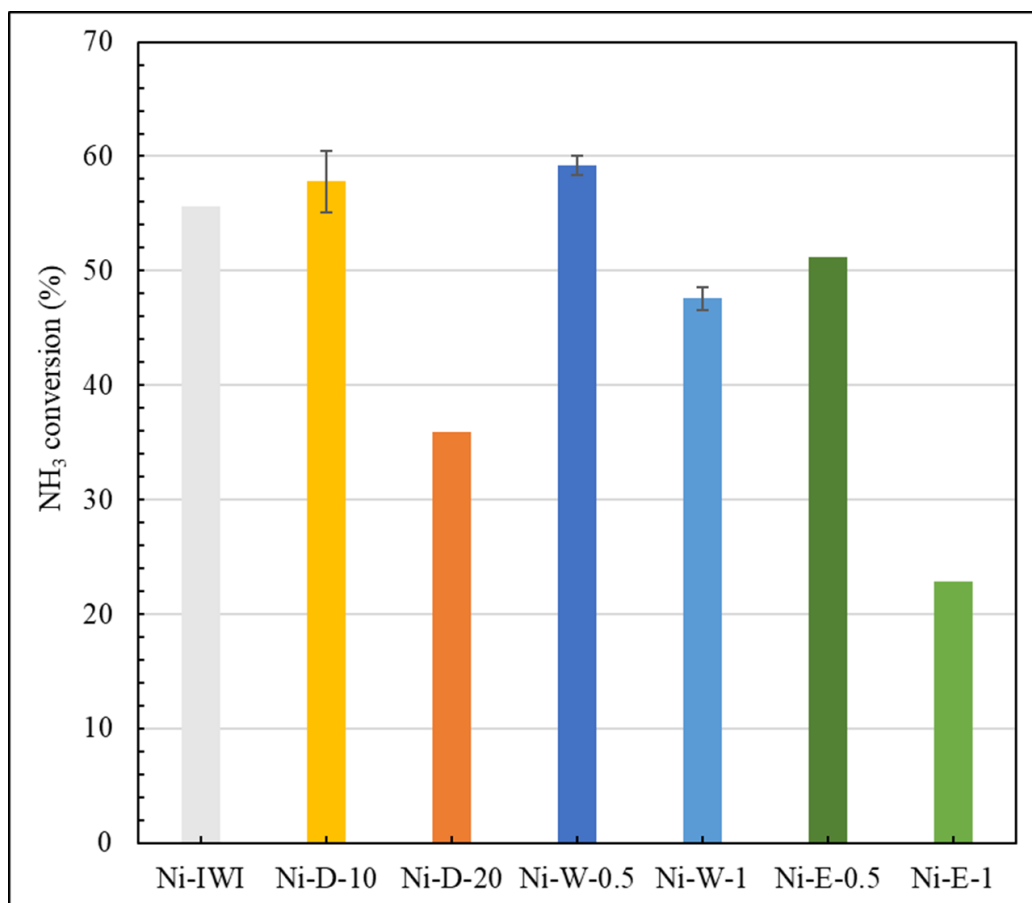


Figure 5.2. Ammonia conversion for Ni catalysts, at 450 °C (Ni-D-X indicates the dry samples and the milling time (X); Ni-W-Y, the addition of water (W) and their amount (Y) and Ni-E-Z, the addition of ethanol (E) and their amount (Z)). The error bars indicate the range of variation of some conversion values of the samples.

The Ni catalysts presented the following tendency: Ni-D-10 ~ Ni-W-0.5 > Ni-IWI > Ni-E-0.5 ~ Ni-W-1 > Ni-D-20 > Ni-E-1. The better performing catalysts were the Ni-D-10 and Ni-W-0.5, which both were prepared with BM, but the latter had 0.5 mL water added. Ni-E-0.5 was prepared with 0.5 mL ethanol, Ni-W-1 with 1 mL water and Ni-E-1 with 1 mL ethanol. Ni-D-20 was performed under different conditions than the rest. It was grinded during 20 min, whereas the others, 10 min.

It can be extracted from Figure 5.2, that the addition of 1 mL of liquid (ethanol or water) worsened the conversion of ammonia. However, while for the addition of less quantity of ethanol (0.5 mL) did not improve the results obtained for Ni-D-10, it did slightly enhance Ni-W-0.5 by adding 0.5



mL water. In addition, dry ball milling (Ni-D-10) appeared to be a better technique than IWI (Ni-IWI), for the catalyst studied. Moreover, it was verified, that the BM conditions of Ni-D-10 were better than the ones chosen for Ni-D-20. Therefore, in terms of ammonia converted, grinding time and quantity of liquid added did affect.

#### 5.1.1.1. Ethanol nickel catalysts

The wet BM samples shown in Figure 5.2 were the last repetitions obtained, at the reference temperature of 450 °C. Ni-E-1 and Ni-E-0.5 were repeated with a two-month difference under the same conditions, obtaining two different results (see Figure 5.3). The first outcome from Ni-E-1 exhibited higher ammonia conversion values. However, after two-month, the values were approximately 40% lower, as can be seen in Figure 5.3. In the case of Ni-E-0.5, the decrease in the conversion is not as low as for Ni-E-1, but still significant, with a reduction of almost 10% at 450 °C (see Figure 5.3). Therefore, catalysts prepared with ethanol presented an evolution over time, as they did not remain stable, and deteriorated.

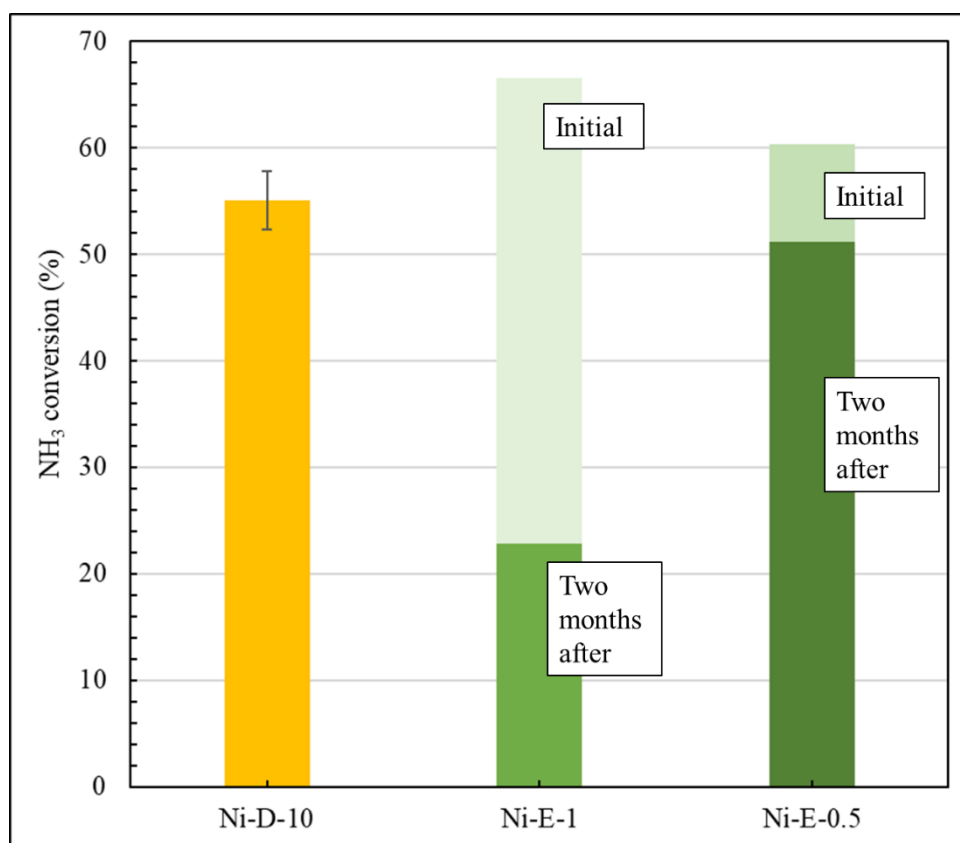


Figure 5.3. Evolution over time of Ni-E-1 (ethanol, 1 mL) and Ni-E-0.5 (ethanol 0.5 mL), compared to Ni-D-10 (dry conditions, milled for 10 min), at 450 °C. The error bars indicate the range of variation of some conversion values of the samples.

#### 5.1.2. Nickel and ruthenium catalysts

As seen in the **Methodology**, six different samples were prepared with two different Ni and Ru ratio, and for each, a different order of addition was used. In Figure 5.4 the results obtained are

presented. First, it should be pointed out that the samples prepared with 0.5% and 2.5% Ru and Ni, respectively, were not fully analysed. In Figure 5.4 the results for Ni-Ru-s are represented. This, compared to the samples with 1% and 5% Ru and Ni, respectively, presented low values, only slightly over the conversion for Ni-D-10, a 450 °C. Therefore, it was found unnecessary to keep analysing the rest of the samples.

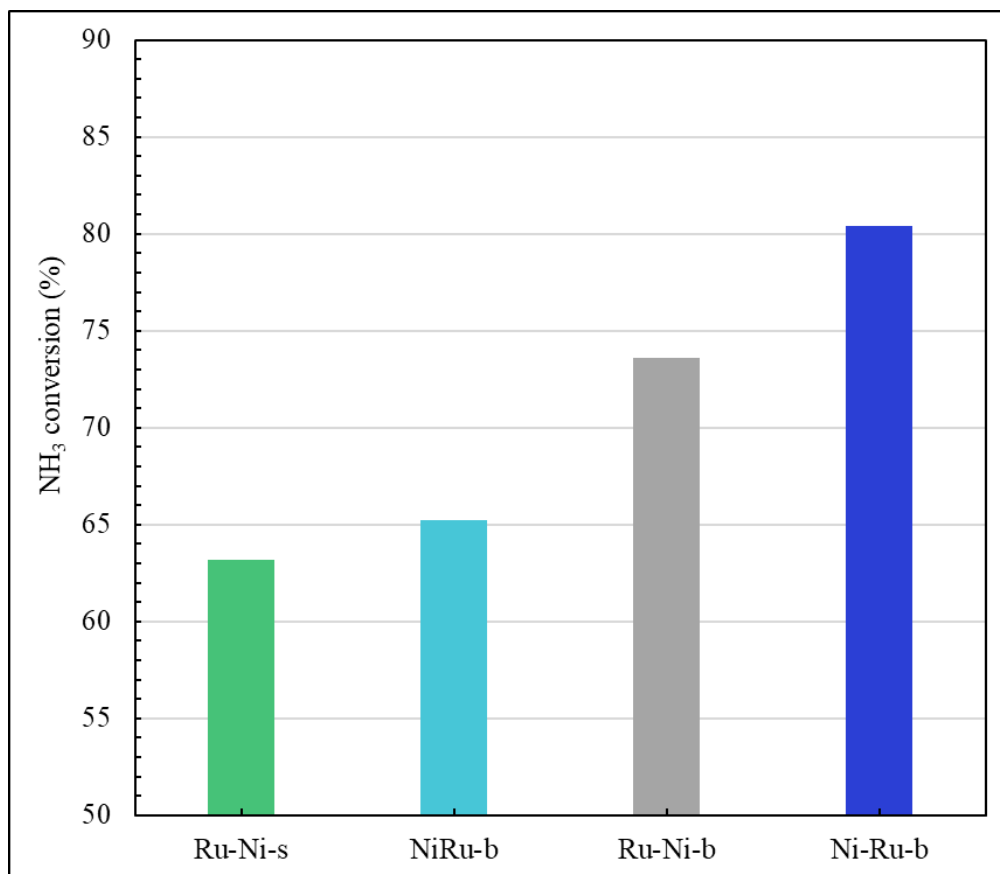


Figure 5.4. Ammonia conversion for bimetallic catalysts at 450 °C (-b, and -s for 5% Ni and 2.5% Ni, respectively, and Ru-Ni indicates that the first addition to the milling was Ru; Ni-Ru, was Ni and NiRu, were both added at the same time).

In Figure 5.4, it is shown how all the other catalysts performed better than Ni-D-10 and Ni-IWI. In addition, the bimetallic catalysts, presented in Figure 5.4 at 450 °C, showed significantly different conversion values regarding the sequence of addition. In terms of the performance in ammonia decomposition: Ni-Ru-b > Ru-Ni-b > NiRu-b. Ni-Ru-b was prepared by adding Ni first, then Ru; for Ru-Ni-b, Ru was added first; and for NiRu-b, both metals at the same time. So, as it is shown, the order of addition in bimetallic BM samples did change the conversion values obtained.

### 5.1.3. Ruthenium catalysts

In Figure 5.5 the results obtained from a small-scale study about the optimal parameters in BM for Ru catalyst are shown.

The conversion curves obtained for the Ru catalysts have higher values than the Ni catalysts (see **Annex 5**) as their tipping point occurs at lower temperatures (between 350 °C-400 °C). These results are in accordance with the volcano type graph for ammonia decomposition in Figure 3.3, where it showed that Ru is the best element for this reaction (see **State of art**).

At 400 rpm, as seen in Figure 5.5 (a), better performing catalysts were prepared with less grinding times (5 and 10 min), whereas the sample with 30 min did worse than the others. Moreover, compared to Ru-IWI (reference), Ru-400-5 and Ru-400-10 had higher conversion values. As both had similar results (considering that the mass spectrometer has an estimated error of  $\pm 5\%$ ), it was assumed that the optimal grinding time was 5 min. Thus, in order to analyse different speeds, the catalysts in Figure 5.5 (b) were prepared at 5 min milling time. Ru-400-5 was the catalyst that presented better ammonia conversion. In fact, the other speeds tested did not improve the conversion.

As a consequence, grinding time and speed affected Ru catalysts prepared by BM. Moreover, it appeared short grinding times (5, 10 min) favour the performance of the samples. For the speed, 400 rpm seemed to be an optimal value. Then, the data suggested that the ideal conditions to prepare Ru by BM was with a speed of 400 rpm during 5 min.

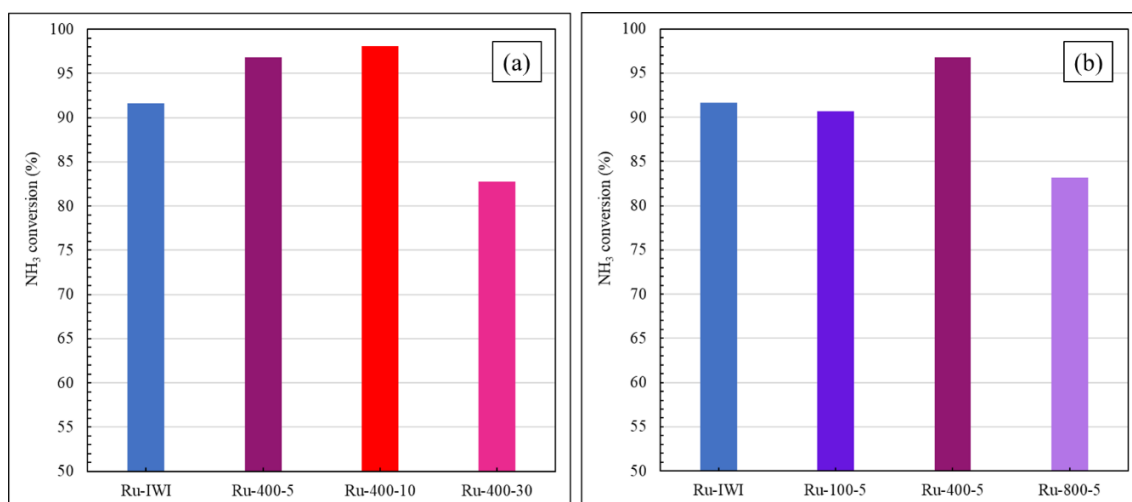


Figure 5.5. Ammonia conversion of Ru catalysts, at 450 °C a) at the same speed but different grinding time and b) at different speed but same grinding time (Ru-X-Y, where indicates X and Y indicate the speed and the duration of the milling).

#### 5.1.4. Final catalysts

A new catalyst was prepared with the conditions found to be the best amongst the different options. The results can be seen in Figure 5.6, as well as Ni-D-10, Ru-400-5 and Ni-Ru-b for comparison.

According to the best parameters found for both Ni (400 rpm, 10 min) and Ru (400 rpm, 5 min), plus firstly adding Ni (see **Nickel and ruthenium**), a new catalyst (Ni10-Ru5-b) was prepared and compared with Ni-Ru-b, which had shown, until now, the best results.

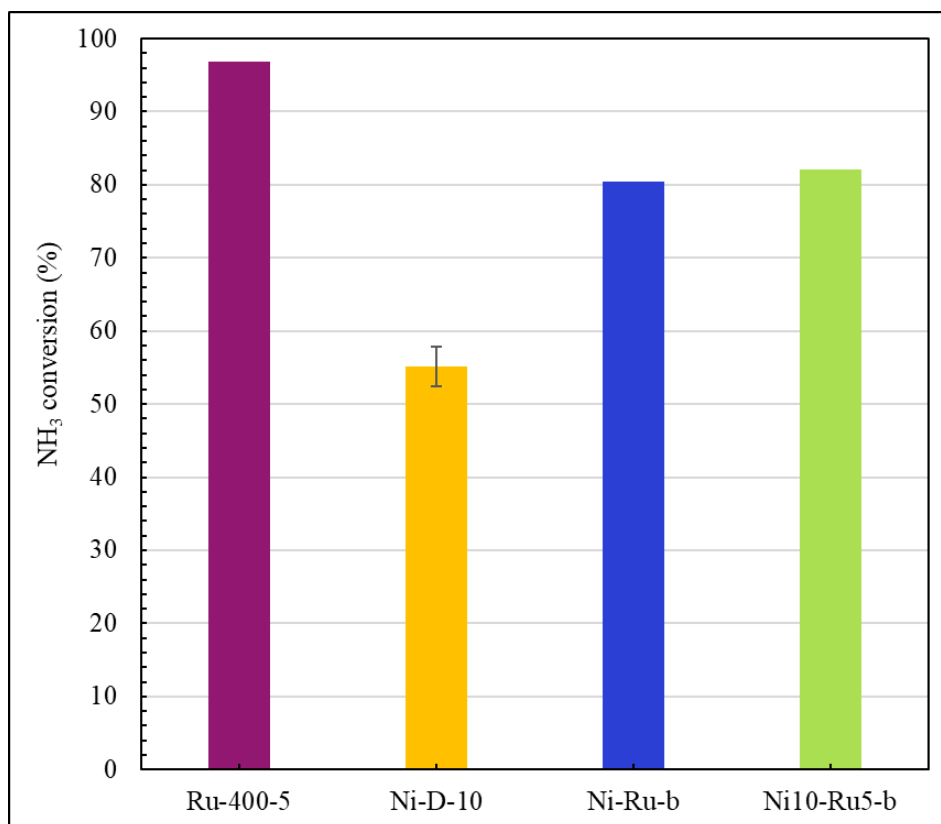


Figure 5.6. Ammonia conversion, at 450 °C, for Ru-400-5 (milled at 400 rpm during 5 min), Ni-D-10 (dry conditions and milled during 10 min), Ni-Ru-b (5% Ni, addition of Ni first) and Ni10-Ru5-b (5% Ni, addition of Ni first and milling Ni for 10 min and Ru for 5 min). The error bars indicate the range of variation of some conversion values of the samples.

Ni10-Ru5-b had a similar behaviour to Ni-Ru-b, although being prepared under different conditions. Both presented intermediate values between Ru-400-5 and Ni-D-10. Bimetallic catalysts represented an improvement with respect of Ni catalyst but not for Ru catalysts. Therefore, regarding Ru catalysts, and addition of 5% Ni in the bimetallic catalysts prepared by BM did not improve their conversion rates.

## 5.2. Characterisation: Raman spectroscopy

After performing the analysis of the ammonia decomposition of the catalysts specified in Table 4.4, a smaller group of samples were studied with a Raman spectrometer. These were: NiRu-b, Ru-Ni-b and Ni-Ru-b before (fresh) and after reaction. For a complete analysis Ni-D-10, Ru-400-10, Ni-IWI and Ru-IWI, also before and after reaction, were done as well. In Table 5.1, it is presented the legend used to identify the species exhibited in the spectra obtained. It is worth to note that to facilitate the compression of these data, it will not be depicted the single spectra of each samples. Therefore, for more detail on the peaks, see **Annex 6**.

Table 5.1. Legend of the symbols used to identify the species and their characteristic Raman shift values.








Species	Symbol	Raman shift (cm <sup>-1</sup> )	Reference
NiO		500 906 1090 1490	(Mironova-Ulmane <i>et al.</i> , 2007)
Ni(OH) <sub>2</sub>		315 450 880	(Murli <i>et al.</i> , 2001)
Ni(NO <sub>3</sub> ) <sub>2</sub>		741 1050	(Vasilchenko <i>et al.</i> , 2020)
CeO <sub>2</sub>		465 600 257 1170	(Loridant, 2020)
RuO <sub>2</sub>		528 646 716	(Huang and Liao, 1998)
Ru-Ce-O		694 968	(He <i>et al.</i> , 2019)
RuCl <sub>3</sub>		155 210 260 396 503	(Li <i>et al.</i> , 2019)

Figure 5.7 depicts the Raman spectra obtained for two different spots (1 and 2) of the sample NiRu-b fresh. To compare ceria, Ni-D-10 and Ru-400-10 were shown as well. For ceria it can be seen the most intense peak (at 465 cm<sup>-1</sup>) followed by less intense peaks at 257 cm<sup>-1</sup>, 600 cm<sup>-1</sup> and 1170 cm<sup>-1</sup>. It should be mentioned that the peak at 600 cm<sup>-1</sup> represents the characteristic oxygen vacancies or defects of ceria. Ni-D-10 fresh catalyst showed peaks at similar Raman shifts as ceria (249 cm<sup>-1</sup>, 462 cm<sup>-1</sup>, 600 cm<sup>-1</sup>) as well as peaks belonging to Ni(NO<sub>3</sub>)<sub>2</sub> signal (741 cm<sup>-1</sup> and 1051 cm<sup>-1</sup>). Ru-400-10 also presented peaks at similar shifts as ceria (237 cm<sup>-1</sup>, 450 cm<sup>-1</sup>, 589 cm<sup>-1</sup> and 1171 cm<sup>-1</sup>). Moreover, other peaks appeared in this spectrum, corresponding to the bond Ru-Ce-O (690 cm<sup>-1</sup> and 969 cm<sup>-1</sup>).

Regarding the bimetallic catalyst (NiRu-b) at two separate spots, different peaks were recorded. Both positions presented some of the characteristic peaks of ceria, slightly shifted from single

ceria sample and between them. For NiRu-b (1) they were at  $460\text{ cm}^{-1}$  and  $1181\text{ cm}^{-1}$ , and for NiRu-b (2) at  $209\text{ cm}^{-1}$ ,  $453\text{ cm}^{-1}$ ,  $600\text{ cm}^{-1}$  and  $1183\text{ cm}^{-1}$ . Then, each spot had different compositions as it can be seen from the difference in peaks shown in Figure 5.7. On one hand NiRu-b (1) presented peaks corresponding to  $\text{Ni}(\text{OH})_2$  ( $328\text{ cm}^{-1}$  and  $894\text{ cm}^{-1}$ ),  $\text{RuO}_2$  ( $506\text{ cm}^{-1}$  and  $654\text{ cm}^{-1}$ ),  $\text{NiO}$  ( $483\text{ cm}^{-1}$ ) and  $\text{Ni}(\text{NO}_3)_2$  ( $742\text{ cm}^{-1}$  and  $1050\text{ cm}^{-1}$ ). On the other hand, NiRu-b (2) did not exhibit any of the signals mentioned before, except for Ru-Ce-O ( $976\text{ cm}^{-1}$ ).

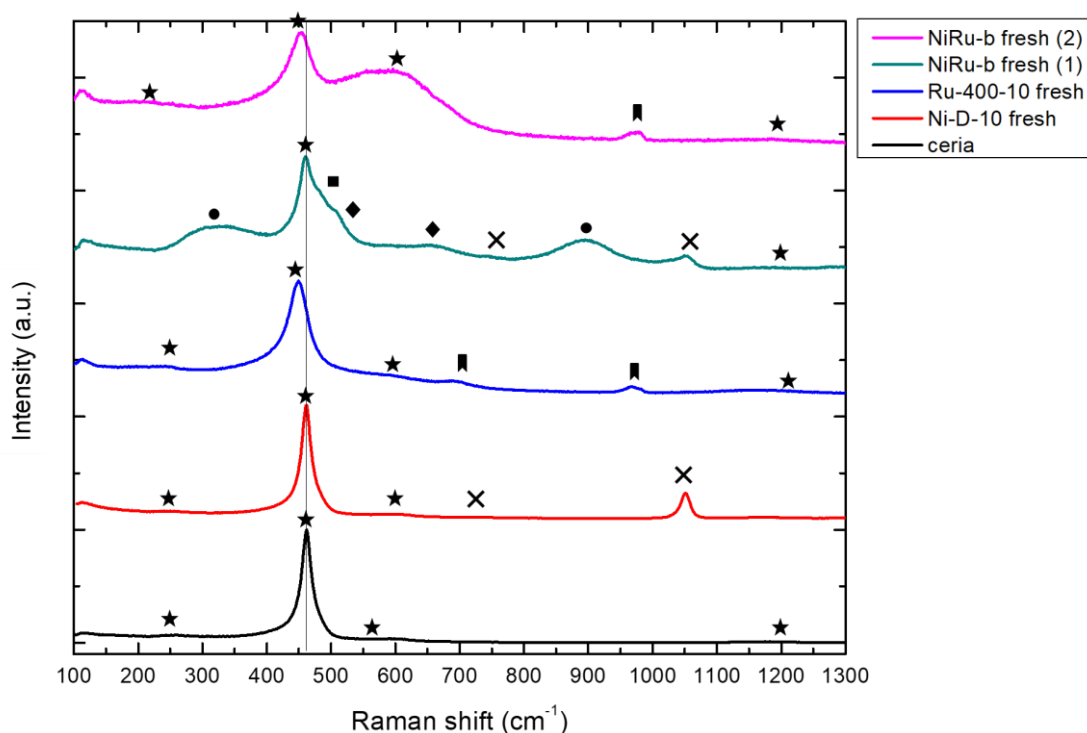


Figure 5.7. Raman spectra of ceria, Ni-D-10, Ru-400-10, and NiRu-b (1 and 2), before reaction.

The next sample analysed was Ru-Ni-b, as shown in Figure 5.8. Similar to Figure 5.7, Ni-D-10, Ru-400-10 and ceria are displayed for comparison. In this case, two separate spots exhibited alike compositions, showing peaks corresponding to ceria at  $211\text{ cm}^{-1}$ ,  $453\text{ cm}^{-1}$ ,  $576\text{ cm}^{-1}$  and  $1159\text{ cm}^{-1}$  for Ru-Ni-b (1) and  $221\text{ cm}^{-1}$ ,  $446\text{ cm}^{-1}$ ,  $573\text{ cm}^{-1}$  and  $1168\text{ cm}^{-1}$  for Ru-Ni-b (2). Moreover, the Raman spectra of both positions depicted the presence of Ru-Ce-O at  $973\text{ cm}^{-1}$  and  $968\text{ cm}^{-1}$ , for Ru-Ni (1) and (2), respectively. It is worth to note that Ru-Ni-b (1) presented relatively more intense peaks than Ru-Ni-b (2), thus exhibiting a more prominent presence of Ru-Ce-O and at the defects peak of ceria. No peak from a Ni species was recorded.

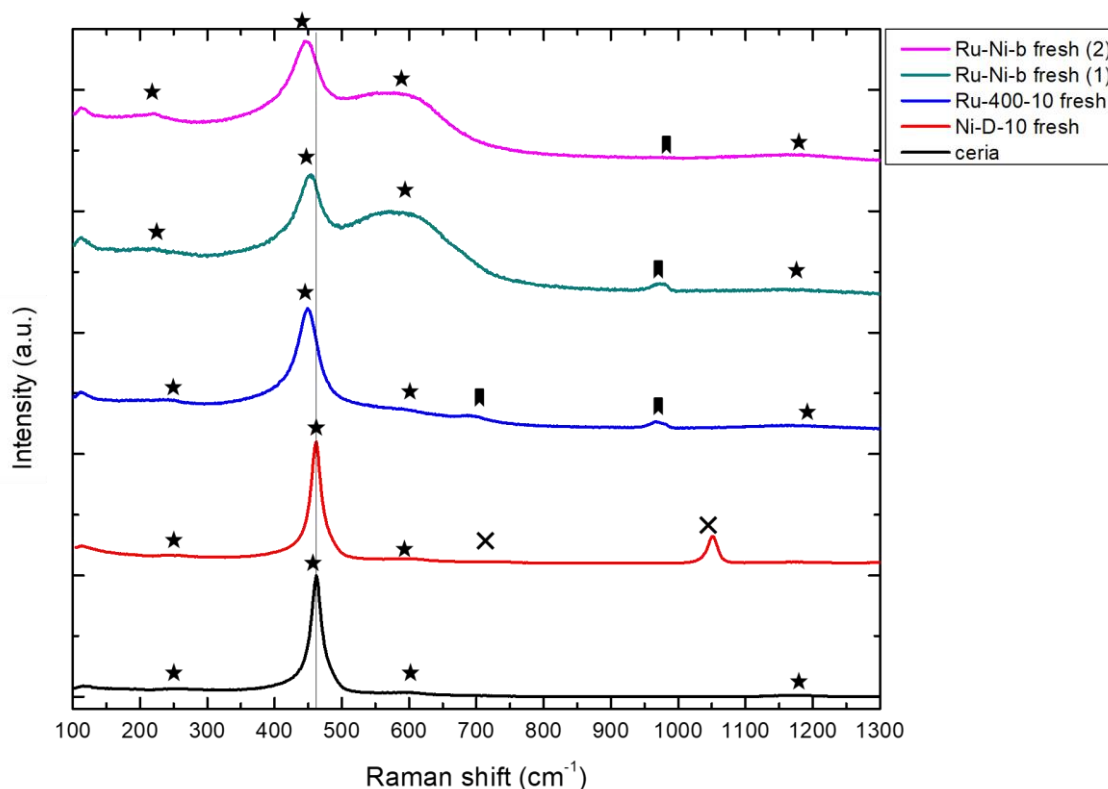


Figure 5.8. Raman spectra of ceria, Ni-D-10, Ru-400-10, and Ru-Ni-b (1 and 2), before reaction.

The last fresh bimetallic catalyst analysed was Ni-Ru-b. In Figure 5.9 are depicted the spectra, as well as Ni-D-10, Ru-400-10 and ceria, for comparison. Three different spots were recorded and, all of them showed a singular composition. Ni-Ru-b (1) presented peaks from Ni(OH)<sub>2</sub> (316 cm<sup>-1</sup> and 888 cm<sup>-1</sup>), ceria (459 cm<sup>-1</sup> and 603 cm<sup>-1</sup>), NiO (480 cm<sup>-1</sup>) and Ru-Ce-O (698 cm<sup>-1</sup> and 991 cm<sup>-1</sup>). For Ni-Ru-b (2) there were no peaks belonging to Ni species, only corresponding to ceria (221 cm<sup>-1</sup>, 452 cm<sup>-1</sup>, 572 cm<sup>-1</sup> and 1160 cm<sup>-1</sup>) and Ru-Ce-O (975 cm<sup>-1</sup>). The last spot recorded (Ni-Ru-b (3)) had also a high presence of Ru species but showed as well, the presence of Ni, although not as significant as Ni-Ru-b (1). In this case, ceria peaks were found at 459 cm<sup>-1</sup> and 609 cm<sup>-1</sup>, while RuO<sub>2</sub> appeared at 532 cm<sup>-1</sup> and Ru-Ce-O at 992 cm<sup>-1</sup>. Because of the presence of these last two peaks, the one at 707 cm<sup>-1</sup> could belong to any of these two. The presence of Ni(NO<sub>3</sub>)<sub>2</sub> was noted at 1053 cm<sup>-1</sup>. It was noteworthy to mention that Ni-Ru-b (2) had the highest relatively intense peak from the defects of the ceria.

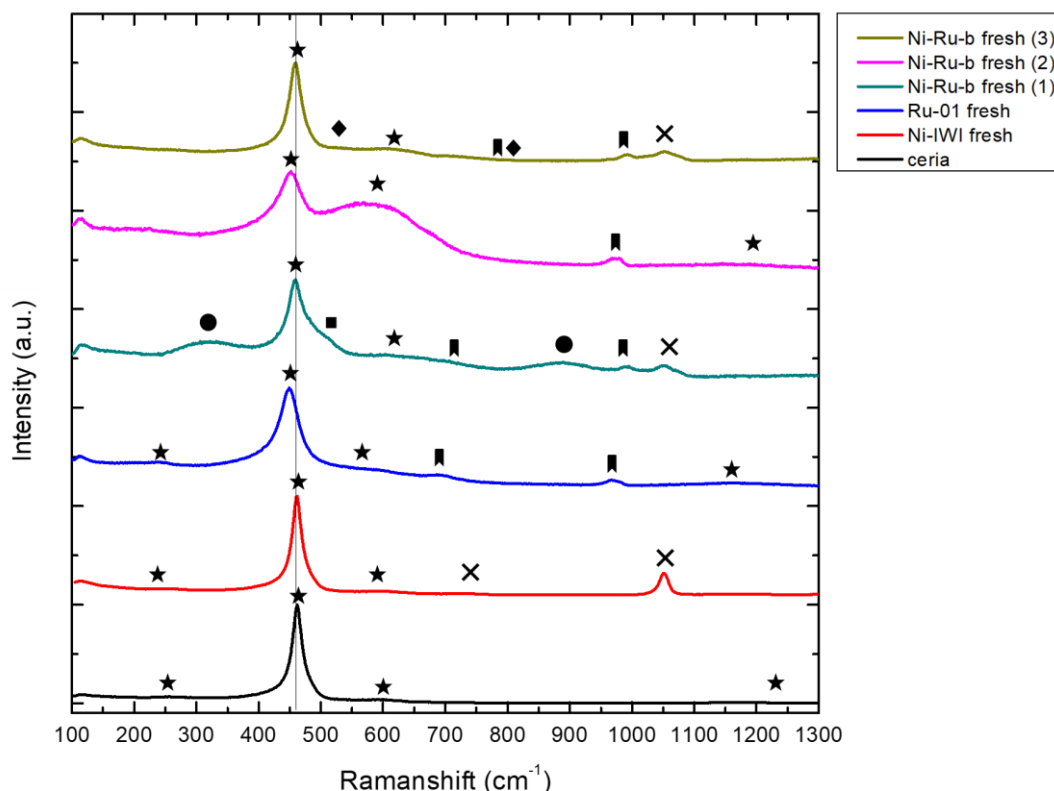


Figure 5.9. Raman spectra of ceria, Ni-D-10, Ru-400-10, and Ni-Ru-b (1, 2 and 3), before reaction.

Regarding the analysis of the samples after reaction, it would only be showed the most representative out of the three bimetallic. The reason was because they present the same peaks and composition, with slightly different features. In Figure 5.10 there is exhibited the spectra of ceria, Ni-D-10 (after reaction), Ru-400-10 (after rection) and NiRu-b (after reaction).

In this case, Ni-D-10 after reaction presented peaks from ceria ( $221\text{ cm}^{-1}$ ,  $455\text{ cm}^{-1}$ ,  $570\text{ cm}^{-1}$ ,  $771\text{ cm}^{-1}$  and  $1173\text{ cm}^{-1}$ ) and NiO ( $771\text{ cm}^{-1}$ ). Ru-400-10 after reaction had, apart from ceria peaks ( $237\text{ cm}^{-1}$ ,  $450\text{ cm}^{-1}$ ,  $591\text{ cm}^{-1}$  and  $1162\text{ cm}^{-1}$ ), presence of oxide species, Ru-Ce-O at  $968\text{ cm}^{-1}$ , like for Ni-D-10.

NiRu-b after reaction depicted peaks from ceria ( $239\text{ cm}^{-1}$ ,  $457\text{ cm}^{-1}$ ,  $580\text{ cm}^{-1}$  and  $1164\text{ cm}^{-1}$ ), and Ru-Ce-O ( $970\text{ cm}^{-1}$ ). None of the bimetallic samples after reaction exhibited peaks from Ni species. However, as NiO has its characteristic peak at shifts around  $500\text{ cm}^{-1}$ , it could be shadowed by the wide band corresponding to ceria defects.

Comparing NiRu-b to Ni-Ru-b (see Figure 10.17), there were no differences between both spectra, because they presented the same peaks, although the presence of Ru-Ce-O could be stronger in NiRu-b than in Ni-Ru-b. Moreover, Ru-Ni-b had the same peaks but an even stronger presence of Ru-Ce-O, thus it appeared the second peak at  $766\text{ cm}^{-1}$  (see Figure 10.15).



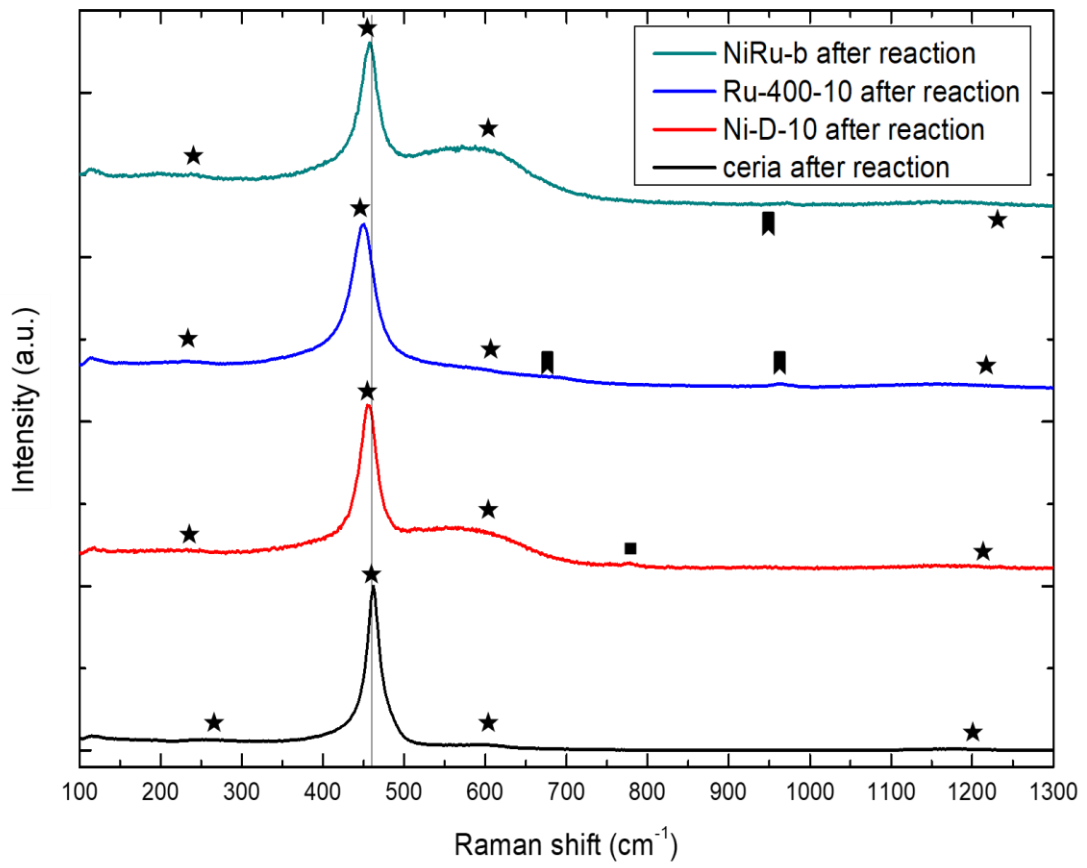


Figure 5.10. Raman spectra of ceria, Ni-D-10, Ru-400-10, and NiRu-b, after reaction.

## 6. Discussion

In the literature there is a wide range of catalysts for the decomposition of ammonia prepared under different conditions, techniques, supports and metallic concentrations, to name a few (Lucentini *et al.*, 2021b). To illustrate that, there are three tables in **Annex 7**, **Annex 8** and **Annex 9** with some representative mono- and bimetallic catalysts.

It is worth to note that the values presented have been, sometimes, analysed under different conditions. Moreover, in this study it has been specified how the ammonia conversion has been calculated (see Eq. 12), whereas in most of the publications have not clearly stated how. However, for the sake of the discussion, they will be assumed as comparable, and some outcomes will be extracted.

Regarding Ni catalysts (**Annex 7**) found in the literature, they exhibit low conversion values for ammonia decomposition, even at higher temperatures, whereas the outcomes of this study are higher. This is remarkable when considering the amount of Ni used in this work in contrast with the literature: a 5% Ni was applied for each catalyst, whereas, they mostly use more than 10% (Chellappa, Fischer and Thomson, 2002; Yin *et al.*, 2004a; Li *et al.*, 2005; Liu *et al.*, 2008; Choudhary, Sivadinarayana and Goodman, 2009; Makepeace *et al.*, 2015; Bell and Torrente-Murciano, 2016b; Okura *et al.*, 2016; Lucentini, Casanovas and Llorca, 2019; Lucentini, *et al.*, 2021b). Assuming that the different reaction conditions performed had no significant effect in the outcomes in the literature, it seems that as support, ceria might improve catalyst's performance, as Lucentini *et al.* (Lucentini, Casanovas and Llorca, 2019) had already stated in their comparison with Al<sub>2</sub>O<sub>3</sub>. Moreover, even at higher Ni concentration, different supports did not obtain values as high as Ni/CeO<sub>2</sub>.

Similar to the comparison between Ni catalysts, the Ru samples of this study exhibit better performance than the rest of Ru catalysts, some of them are presented in **Annex 8**. However, there are three studies of Ru catalysts that show better ammonia conversion values than the results obtained in this work (Lucentini, Casanovas and Llorca, 2019; McCullough *et al.*, 2020; Pinzón *et al.*, 2021). Firstly, Lucentini *et al.* (Lucentini, Casanovas and Llorca, 2019) used the same support and conditions as this study, but with 2% Ru instead of 1% (see **Methodology**). As less of the metallic element is added, less ammonia is converted, as seen in Ni-Ru-s, compared to the other bimetallic samples. The second example is the publication of Pinzón *et al.* (Pinzón *et al.*, 2021), where they use a different support and a higher Ru content. Therefore, as more Ru is available, more products could be obtained. For the last case with better performing results, McCullough *et al.* (McCullough *et al.*, 2020) have used 1% Ru over SBA 200- $\gamma$ -Al<sub>2</sub>O<sub>3</sub>. As the support in this work is promoted with potassium (12%), that could have enhanced the performance of the catalyst (McCullough *et al.*, 2020). Therefore, increasing the amount of Ru or promoting

the support might increase the results obtained in this work. Nevertheless, ceria as a support for Ru catalysts is still a suitable choice.

As for the comparison between the bimetallic catalysts, this study had higher conversion values in general. Similar reasoning to the previous discussion, it appears that ceria might be a suitable candidate as support of bimetallic catalyst for ammonia decomposition. There is only one of the examples presented in **Annex 9** with better results (Lucentini, Casanovas and Llorca, 2019). As the content of Ni and Ru in (Lucentini, Casanovas and Llorca, 2019) is 10% and 2%, respectively, they had use double concentrations than this study. Thus, as previously seen (see Nickel and ruthenium catalysts), an increase of the amount of metal used, improved the ammonia conversion. Considering the error of the mass spectrometer ( $\pm 5\%$ ), the results of Lucentini et. al. (Lucentini, Casanovas and Llorca, 2019) are only less than 10% higher than the outcomes of this study, at 450 °C. Therefore, as Ru is remarkably expensive, it is suggested that it may not be worth doubling the concentration.

### 6.1. Nickel catalyst

In this study, the different Ni/CeO<sub>2</sub> catalysts prepared under various BM conditions have shown distinct behaviours regarding ammonia conversion. As well, similar results to this study in the literature have been found. Marin et. al. (Marin, 2020) tested Ni/CeO<sub>2</sub> under different BM parameters like ball to powder ratio, speed, grinding time and ball diameter. They concluded that there is an improvement by using BM in front of IWI, which can be seen, as well, in Figure 5.2. Moreover, they suggested that the best conditions to prepare Ni catalyst by BM were at 400 rpm during 10 min. Similar results have been obtained in the current study where Ni-D-20 converted less ammonia than Ni-D-10 (see Figure 5.2). This could be explained by the results in House et. al. publication (House *et al.*, 2015). According to them, as the grinding time increased, the Ni particles were embedded further in the support's structure causing the appearance of intermetallic bonds, and lower efficiencies. Therefore, as the grinding time in this study went from 10 min (Ni-D-10) to 20 min (Ni-D-20), it is possible that more Ni particles were not able to be on the surface, so Ni-D-20 converted less. Further analysing the best option (Ni-D-10), the values obtained in the present work are lower compared to the same sample as Marin et. al. (Marin, 2020). They obtained values of ammonia conversion of 69% at 450 °C (approximately), while this study reached 58 ± 3% (see Figure 5.2). More investigations needed to be done to discern this rough 10% difference.

Regarding the use of ethanol in the BM preparation, publications that use Ni catalysts for ammonia decomposition have not been found. Therefore, the values in this study cannot be compared. However, there are, indeed, publications that analyse the effect of ethanol as a grinding media in BM (Kang *et al.*, 2008; Sayyah *et al.*, 2013; Kozawa, 2021). Kang et. al. (Kang *et al.*, 2008) and Kozawa (Kozawa, 2021) had found the presence of organic species derivative from the

ethanol and some carbon bonds with the support. The formers did not intervene in the processes occurring per se and, by thermal treatments they could be removed. Nevertheless, carbon bonds did affect the reaction and increased its efficiency, as the carbon acts as a doping agent and ethanol allowed to reduce particle size (Kang *et al.*, 2008). Then, it might be possible, that the initial results from Ni-E-1 and Ni-E-0.5 of this study performed better because of the presence of these bonds with ceria (see Figure 5.3).

However, after two months, Ni-E-1 and Ni-E-0.5 presented significantly lower conversion values. In fact, at 450 °C a reduction of 40% and 10%, approximately and respectively was recorded (see Figure 5.3). It is worth to note that the decrease in both samples seemed proportional to the amount of liquid used. Then, Sayyah *et. al.* (Sayyah *et al.*, 2013) exhibited in their publication, that their samples (prepared with ethanol) sintered after 50 cycles of the reaction, although they did not consider it as a major issue. That means that the catalysts' particles became bigger, and that produced a decrease in their performance. It is probable that this effect could have happened in the samples of this work (Ni-E-1 and Ni-E-0.5), even though repeated cycles of the same catalysts have not been done. Maybe, if an experiment similar to Sayyah *et. al.* (Sayyah *et al.*, 2013) would have been done, a decrease in the ammonia conversion values would be obtained.

Similar to the ethanol case, no publications were found using the same conditions as the water samples analysed in the current study. Thus, comparing our results with the literature was not possible. In the same manner, it could be explained the behaviour of Ni-W-1 and Ni-W-0.5 by adapting literature results to this study. Kozawa (Kozawa, 2021) found that water allowed the metallic species to disperse better on the surface of the support. This resulted in the reduction of the size of the particle, when compared with dry milling (Kozawa, 2021) or IWI (Zhang *et al.*, 2014) methods. That produced catalysts that could perform more efficiently. Ni-W-0.5 could have presented an improvement compared with Ni-D-10; however, when considering their error range, they have similar values. Moreover, Ni-W-1 had 10% lower conversion values than Ni-D-10, at 450 °C. Both samples were not better than Ni-D-10, which disagreed with the statement of Kozawa (Kozawa, 2021). However, as the support used in their work is Al<sub>2</sub>O<sub>3</sub>, it is suggested that the effect of water could not be as significant as expected. In their publication, Zhang *et. al.* (Zhang *et al.*, 2014) used ceria as support, and when compared to an IWI sample, they concluded that water did improve the conversion. This result agrees partially with the current study, where Ni-W-0.5 had better values than Ni-IWI, but not Ni-W-1. Nevertheless, it has to be considered that both studies did use different catalyst to liquid ratio, 3:5 (Zhang *et al.*, 2014) and 2.5:1 (Kozawa, 2021). As the present study used 1 mL and 0.5 mL, to prepare 2 g of catalysts, the effect of water could not be as significant or even the same, as previously described. In addition, as the chosen parameters of BM were analysed in dry conditions, it is proposed that adding any liquid

might change them. Thus, more analysis in regard of the effectiveness of water in BM Ni/CeO<sub>2</sub> samples needs to be conducted.

It is remarkable that Zhang *et al.* (Zhang *et al.*, 2014) states that Ni catalysts prepared by BM in the presence of water were stable after consecutive repetitions. As the error obtained for both Ni-W-1 and Ni-W-0.5 was smaller than 1%, the current study also verifies the stability of these type of catalysts over time. Furthermore, as the measurements were repeated with a time difference of 4 months, it can be assured the reproducibility and the accuracy of the experiment.

It is worth to mention that all wet samples, regardless of ethanol or water, had a different colour than dry ones. In Figure 6.1, two samples are shown: Ni-D-10 (yellowish green) and Ni-W-0.5 (apple-green). After some research in the literature, it was found that Ni(OH)<sub>2</sub> was apple green (Chen *et al.*, 1999). Therefore, as no characterisation technique was performed in these samples, that remained as a hypothesis. Moreover, it has not been found mentions of this molecule in Ni/CeO<sub>2</sub> catalysts. However, as it has been seen, the signal of this element appeared in the Raman spectra of some of the bimetallic samples analysed in the current work. It is suggested that maybe the presence of this element could potentially affect the performance of the reaction. Some publications in literature supported that the use of Ni(OH)<sub>2</sub> in their catalyst in the hydrogen evolution reaction (HER) or in the oxygen evolution reaction (OER) improved their catalytic activity (Stern and Hu, 2014; Lv *et al.*, 2020). However, regarding ammonia decomposition, further analysis should be done.

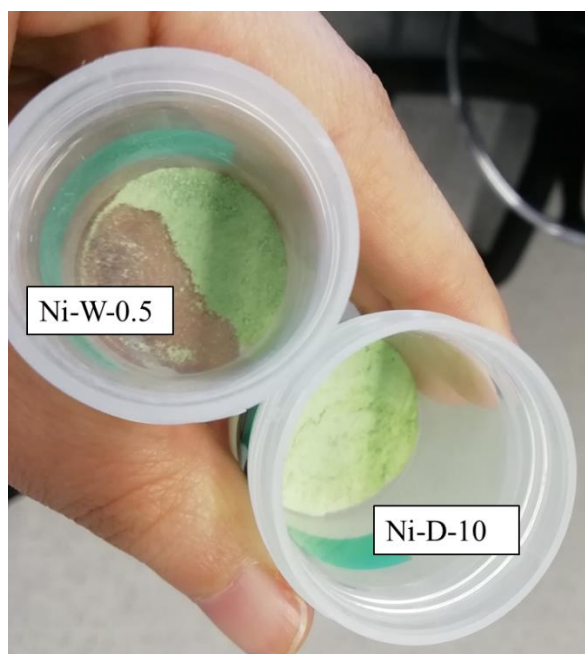


Figure 6.1. Image of Ni-W-0.5 and Ni-D-10 (own elaboration).

As a result of this discussion and comparing Ni-D-10 and Ni-W-0.5, it was chosen the former as the most optimal conditions to apply to Ni in the bimetallic catalysts. The difference between both

samples is not significant, and because the lack of studies backing the effectiveness of such amounts of water in Ni/CeO<sub>2</sub> catalysts, Ni-W-0.5 was discarded. Moreover, even if there were enough studies agreeing with the impact of small amounts of water on Ni/CeO<sub>2</sub>, there is no guarantee that these same conditions would be the same as for bimetallic catalysts using Ni. Furthermore, because Ni-D-10 needed less elements to be produced, its synthesis was more sustainable than Ni-W-0.5.

## 6.2. Ruthenium catalyst

Likewise, no publications that have studied the effect of BM parameters on Ru catalysts have been found. Therefore, the results exhibited in Figure 5.5 could not be verified. As Ru is expensive, it is not feasible to develop a large-scale catalyst.

Returning to Figure 5.5, it can be seen that there is an optimal parameter to prepare Ru with BM, that was slightly different than Ni: 400 rpm, 5 min (versus 10 min). It was shown that high milling energy was detrimental to the sample (Ru-400-30) and (Ru-800-5), as the efficiency dropped more than 13% (at 450 °C) when compared to the rest of the samples. This could be argued similarly to Ni-D-10 and Ni-D-20. As the energy increased, the metals can be further embedded in the support's structure preventing them from being an active site to perform in the reaction (House *et al.*, 2015). Applying less energy did not mean low conversion values as for the previous case. When decreasing the speed (constant time, at 450 °C), the reduction is about 6%, which was only slightly over the error of the mass spectrometer (Ru-100-5). Even less significant decrease is obtained (1%) between Ru-400-5 and Ru-400-10 (at 450 °C). Both samples have similar ammonia conversion, thus less time implies a more overall efficient process.

Hence, this study could have been done in more detail, apart from considering the effect of other parameters involved, to find a more precise optimal value. Nevertheless, it is suggested that such study could not be necessary for two reasons: (i) similarly stated for Ni, if the aim is to determine the conditions to prepare a bimetallic catalyst, it cannot be assured that those could be the same, when combined with another metal, and (ii) Ru is an expensive metal, as already mentioned, therefore it is more attractive to study different materials that could substitute it rather than a more in depth study of Ru.

## 6.3. Nickel and ruthenium catalyst

The NiRu bimetallic catalysts prepared with BM have not been found in other publications in order to conduct a comparison. There are, indeed, articles regarding bimetallic catalysts applied to the ammonia decomposition (Han *et al.*, 2007; Choudhary, Sivadinarayana and Goodman, 2009; Simonsen *et al.*, 2012; Lucentini, Casanovas and Llorca, 2019; Kirste *et al.*, 2021).

Nevertheless, most of these cannot be used to compare or to extract explanations about the reason why the order of addition in BM affects its conversion. Some have explored this idea, like Lucentini et. al. (Lucentini, Casanovas and Llorca, 2019) and Álvarez et. al. (Álvarez M, Centeno and Odriozola, 2016) but with catalysts prepared with IWI method. Lucentini et. al. (Lucentini, Casanovas and Llorca, 2019) have found that the addition did not affect the conversion of ammonia, as they obtained differences about 4%. In the case of Álvarez et. al. (Álvarez M, Centeno and Odriozola, 2016), the reaction analysed was the dry-steam reforming of methane over NiRu based catalyst. They found out that the simultaneous addition of Ru and Ni was the best combination. Thus, the results of this current study did not agree with the literature. It is suggested that preparation techniques chosen could have a significant effect on the performance of the catalysts. Moreover, returning to an idea previously mentioned, the use of BM can induce different levels of incorporation of the metal into the support, depending on the energy used (House *et al.*, 2015). When preparing a bimetallic catalyst, the first metal incorporated could be potentially covered by the second addition, decreasing the activity of the first one or maybe the first one could have created stronger interactions with the support than the last addition. Both hypotheses could be further explored in the discussion of the Raman spectra obtained.

In the publication of Lucentini et. al. (Lucentini, Casanovas and Llorca, 2019), they did indicate that the combination of Ni and Ru did improve the conversion, regarding Ni based catalyst, but not for Ru catalysts. In the present study, the same conclusion is obtained. Nevertheless, it is contradictory to results found in other works (Han *et al.*, 2007; Choudhary, Sivadinarayana and Goodman, 2009; Simonsen *et al.*, 2012; Kirste *et al.*, 2021), where the combination of two metals produced a better catalysts than the monometallic counterparts. The highest conversions obtained at 450 °C, for bimetallic catalysts were 80.4% and 82.1% (Ni-Ru-b and Ni10-Ru5-b, respectively). While Ni-D-10 achieved the 55.1%, at the same temperature, Ru-400-10 had values of 96.8% conversion. Thus, an addition of 1% Ru did improve the performance of 5% Ni based samples, by 30%, roughly. However, it worsened the values obtained with Ru monometallic samples. Although the decrease is only around 15%, maybe it could be explored, whether different concentrations of Ni and Ru perform better than Ru catalysts, like smaller amounts of Ru (<1%) and higher of Ni (>5%).

### 6.3.1. Raman spectroscopy

Figure 6.2 depicts a comparison of the three bimetallic samples (before reaction), analysed with Raman (NiRu-b, Ru-Ni-b and Ni-Ru-b). Some initial conclusions from this graphic can be extracted: (i) catalysts produced by BM method were not as homogeneous in composition as expected and (ii) the presence of the Ni precursor was more evident than the Ru. The latter can be understood as the quantity used for Ru was much smaller than for Ni, thus the intensity of the

signal would be proportional to the amount present in the sample. The former conclusion did appear unexpected as it was believed that BM could produce more homogeneous catalysts. This idea was supported by the spectra obtained (see Figure 6.2). For example, for Ni-Ru-b three different spots of the sample showed three different compositions. It has not been found any literature about this topic, as most of the publications did apply larger times than this work (Sayyah *et al.*, 2013; Zhang *et al.*, 2014; House *et al.*, 2015; Kozawa, 2021). Therefore, it could be possible that more grinding times could have produced more homogeneous catalysts, but it was also proven that an increase of time reduced its performance. It is suggested that maybe this heterogeneity helped increase the activity of the catalysts. However, after reaction, between spots of the same sample only varied the intensity between peaks, thus samples became more homogeneous in composition (see Annex 6).

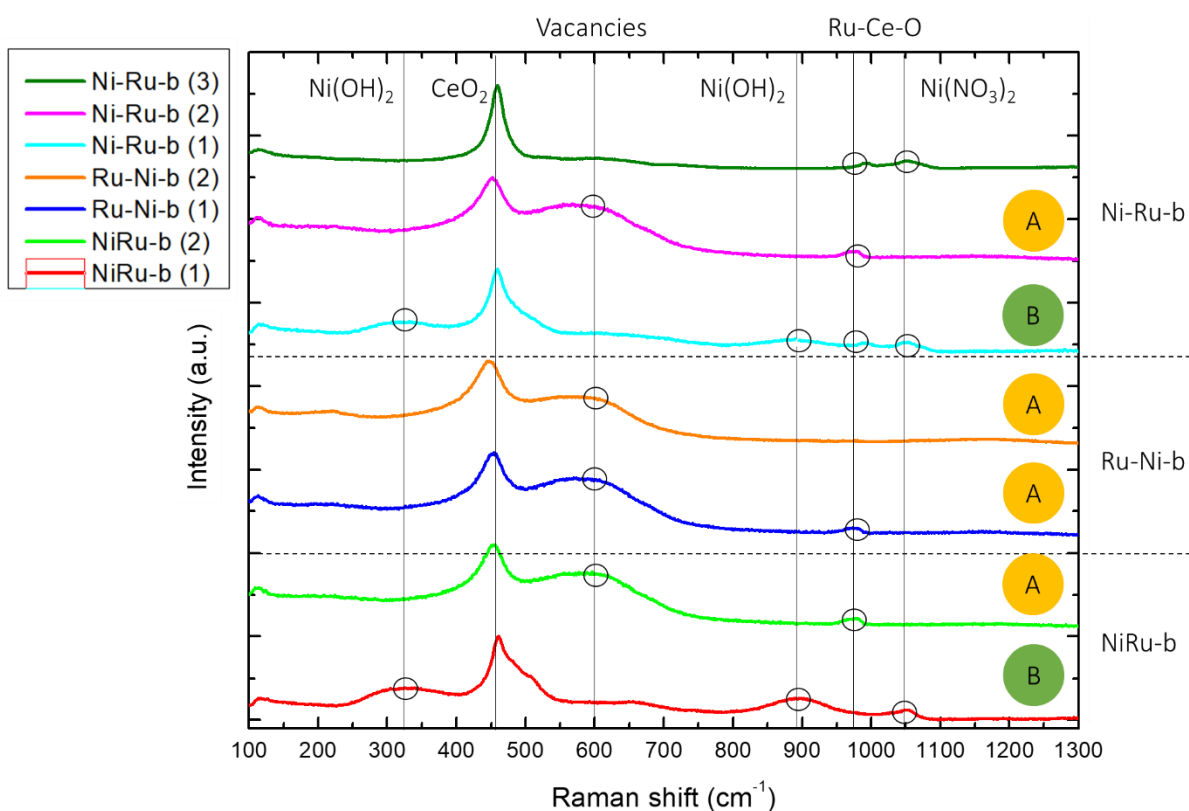


Figure 6.2. Raman spectra of the three bimetallic catalysts: NiRu-b, Ru-Ni-b and Ni-Ru-b. Some of the most significant peaks are marked, as well as the two different types of spectra, labelled as A and B.

The heterogeneity of fresh samples was expressed as two distinct profiles, which can be represented by Ni-Ru-b (2) and Ni-Ru-b (1) and will be referred from now on as A and B, respectively. The A profiles were Ni-Ru-b (2), Ru-Ni-b (1), Ru-Ni-b (2) and NiRu-b (2). The B profiles were Ni-Ru-b (1) and NiRu-b (1). The spectrum of Ni-Ru-b (3) did not follow any of the types mentioned, it exhibited a similar profile as the single ceria (see Figure 10.3). It is suggested that this was an evidence of the heterogeneity of the sample, but this profile did not provide information on the activity of the catalysts.



The A profile showed a significant shift of the position of CeO<sub>2</sub> peak towards the left side of the graph (see Figure 6.2). The Raman shift values ranged from 446 cm<sup>-1</sup> to 453 cm<sup>-1</sup>, as Ru-Ni-b (2) had the strongest shift and NiRu-b (2) the smallest, compared to the original peak, at 465 cm<sup>-1</sup> (see Figure 10.3). This change of position was due the strong interaction between metals and support, which meant that new bonds are generated between Ni, Ru and ceria; thus, the original bonding energy of the peak is modified because of the contribution of the metals into the structure (Barrio *et al.*, 2010; Stojmenović *et al.*, 2016). More evidence of this strong interaction was that three of the four spectra with A profile displayed the Ru-Ce-O signal.

Regarding the peak of oxygen vacancies in ceria (vacancies, in Figure 6.2), compared to the original (see Figure 10.3), it has broadened (500-700 cm<sup>-1</sup>) and the difference of intensity with the largest peak has decreased too (see Figure 6.2). As aforementioned, the largest peak of ceria shifted as the interaction metal-support increases, which is linked to this broadening. This occurred because the increase of intensity of the original peak at 600 cm<sup>-1</sup> and the appearance of two other peaks. This former signal represented the intrinsic defects ceria had because the absence of an oxygen in the structure or the presence of the reduced atom of cerium (Ce<sup>3+</sup>) (Sartoretti *et al.*, 2019). The other two were caused by the addition of the metals as they interacted with the support and originated new defects, as stated by Sartoretti *et al.* (Sartoretti *et al.*, 2019). It is worth to mention that the peaks for NiO (500 cm<sup>-1</sup> and 730 cm<sup>-1</sup>) and RuO<sub>2</sub> (528 cm<sup>-1</sup>, 646 cm<sup>-1</sup> and 716 cm<sup>-1</sup>) had Raman shifts similar to the band exhibited in these spots analysed. Indeed, it was possible that there was presence of these species, but they were overlapped by the appearance of defects.

It can be seen that out of these four A profiles, Ni-Ru-b (2) presented (i) one of the largest shifts, changing from 465 cm<sup>-1</sup> to 452 cm<sup>-1</sup> and (ii) the least difference in intensity between CeO<sub>2</sub> peak and the band (vacancies). It could be assumed that the interaction metal-support could be a key parameter to achieve better performing catalysts, as the Ni-Ru-b exhibited the best values of ammonia conversion out of the three bimetallic samples.

Raman spectra with A profiles have been found in literature (Lucentini *et al.*, 2021a). Nevertheless, Figure 6.2 shows another profile which has not been found in any publication, B profile (Ni-Ru-b (1) and NiRu-b (1)). The position of the CeO<sub>2</sub> peak was not as shifted as the previously explained, but it had a strong asymmetry towards the right side, corresponding to smaller peaks from the signals of NiO and RuO<sub>2</sub> (see Figure 5.7 and Figure 5.9). Moreover, as these signals were present, the characteristic band mentioned above disappeared. Only the peak at 600 cm<sup>-1</sup> remained but the intensity was not as significant as in the other samples, thus it cannot be seen in Figure 6.2. The spots analysed presented a high presence of oxidised elements, and a smaller interaction between metal and ceria, compared to A profiles. When Ru and Ni were added

simultaneously (NiRu-b (2)) the signal of NiO and RuO<sub>2</sub> appeared stronger than Ni-Ru-b. It is suggested that the structure of the support remained similar to the original because instead of becoming part of it, they recombined to form RuO<sub>2</sub> and NiO. It is worth to note, that both compounds were proven to be the active sites where the reaction occurred once they were reduced (Lucentini, Casanovas and Llorca, 2019).

It seemed like A profiles had stronger interactions between metal and support, inducing more defects and vacancies into the structure. However, B profile had potentially less-defect structure but higher presence of oxide species. It could be argued that defects in the support played a more significant role in the conversion of ammonia, when compared to the NiO and RuO<sub>2</sub>. The reason was because, although NiRu-b and Ni-Ru-b might have presented both type of spectra, one of the profiles could be more active in terms of reaction. For Ni-Ru-b, the spectrum related to the defects (A profile) had the strongest interaction out of the other profiles and the least relative intense peaks of NiO and RuO<sub>2</sub> (B profile). Meanwhile, the behaviour of NiRu-b was the other way around. Ru-Ni-b only presented A profile, related with the high presence of defects. Therefore, as Ni-Ru-b did perform better, in terms of ammonia decomposition (see Nickel and ruthenium catalysts), the presence of defects could be potentially more important to decompose ammonia, than the presence of RuO<sub>2</sub> and NiO. However, these oxides could not be detrimental to the reaction, but could enhance the conversion, as Ru-Ni-b spectra only recorded one type of profile and did perform worse than Ni-Ru-b.

There is another unusual feature in this last type of spectrum, which is the signal of Ni(OH)<sub>2</sub>. No publication regarding this issue has been found. It is suspected that during BM method some water could have been produced, as the catalysts resultant had a wet appearance, even though no liquid was added. This hypothesis was based in the colour of the wet Ni samples. They had an apple green colour, which might be caused by Ni(OH)<sub>2</sub> as it has this characteristic colour. So, because these samples acquired such colour due to the addition of a liquid, it could be possible that both reagents (RuCl<sub>3</sub> and Ni(NO<sub>3</sub>)<sub>2</sub>·6H<sub>2</sub>O) were hygroscopic<sup>9</sup> (Fischer, 2013) and that favoured the generation of such compounds. Whether it helped or not during the reaction it is unclear, as more studies should be done.

The idea that defects could have a more significant role than the oxide elements could be partially confirmed with the spectra obtained for the samples after reaction. They mostly had an A profile (see **Annex 6**) which exhibited the high interaction of the metals with the support and the presence of defects in its structure. It is worth mentioning that there could also be signals of RuO<sub>2</sub> and NiO but overlapped by the characteristic band. As they were calcined at 600 °C, the catalysts were oxidized, therefore it was sure that NiO and RuO<sub>2</sub> should have been present. They all have a

---

<sup>9</sup> Hygroscopic compounds are those materials with high affinity to water and they are able to absorb a significant amount of it (Fischer, 2013).

strong shifting towards lower frequencies of the graph and quite symmetrical peaks, from 446 to 457  $\text{cm}^{-1}$ . These signals were paired with the broad band at 500-700  $\text{cm}^{-1}$ , as previously stated. Then, out of the three bimetallic catalysts, Ni-Ru-b presented the most shifted peak, and the least difference between intensities in these two signals, once again. Thus, the hypothesis that the defects might play a more important role than the presence of oxides could be possible.

Hence, it has been showed the possibility that the BM technique could induce heterogeneous catalysts in composition and perhaps both the presences of defects and oxide compounds improved the reaction.

Previously it has been suggested the effect of the order of addition in BM. It was clear from the values of ammonia conversion obtained, that the best option was to introduce first Ni, and then Ru. Two options have been mentioned as to why this combination did obtain the best results. Firstly, by incorporating Ni first, and then Ru, the latter could have covered part of the Ni particles and because the high affinity of Ru with the reaction, it did improve the results. Secondly, Ni created stronger interactions with the support and Ru did not.

After analysing the Raman spectra obtained, the first hypothesis can be ruled out. If this idea were true, more presence of  $\text{Ni}(\text{NO}_3)_2$  in Ru-Ni-b should have been exhibited, as it did for the other two bimetallic samples. According to second explanation, it could be feasible that the first metal added should have created stronger interactions than the second. However, as the grinding times applied were the most optimal for monometallic catalyst (Ni and Ru) it should be assumed that the interaction should have been as strong as for their monometallic counterparts.

With only Raman spectra it cannot be argued the reason why the order of addition in BM changed the activity of the catalysts. It is suspected that the structure did played a key part into the ammonia conversion, thus an XPS will be done in a near future.

## 7. Fuel analysis: viability of NH<sub>3</sub> as a fuel

One of the aims of this work is to find a catalyst that could allow an efficient way to convert ammonia to obtain hydrogen. The importance of this section is to determine whether using ammonia as an energy carrier could be a feasible and competitive option to consider as a future solution.

Therefore, in this chapter, advantages and disadvantages of ammonia, as a fuel, will be compared to the other available alternatives. There will be an explanation of the production of fossil fuels (gasoline, diesel and natural gas), as well as electricity and hydrogen from steam reforming and from renewables. For each type, the emissions in the generation process and during the usage for mobile application will be exposed. Other characteristics such as the price of the fuel, car and energy achieved with each one will be presented. With this data, a discussion will be conducted to determine whether or not ammonia is a feasible fuel. Other aspects will also be discussed, like the potential environmental impacts that fuels cells and Li-ion batteries can have when disposed.

### 7.1. Fossil fuels

#### 7.1.1. Gasoline and diesel

Gasoline or diesel are some of the multiple products that can be obtained from crude oil. The extraction of the oil depends on the geological characteristics of the soil, and different methods must be considered. However, the most conventional way is to drill and pump the liquid (CAPP, 2020).

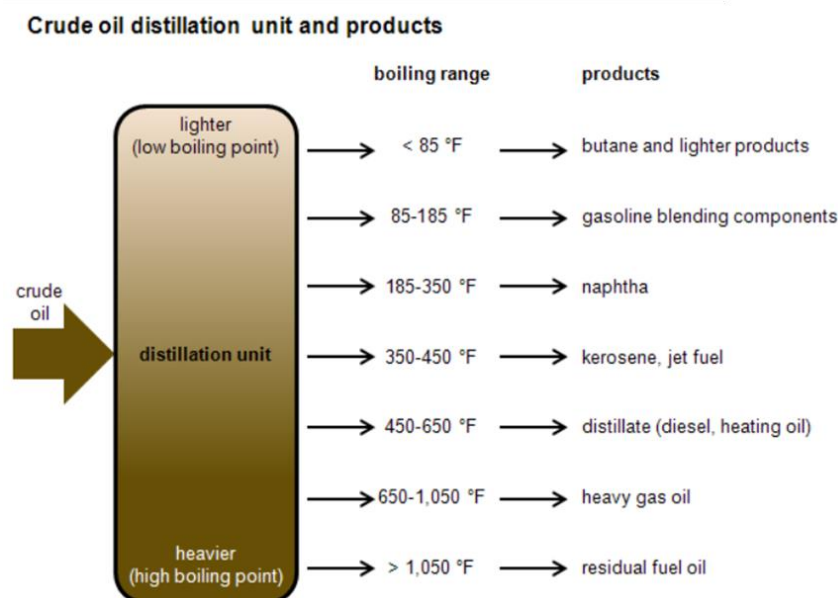


Figure 7.1. Scheme of the distillation tower of the refining process of crude oil (EIA, 2020c).

The refining process consists in three steps: separation, conversion and treatment. At first, the crude oil is pumped into tall hot furnaces, up to 600 °C (1050 °F) approximately, as seen in Figure

7.1. As the different components of the oil have different boiling points, these fractions can be separated. Lighter components, like gasoline, can be extracted at the top, while medium liquids like diesel, which have a heavier boiling point, stay in the middle. Heavier fractions have low value *per se*; therefore, they can be processed into lighter fractions. This method is known as cracking, which consists in breaking hydrocarbon molecules into lighter components, by the use of heat, pressure and the presence of a catalyst. The last step is the treatment which assures the high quality and safety of the final products (EIA, 2020c).

Any process has environmental impacts associated. For these fuels, the climate change factor will be discussed by means of the grams carbon dioxide equivalent<sup>10</sup> per megajoule in the fuel (g CO<sub>2</sub> eq/MJ). This value can express direct and indirect emissions during the process, but it does not contemplate other impacts that the whole process creates, like: the disturbance of the wildlife because of the land use or the noise, the water pollution or the risk of polluting nearby aquifer when drilling, or the emission of toxic compounds to the ecosystem (air, water, soil), such as VOC, NO<sub>x</sub> or PAH (Ngene *et al.*, 2016).

JEC (JRC-Eucar-Concawe) presented in 2020 a Life-Cycle-Analysis (LCA) report for different fuels from Well-To-Tank (WTT). This term, used mainly for fossil fuels, pretends to describe the path a fuel follows from its extraction, through its processing and until the gas station. Other LCA studies of the same subject may obtain different values because their initial assumptions. In this case, the emissions associated to the following aspects have not been considered (Prussi *et al.*, 2020):

- Production and disposal of the vehicle, corresponding to its fuel.
- Production and distribution facilities that produce the fuel.

According to this report, the environmental impact for gasoline is 17.0 g CO<sub>2</sub> eq/MJ and for diesel is 18.9 g CO<sub>2</sub> eq/MJ. These values include the emissions related to the use of energy and potential leakage from extraction of the crude oil, the refining process and the transportation to the gas station (Prussi *et al.*, 2020).

As a combustion product, gasoline has a specific energy of 12.8 kWh/kg and an energy density of 9.5 kWh/dm<sup>3</sup>, while diesel has 12.6 kWh/kg and 10.6 kWh/dm<sup>3</sup>, as it can be seen in Table 1.1. Both fuels are, amongst the different options, the ones that have the highest energy density. However, in terms of internal combustion engines, their efficiency is about 25%. Plus, considering that the refining process in general only has losses about 15%, the overall efficiency is no more

---

<sup>10</sup> Carbon dioxide equivalent (CO<sub>2</sub> eq) is a metric measure that expresses the amount of greenhouse gases emitted in terms of carbon dioxide emissions by considering the global warming potential of each gas (Eurostat Statistics Explained, 2017).

than 20%. However, due to their high energy density, they can compensate such a deficiency (Nave, 2001; Cook, 2002).

However, the greenhouse gases and pollutants produced by gasoline and diesel are harmful for humans and ecosystems. Figure 7.2 shows the average percentages of the products from the exhaust gas for gasoline and diesel. It can be seen that the exhaust gas is mostly composed by  $N_2$ , which is in consonance due to the use of air as a source of  $O_2$ . Ideally, the combustion of the fuel would only produce  $CO_2$  and water. However, because of the incomplete combustion and high temperatures associated to combustion engines, the products are various and some of them are harmful, like CO, soot,  $NO_x$  or hydrocarbons (Geng *et al.*, 2017).

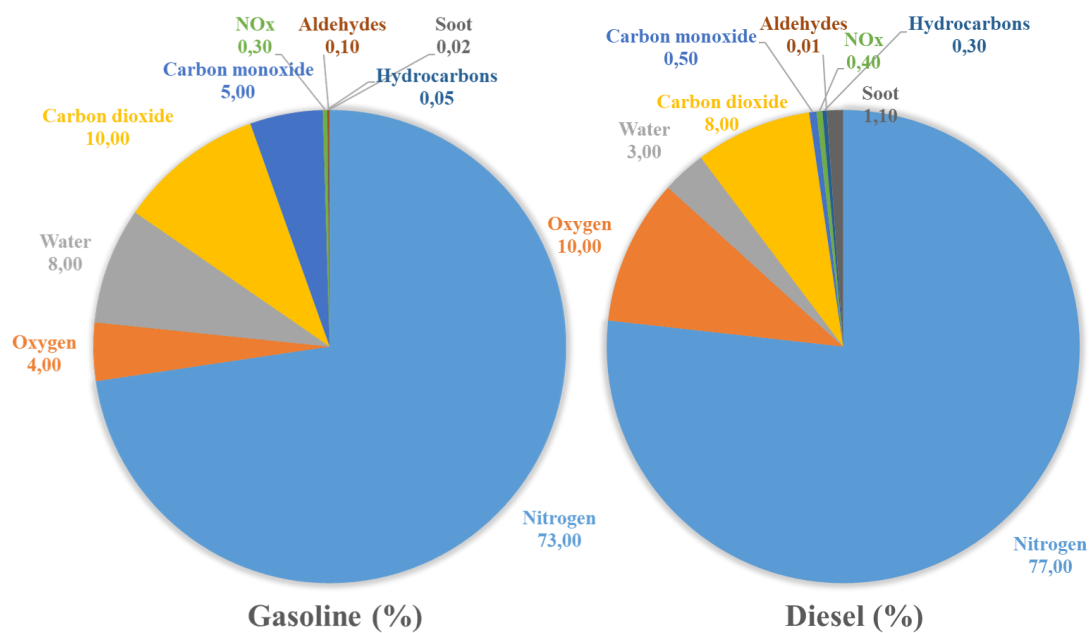


Figure 7.2. Composition of the exhaust gas from the combustion of gasoline and diesel in percentage (Data extracted from: (Sassykova *et al.*, 2019)).

According to the unit established before to express the environmental impact, for the combustion of gasoline is 73.0 g  $CO_2$  eq/MJ; and for the diesel is 72.5 g  $CO_2$  eq/MJ (Zijlema, 2018). At first, diesel could be considered a better option than gasoline, taking into account that emits less carbon dioxide and contains more energy per unit volume. However, as it is seen in Figure 7.2, diesel engines produce more pollutants, contributing into worsening the air pollution. Specifically, its combustion emits a higher concentration of soot, containing particles smaller than 2.5  $\mu m$ , which are known to produce in human's cancer, respiratory or cardiovascular health effects (Prasad and Venkateswara, 2010; EIA, 2020a).

Gasoline is one of the most used fuels. By 2020, 51.9% of the vehicles sold used gasoline while 29.4% used diesel. Although this amount is larger than any other that uses an alternative fuel, both diesel and gasoline cars have been experiencing a decrease in their sales (ACEA, 2020). An example of gasoline and diesel cars are the Hyundai i10, at 17390€ and

100HP<sup>11</sup> and the Fiat Tipo Cross MCA, at 27150€ and 130HP, respectively (Fiat, 2021; Hyundai, 2021b). The price for the gasoline car is 1.367 €/10kWh while for the diesel is 1.065 €/10kWh (Geoportal, 2021). The following table (Table 7.1) shows all the values presented in this section, for the gasoline and the diesel.

Table 7.1. Summary of the characteristics and the impacts associated with gasoline and diesel (Data extracted from: (Nave, 2001; Cook, 2002; Kolb, 2017; Masnadi, El-Houjeiri and Schunack, 2018; OCU, 2018; Zijlema, 2018; Edwards *et al.*, 2020; Hoekstra, 2020; Lazard, 2020)).

	Gasoline	Diesel
Specific energy (kWh/kg)	12.8	12.6
Energy density (kWh/dm <sup>3</sup> )	9.5	10.6
WTT* impact (g CO <sub>2</sub> eq/MJ)	17.0	18.9
Combustion impact (g CO <sub>2</sub> eq/MJ)	73.0	72.5
Price (€)	17390 (100HP)	27150 (130HP)
Fuel price (€/10 kWh)	1.367	1.065

\*WTT: Well-To-Tank.

### 7.1.2. Natural gas

Natural gas is the other main fossil fuel used in cars and is mainly composed by methane (CH<sub>4</sub>). The process of extraction, production and distribution is shown in Figure 7.3. Generally, natural gas is present in cracks, spaces or pores in the soil and rocks. It also can be found in the same well where crude oil is extracted. The main process of extraction is by drilling wells vertically or horizontally, depending on the geological formations. It is worth to note another method: hydraulic fracturing or fracking. It consists in breaking the rock which contains natural gas with a beam of high-pressure water. The product obtained needs to be processed because it contains compounds not suitable for its consumption (CO, H<sub>2</sub>S, N<sub>2</sub>, He, S, C<sub>2</sub>H<sub>6</sub> or C<sub>3</sub>H<sub>8</sub>). The outcome of this treatment is methane. It can be used as compressed gas (CNG) or in liquefied state (LNG) (EIA, 2020b; U.S. Department of Transportation, 2020).

<sup>11</sup> HP: horsepower

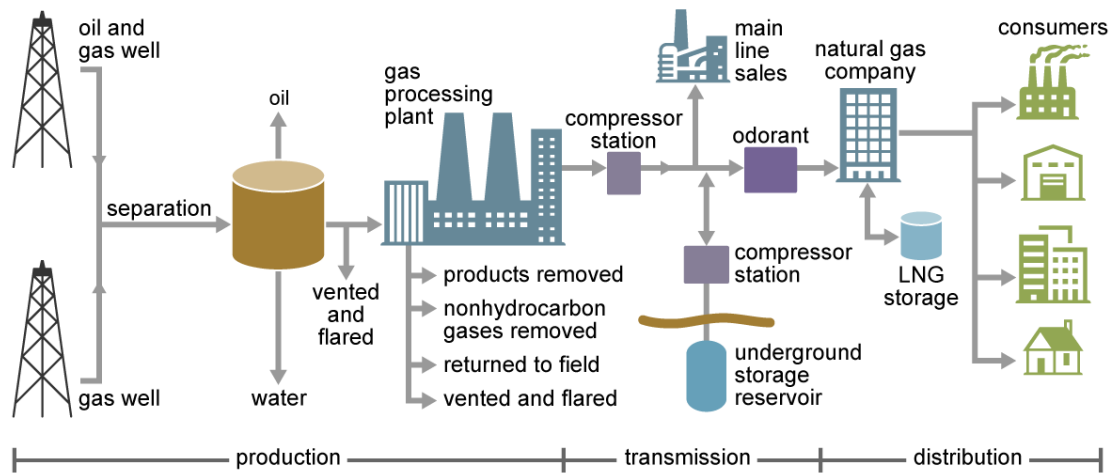


Figure 7.3. Scheme of the production, transmission and distribution of the natural gas (EIA, 2020b).

The environmental impact of natural gas from a WTT perspective varies according to the transportation distance and the purity of the natural gas extracted to be processed. On one hand, the greater the distance is, the larger is the probability of having leakage. On the other hand, as the natural gas has more impurities, more energy to treat it is needed. (Gan *et al.*, 2020).

For a gas transported by pipeline from South-West Asian locations to any Asian country (assumed distance of 4000 km), the environmental impact is 15.1 g CO<sub>2</sub> eq/MJ. This situation is becoming popular in Asia to substitute diesel. The case for Europe is the production and transport of LNG, which has an environmental impact of 17.4 g CO<sub>2</sub> eq/MJ. This value is higher than the Asian situation, even when the transporting distance is shorter. The reason is that the process of liquefaction requires extra energy to convert the CNG into LNG (Prussi, M., Yugo, M., De Prada, L., Padella, M. and Edwards, 2020). Apart from the emissions, there are other environmental impacts associated with the extraction, processing and distribution of natural gas. In the previous section, about gasoline and diesel, the effects of the drilling have already been explained. Moreover, natural gas can be extracted from a well where there is no crude oil. Even though the impacts are the same: disturbance of wildlife, water pollution, noise and the emission of toxic compounds (Ngene *et al.*, 2016; EIA, 2020b).

In Table 1.1 the characteristics for the natural gas are presented at 200 bar (CNG), which are 13.9 kWh/kg for the specific energy and 2.3 kWh/dm<sup>3</sup> for the energy density. If the natural gas is used in its liquefied state (LNG), the values are 13.9 kWh/kg and 5.6 kWh/dm<sup>3</sup>, respectively (Nave, 2001; Cook, 2002).

Amongst the fossil fuels, natural gas is the cleanest in terms of combustion. There are two reasons: (i) it emits less pollutants than diesel and gasoline (NO<sub>x</sub>, SO<sub>2</sub>, CH<sub>4</sub>, soot and CO<sub>2</sub>) and (ii) the combustion is more efficient, thus, these concentrations are smaller in the case of natural gas. (Ministerio para la Transición Ecológica, 2019; EIA, 2020b).



The impact of the combustion for the CNG and LNG is 56.6 g CO<sub>2</sub> eq/MJ (Zijlema, 2018). Compared to the values mentioned in the previous section, natural gas is indeed a cleaner fuel and contributes less to the climate change.

Natural gas produces cleaner combustion products, and regarding the environmental impact, it is the best option amongst the other fossil fuels. The price of CNG is 0.701 €/10kWh and 0.503 €/10kWh for the LNG (Geoportal, 2021). In Spain, a market option with a CNG engine is the Skoda Octavia, at 29390 € and 130 HP. There are not cars with LNG engines because they require high pressure to maintain the liquid state (Skoda, 2021). However, there are only 144 recharging points in Spain, concentrated around major cities like Barcelona or Madrid (Geoportal, 2021). In addition, as well as the other fossil fuel cars, in the last years the sales have been decreasing, representing less than 1.9% of the sales of vehicles in 2020 (ACEA, 2020).

A summary of the characteristic values for LNG and CNG is displayed in Table 7.2.

Table 7.2. Summary of the characteristics of the CNG and the LNG (Data extracted from: (Nave, 2001; Cook, 2002; Zijlema, 2018; Prussi *et al.*, 2020; Skoda, 2021)).

	CNG	LNG
Specific energy (kWh/kg)	13.9	13.9
Energy density (kWh/dm <sup>3</sup> )	2.3	5.6
WTT* impact (g CO <sub>2</sub> eq/MJ)	15.1 (Asia)	17.4 (Europe)
Combustion impact (g CO <sub>2</sub> eq/MJ)	56.6	56.6
Price (€)	29390 (130 HP)	-
Fuel price (€/10 kWh)	0.701	0.503

\*WTT: Well-To-Tank.

## 7.2. Electricity

Electric cars have become one of the best current alternatives in terms of clean means of transport. In circulation, their emissions are 0 g CO<sub>2</sub> eq/MJ because it depends on the energy stored in the Li-ion battery. Nevertheless, most of the times, the electricity needed to fuel the vehicle does not come from renewable sources.

As it has been previously discussed in **Introduction**, the energy sector is the main producer of greenhouse gases, due to the use of fossil fuels in combustion. The generation of electricity constitute the 42% of the emissions of this sector (Climate Watch, 2020; World Resources

Institute, 2020). Globally, the fossil fuels are the main source to generate electricity, as displayed in Figure 7.4 (BP, 2020).

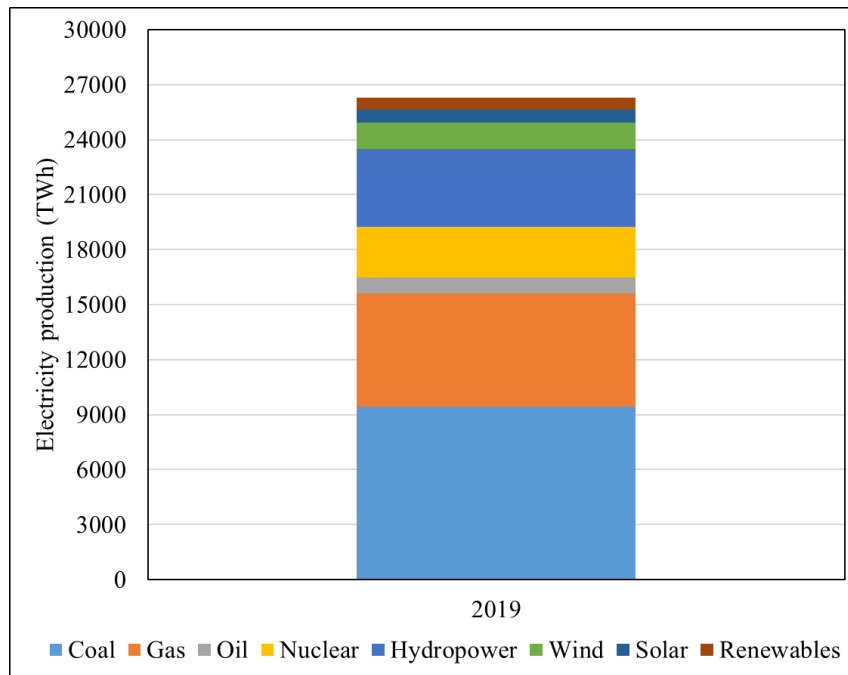


Figure 7.4. Distribution of the global energy production per source (2019) (Data extracted from: (BP, 2020)).

From these data, it can be extracted that the total global electricity production, in 2019, was 26296.51 TWh. This value has been increasing since the pre-industrial era and the tendency will continue like so. About 27% of the production is from renewable sources (nuclear not included). This low proportion is mainly because developing countries like China or India use fossil fuels to generate the electricity needed to run their industries. In order to compete with developed countries, they need to generate as much as they can, without having huge investments. Thus, they choose the option that offers the energy needed at the lowest price possible. Furthermore, a common situation, amongst their population is the use of coal or biomass to heat and cook (Ritchie and Roser, 2014; Butler, Frost and Walsh, 2015).

Nonetheless, the electricity mix presented in Figure 7.4, does not match with the characteristic ratio of some developed countries like Spain. Figure 7.5 shows the distribution of the production of electricity in Spain by 2020. Its energetic infrastructures have generated about 250000 GWh, with a distribution of renewables and non-renewables, almost equally (46.2% and 53.8%, respectively) (REE, 2021a). Each year, European members increase the use of renewable sources by stablishing policies that favour them. For example in Spain, there is the Real Decreto-Ley 17/2019, published in 2019, where thermal coal generation plants are closed, to be substituted by renewable plants (RDL 17/2019, de 22 de noviembre).

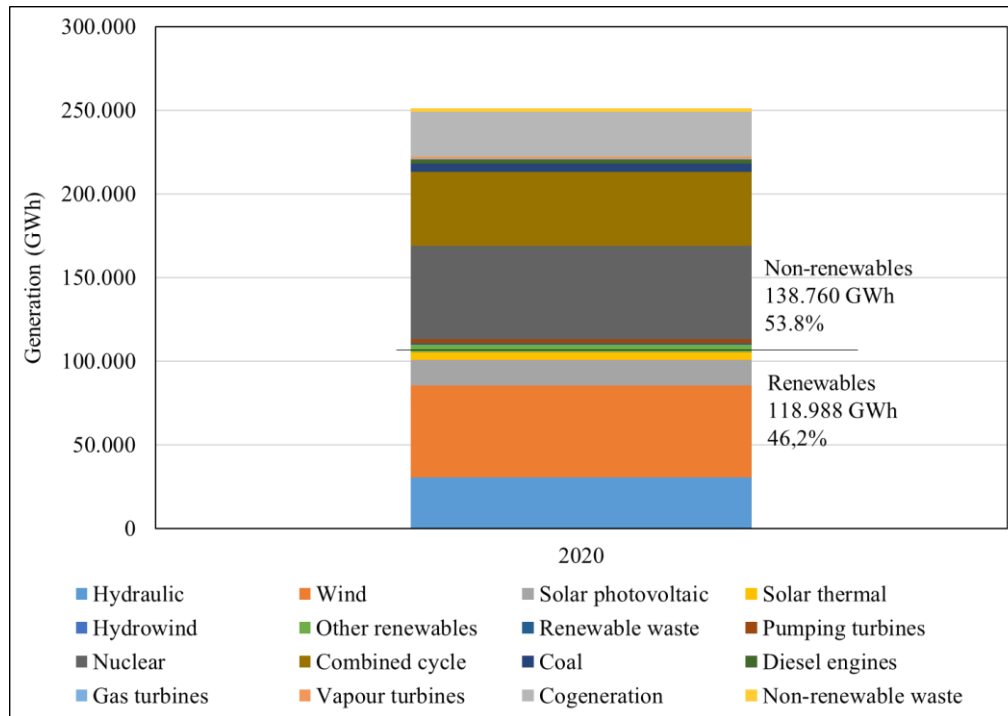


Figure 7.5. Distribution of the generation of electricity by power plant in Spain (2020)(Data extracted from: (REE, 2021a)).

The generation of electricity has emissions associated, determined by the amount of fossil fuel-based plants. For Spain in 2020, there was an emission of 27.8 g CO<sub>2</sub> eq/MJ. Within this value the emissions related to the maintenance, or the construction of electricity plants are not included. Therefore, this will be assumed as the environmental impact associated with the production of the fuel for the electric cars (REE, 2020).

In average, the price of electricity in the peninsular region of Spain, in 2020, was 0.404 €/10 kWh (expressed in the same units as the other fuels) (REE, 2021b). However, this is not the final price users pay to charge their vehicle. On one hand, if the owners have a garage or a parking space, they can install their own charging point for 1500 € on average. On the other hand, there are public charging points. In fact, currently in Spain, there are 19790 charging points, 4545 of them are public (González, 2019; Electromaps, 2021). Nonetheless, the majority are from private enterprises, and on average, the price of the charging is 0.500 €/kWh (Electromaps, 2021).

Moreover, the Spanish government offers state grants for the vehicle users that change from a 10-year-old car for a new alternative vehicle, under the *Programa de Incentivos a la Movilidad Eficiente y Sostenible* (MOVES). Depending on the price of the new acquisition, and the conditions of the old one, the grants can range from 400 € to 4000 € (RDL 266/2021, de 13 de abril). Because of these policies, in Europe, the sale of electric cars have increased by 53.3% in 2020, compared with 2019; becoming the 7.2% of vehicles sold (ACEA, 2020). Nevertheless, because the price is still high, it is not as competitive as the combustion cars. An example in

Spain, is the Peugeot e-208 that costs 31850 € (136 HP), which is twice the price of a gasoline car, approximately (Peugeot, 2021).

In terms of energy density and specific energy, for this fuel, it is determined by the characteristics of the lithium-ion battery of the vehicle. The device consists in an anode, a cathode and electrolyte. By charging it with electricity, the energy is transformed into chemical energy. Considering the losses due to the efficiency of the conversion, the electric grid, and the conversion from the DC (battery) to AC (electric grid and car), electric cars have an overall efficiency of 80% (approximately). With all taken into account, (Wilberforce *et al.*, 2017) on average, considering the values from Table 1.1, the current batteries have 0,85-1,2 kWh/kg and 0.47 kWh/dm<sup>3</sup> (Shen *et al.*, 2018; Ding *et al.*, 2019).

Nevertheless, electric batteries have two major drawbacks. Firstly, it is the time it takes to fully charge the car. Generally, it is needed more than an hour, depending on the capacity of the battery and the electric grid. This problem is mostly solved by charging it during the night. Secondly, it is that even when fully charged, the range of the car goes from 200 km to 490 km, whereas a combustion car has an average range of 650 km (approximately). However, in order to increase the autonomy of an electric car, the battery will have to weigh more. The mass is related to the capacity to store energy; thus, the car would need to be heavier and the structure of the vehicle must be strengthened to be able to support the weight (Wilberforce *et al.*, 2017).

Electric cars are being chosen as a clean alternative to the combustion cars. However, apart from the origin of the electricity, there is another aspect to be taken into consideration in terms of pollution. These lithium-ion batteries are made of scarce elements that their extraction and refinement involve emissions of hazardous elements, such as Li itself. Moreover, the production of the batteries may produce or emit pollutants, as well as some losses of the materials that constitute the battery. As a previous study reported (Ordoñez, Gago and Girard, 2016), from 4000 t of spent lithium-ion batteries, 1100 t of heavy metals and 200 t of toxic electrolytes are generated. This impact constitutes an environmental and health issue. Therefore, the right disposal is necessary. Nevertheless, because the scarcity of these elements and their environmental impact, they need to be processed. That is why, the best option is to recycle the batteries and extract those materials (Shen *et al.*, 2018; Yang, Gu and Guo, 2020).

It is worth to note that there is a misconception around the scarcity of Li. It is in fact a rare element, and it is present in the world as 1:1000 of sodium or potassium (Eftekhari, 2019). However, the idea of Li scarcity because of their increasing use in electric batteries appeared in 2015 when a deficit in the supply happened. That was originated by a rapid consumption and low production of Li, thus an increase in its price (Narins, 2017). This imbalance created the idea of uncertainty. However, it has been published (Jaskula, 2015) that there is not only readily available Li on earth,

but if the demand of the element would triple its current levels, there would be still enough lithium on known reserves for 135 years.

In Table 7.3, there is a summary of the characteristics of the electricity as fuel.

Table 7.3. Summary of the characteristics of the electricity (Data extracted from: (Shen *et al.*, 2018; Ding *et al.*, 2019; REE, 2020; Peugeot, 2021; REE, 2021b).

	Electricity
Specific energy (kWh/kg)	0.85-1.20
Energy density (kWh/dm <sup>3</sup> )	0.47
WTT* impact (g CO <sub>2</sub> eq/MJ)	27.8
Combustion impact (g CO <sub>2</sub> eq/MJ)	0
Price (€)	31850 (136 HP)
Fuel price (€/10 kWh)	0.404

\*WTT: Well-To-Tank.

### 7.3. Hydrogen and ammonia from steam reforming

The use of hydrogen as an alternative fuel is gaining more attention, as it has been promoted by European policies. However, some disadvantage in terms of mobile applications surface when using hydrogen as a fuel (see [Challenges](#)). Therefore, one of the proposed solutions to the multiple issues, is the generation on board by decomposing ammonia to generate it at the moment.

Hydrogen and ammonia might be considered as clean fuels. Nevertheless, according to their source and the way of production, it might not be true. Nowadays, 97% of the produced hydrogen is via natural gas steam reforming. Furthermore, ammonia is also produced with this same hydrogen. In fact, the ammonia industry is responsible of about 1% of the global emissions of carbon dioxide (Koroneos *et al.*, 2004).

In general terms, the steam reforming consists in the catalytically split of the natural gas in presence of water steam. In Figure 7.6, are shown the multiple steps of the process. Firstly, a desulphurisation of the fuel is needed in order to assure enough purity for not poisoning the catalyst used to split the natural gas. Then, at temperatures that range from 800 °C to 900 °C, the hydrocarbon is split producing syngas: CO and H<sub>2</sub>. The former then reacts with water to obtain more H<sub>2</sub> and CO<sub>2</sub>, which needs to be extracted and to obtain a high purity level of hydrogen. This reaction is called the water gas shift-reaction (EPA, 1991; Koroneos *et al.*, 2004).

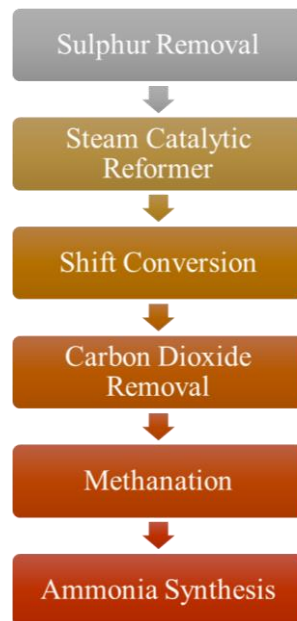


Figure 7.6. Scheme of the steps to produce hydrogen and ammonia (Data extracted from: (Koroneos et al., 2004)).

This would be the process for a typical hydrogen plant. For the production of ammonia, two more steps are needed. Once the CO<sub>2</sub> is removed, another step is done to further extract the residual carbon oxides from the syngas: methanation. Then, the ammonia synthesis or the Haber-Bosh process is performed, as shown in Figure 7.7. Hydrogen from the steam reforming is compressed with nitrogen (H<sub>2</sub>:N<sub>2</sub>, 3:1) at pressures, ranging from 20 MPa to 40 MPa; to be then introduced to a reactor. There, N<sub>2</sub> and H<sub>2</sub> are combined at 450 °C with the presence of a catalyst. As a result, NH<sub>3</sub> is produced and then cooled down and stored in a collector. Some N<sub>2</sub> and H<sub>2</sub> are not transformed, so it is recirculated back into the reactor (Ash and Scarbrough, 2019).

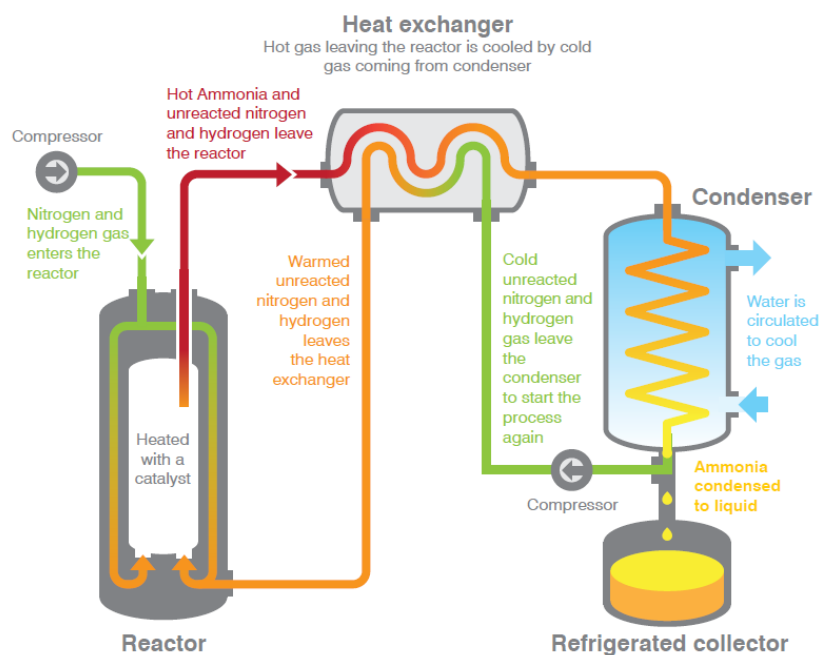


Figure 7.7. Haber-Bosch process scheme (Ash and Scarbrough, 2019).

Both processes emit CO<sub>2</sub> and other GHG directly (emissions) and indirectly (use of energy). For the case of the hydrogen production, following the same conditions stated in the JEC report, the environmental impact from producing hydrogen (compressed) in Europe, considering the transport of the natural gas, is 113.0 g CO<sub>2</sub> eq/MJ. If the hydrogen were to be liquefied, the value of its impact raises to 499.6 g CO<sub>2</sub> eq/MJ (Prussi, M., Yugo, M., De Prada, L., Padella, M. and Edwards, 2020). For the ammonia production the value of its impact is 161.5 g CO<sub>2</sub> eq/MJ (Bicer *et al.*, 2017).

Although both effects have an important impact on the climate change, it is not negligible the damage on the air quality that other emissions have. These are CO, SO<sub>2</sub>, NH<sub>3</sub> and organic compounds (EPA, 1991; Koroneos *et al.*, 2004).

As for their characteristics as a fuel, hydrogen presents a specific energy of 33.3 kWh/kg and an energy density of 2.22 kWh/dm<sup>3</sup>, for liquid, and 0.53 kWh/dm<sup>3</sup>, for gas (Office of Energy Efficiency and Renewable Energy, 2020). Nevertheless, as the DOE<sup>12</sup> has calculated, the specific energy of hydrogen stored in a car is 1.4 kWh/kg, and the energy density is 1.0 kWh/dm<sup>3</sup>. The change is due to the calculation of the values considering that the storage, as a whole, would weight about 125 kg and its volume would be of 250 L. Therefore, the mass of hydrogen gas in the tank would be a small part of the weight but would take up most of the space (U.S. DRIVE Partnership, 2017; Wilberforce *et al.*, 2017).

For the ammonia, the values of specific energy and energy density are 5.16 kWh/kg and 3.14 kWh/dm<sup>3</sup>, respectively. However, for this case, these would only be needed if the combustion of ammonia in cars or the direct use of it in a fuel cell was addressed, which will not be part of this discussion (NH<sub>3</sub> hydrofuel, 2020).

Therefore, considering that the vehicles are powered by a fuel cell that is feed by hydrogen, the only emission would be water vapour (see **Fuel cells**); which is not harmful for the environment or humans. In addition, if the hydrogen is stored in the vehicle, any possible leakage will not cause any damage in the ecosystems. However, if the tank is full of ammonia to generate hydrogen on board, some leakage might happen, and in this case it is toxic. Even though the risk (see **Generation on board: ammonia**) there are mechanisms to assure a better handling of this threats (Dujim, Markert and Paulsen, 2005; Zamfirescu and Dincer, 2009; ARPA-E, 2017).

While a fuel cell is a clean option to power a car, there are certain disadvantages that the currently technology is facing (see **Fuel cells (FC)**). First, the use of platinum as a catalyst is responsible for the high prices of these vehicles. In order to reduce costs, two solutions are being studied:

---

<sup>12</sup> The DOE Hydrogen Program, led by the Office of Energy Efficiency and Renewable Energy, aims to research and develop and infrastructure and a new way of transportation, powered by hydrogen (U. S. Department of Energy, 2020).

using smaller quantities of platinum or other metals that are not precious and recycling the platinum of the fuel cell. Second, their components suffer degradation due to water and the heat, and the catalysts can be poisoned under certain conditions and elements (Wilberforce *et al.*, 2017).

The market for cars based with a fuel cell technology is fairly new. Thus, there are only a few companies that produce light-duty vehicles to sell. One example is the Hyundai NEXO, which costs 69000 € (184 HP) (Hyundai, 2021a). This price is mainly dictated by the fuel cell, composed by precious metals, so it is expensive to produce. In addition, hydrogen produced by steam reforming costs 0.403 €/10kWh (Hydrogen Council, 2020).

Filling a hydrogen tank would take the same time as a gasoline or diesel tank (between 3 to 5 minutes) and allow the vehicle an autonomy of 500 km to 700 km (according to the capacity of tank) (U.S. DRIVE Partnership, 2017; H2, 2021). However, nowadays there are not charging points in Spain, and in the near future only two stations are being planned (H2, 2021).

Moreover, there are no vehicles that generate hydrogen on board, only a few studies and projects have been developed (Zamfirescu and Dincer, 2009). Thus, their prices are not defined. However, The Zero Emission Pollution automobile company developed ZAP. It is based on an alkaline fuel cell, feed by hydrogen, which is produced on board by the decomposition of ammonia. It has a 60 kW fuel cell, and an ammonia tank of 38.32 L, that last until 320 km (approximately). This capacity of the tank and the range are less than the value for the commercial gasoline cars, which generally can get until 600 km and have a capacity of 49 L (Zamfirescu and Dincer, 2009). Nevertheless, the price of the ammonia from steam reforming is 0.601 €/10kWh; which is similar to the other fuels' prices (Boulamanti and Moya, 2017).

### 7.3.1. Hydrogen and ammonia from renewables

In the previous section, it has been shown the impacts of its production by the steam reforming of natural gas. Hydrogen, as well as ammonia, needs to come from renewable sources to be labelled as green<sup>13</sup> fuel.

The method to obtain hydrogen from renewables is electrolysis. Here the electricity is used to split water into hydrogen and oxygen<sup>14</sup>. As presented in Figure 7.8, the process is performed in an electrolytic cell, composed by an anode, a cathode, and an electrolyte. The system is under water, which contain ions, such as potassium hydroxide (KOH) to enhance the electrical conductivity of the water. Thus, the cell becomes a circuit. Once electricity starts to run through

---

<sup>13</sup> Hydrogen can be categorised by different colours depending on the source of its production. The one explained in the last section is the grey where it comes from steam reforming of natural gas. If the source of energy is a renewable is the green hydrogen (Giovannini, 2020).

<sup>14</sup>  $2H_2O_{(l)} \rightarrow 2H_{2(g)} + O_{2(g)}$  (Ash and Scarbrough, 2019)



it, the cathode would attract protons ( $H^+$ ) and on their surface will recombine and produce hydrogen. Concurrently, the anode would attract hydroxyl groups ( $OH^-$ ), and on their surface will recombine to form oxygen and water. Generally, this process has an efficiency of 77%, although, it increases, if less voltage is used and combined with heat (Koroneos *et al.*, 2004; Ash and Scarbrough, 2019).

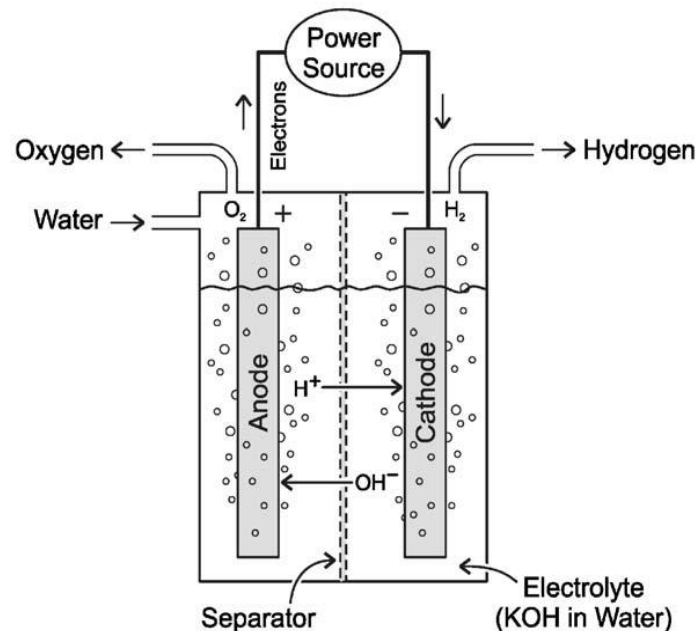


Figure 7.8. Electrolytic cell scheme (Koroneos *et al.*, 2004).

For the same conditions used on the other fuels in the JEC report, if the renewable energy source of choice is wind power, the environmental impact would be of 9.5 g  $CO_2$  eq/MJ. This election is driven under the assumption the use of wind power is the highest amongst the other renewables for most of the State Members of the European Union. Although wind power only produces greenhouse gases during its construction and maintenance, which it is not considered in the JEC report, the value presented is not zero. The reason is because this hydrogen is compressed by electricity from the European mix (Prussi, M., Yugo, M., De Prada, L., Padella, M. and Edwards, 2020).

Nowadays, the technology to produce ammonia in the same electrolytic cell it is no feasible. Ammonia could be produced from green hydrogen by the Haber Bosch process. However, fossil fuels are currently used to produce the heat needed. It has been reported (Smith, Hill and Torrente-Murciano, 2020), that if this process is electrified, the associated  $CO_2$  emissions will decrease, and the efficiency of the process could increase by 50%. Moreover, if this electricity comes from renewables, such as wind power, the environmental impact is 10.8 g  $CO_2$  eq/MJ (Smith, Hill and Torrente-Murciano, 2020).

To analyse the efficiency from its production until its usage in a car, the productivities of the following processes have to be considered: electrolysis (70%), transport and distribution (80%), fuel cell (for PEMFC, 50-65%), conversion from DC to AC (95%). This results in an overall efficiency of 30%, approximately (Transport & Environment, 2021). For the alternative of ammonia as an energy vector, the transport losses could be solved, but because the cracking (the efficiency depends on the catalyst) and the Haber-Bosch process (60%), the final productivity from the power plant to the wheel is around 15% (Brown, 2017).

As for the price, in 2020 green hydrogen costed 1.508 €/10kWh (Hydrogen Council, 2020), while the ammonia was 0.620 €/10kWh. The difference in price could be explained for two reasons: the conversion factor of the specific energy (which for the hydrogen is larger) and because ammonia is more used and easier to transport than hydrogen (Shiozawa, 2020). A summary of all the characteristics for green and grey hydrogen and ammonia are presented in Table 7.4.

*Table 7.4. Summary of the characteristics of green and grey hydrogen and ammonia (Data extracted from: (Bicer et al., 2017; Boulamanti and Moya, 2017; U.S. DRIVE Partnership, 2017; Wilberforce et al., 2017; Hydrogen Council, 2020; NH<sub>3</sub> hydrofuel, 2020; Shiozawa, 2020; Smith, Hill and Torrente-Murciano, 2020)).*

	<b>Grey hydrogen (compressed)</b>	<b>Green hydrogen (compressed)</b>	<b>Grey ammonia</b>	<b>Green ammonia</b>
Specific energy (kWh/kg)	1.40		5.16	
Energy density (kWh/dm <sup>3</sup> )	1.00		3.14	
WTT* impact (g CO <sub>2</sub> eq/MJ)	113.0	9.5	161.5	10.8
Use as a fuel impact (g CO <sub>2</sub> eq/MJ)	0		0	
Price (€)	69000 (184 HP)		-	
Fuel price (€/10 kWh)	0.403	1.508	0.601	0.620

\*WTT: Well-To-Tank.

## 7.4. Discussion and comparison

The different characteristics and their production for fossil fuels (gasoline, diesel and CNG), electricity, hydrogen and ammonia have been explained. In this section, will be discussed which of the stated could be better in terms of price, environmental impact, and power. Furthermore, the future projections related to them will be discussed.

### 7.4.1. Fuel prices

The different prices (€/kWh) for each fuel are displayed in Figure 7.9. Gasoline, diesel, and green hydrogen present the highest fuel prices, while the lowest are for electricity and grey hydrogen.

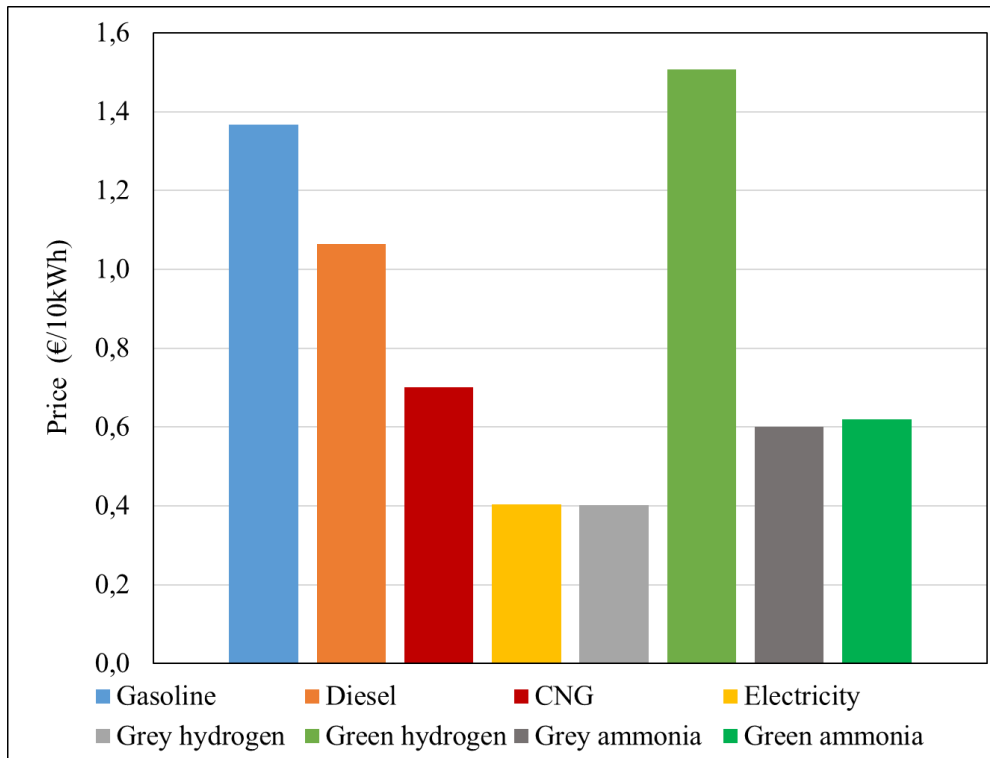


Figure 7.9. Comparison of the price for each fuel (€/kWh) (Data extracted from: (Boulamanti and Moya, 2017; Hydrogen Council, 2020; Shiozawa, 2020; Geoportal, 2021; REE, 2021b)).

Regarding gasoline and diesel, both have been experiencing an increasing price over the last decade in Europe. This cost includes the taxes dictated by Europe. However, the price at which these products are exported have fluctuated around 0.5 €/L. Therefore, taxes are a powerful tool to dissuade the use of these fuels. Europe has two main reasons to support alternative fuels. On one hand, the demand of energy is rapidly growing, as much as the population; thus, more fuel needs to be exported from other countries. This necessity forces Europe to become dependent on other countries to obtain energy. Moreover, promoting other alternative fuels which Europe itself can produce, can prevent from relying on others. On the other hand, due to the aim to become a zero-emissions society, Europe has to change the way the energy is produced. With increasing taxes, both issues can be addressed at once. As it has been explained previously, the demand of fossil fuel cars has been decreasing, which is an indicator that the taxes may have influenced positively (EEA, 2021).

Natural gas is the cheapest amongst the fossil fuels. As it has been seen, its production is much easier and does not require the same infrastructure as petrol refineries. However, as a fossil fuel, their taxes are high in order to prevent its use.

Green hydrogen is the most expensive fuel due to its scarce demand and technology. In fact, there are barely power plants that produce green hydrogen compared to grey hydrogen infrastructures. In addition, fuel cell technology is still new and, because it needs precious metals, it is expensive too. However, lately there have been arising projects to turn over this situation, like the plant that

Iberdrola plans to start in Puerto Llano (Ciudad Real) in 2021 (Iberdrola, 2020). Not only in Spain, but globally there are projects to create plants that could produce hydrogen by renewables, mostly wind power (Harrison *et al.*, 2010). An increase of production would allow to obtain more affordable hydrogen.

As seen in Figure 7.9, electricity and grey hydrogen are the cheapest fuels. The former is presented as an average value over the 2020. A more specific study over this same year could show how it fluctuates over the months and days and therefore, at certain time, it could no longer be the most economic fuel. Grey hydrogen has a low price as well. As a chemical product used in different sectors, contrary to green hydrogen, the production is well-established because the steam reforming method is a process known and optimized.

Similarly, grey ammonia has a established network, transportation and production. However, the price for this product is slightly more expensive than grey hydrogen because its price has to include the cost of grey hydrogen. Nevertheless, this tendency changes regarding the green fuels: ammonia is much cheaper than hydrogen. The ideal green ammonia production would be done next to the hydrogen plants in order to store the energy in ammonia, rather than in hydrogen. Because of storage and transportation terms, green ammonia is, currently a more feasible product than green hydrogen.

With regard to the price of each fuel, the best options could be electricity or grey hydrogen. Those can produce the same amount of energy, for less price than the other alternatives.

#### 7.4.2. Car prices

Figure 7.10 depicts the prices of certain light duty vehicles in the current market, which have a similar horsepower. The most economic options are the internal combustion engines, being gasoline, the most affordable and commonest choice. The novel alternatives have a higher price, and for the case of a hydrogen fuel cell car is almost four times more expensive than a gasoline-powered car.

Its price is determined mainly because of its demand and production. Currently, the sales for 2020 show that more than half of the vehicles acquired are powered by gasoline (ACEA, 2020). The automobile industry has optimised this production in order to make large amounts and at lower prices.

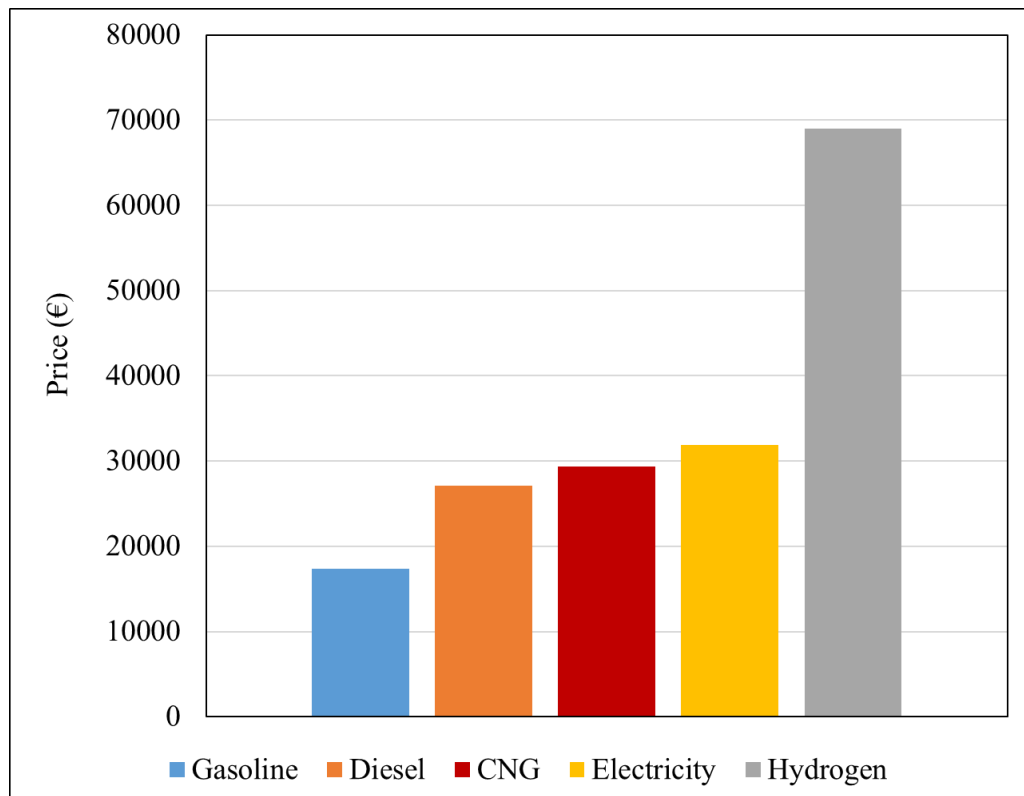


Figure 7.10. Comparison of car prices (€) depending on their fuel (Data extracted from: (Fiat, 2021; Hyundai, 2021b, 2021a; Peugeot, 2021; Skoda, 2021)).

To avoid this trend, other alternatives have to be fostered. Thus, industries would be forced to produce electric or fuel cell cars, and they could decrease in price and be affordable for a common consumer.

Within the European framework, there are norms that aim to reduce CO<sub>2</sub> emissions and improve the air quality by pressuring manufacturers to produce alternative vehicles. The Regulation (EU) 2019/613 and the Regulation (EU) 2019/318 for light-duty and heavy-duty vehicles, respectively, set a limit for the emissions that newly registered cars to be sold can produce. By 2021 for light-duty vehicles, the average emissions per kilometre for all the new models has to be lower than 95 g CO<sub>2</sub>/km. As it is a regulation, the enterprises which overpass the limit have to pay a fee of 95€ per each g/km exceed (Regulations (EU) 2019/813; Regulation (EU) 2019/631).

These regulations imply that the manufactures have to increase the production of alternative cars in order to obtain an average lower than 95 g CO<sub>2</sub>/km. With an increase of electric and hydrogen cars in the market, their price would be reduced.

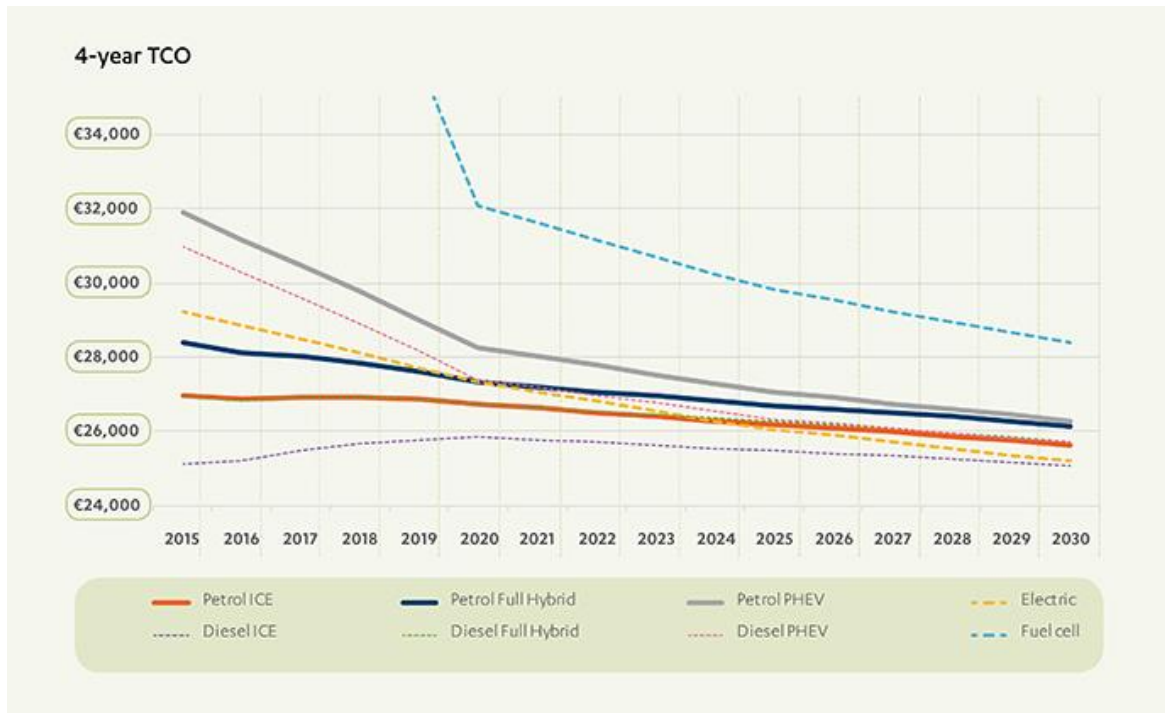


Figure 7.11. Projected evolution of 4 years of TCO for different fuelled vehicles (BEUC, 2016).

As it can be seen in Figure 7.11, the projected evolution of the Total Cost of Ownership (TCO)<sup>15</sup> for 4 years is plotted for different vehicle options. Overall, there is a decrease in the life cycle cost. However, the rate at which the cleaner alternatives reduce the price is steeper. This trend is consequence of Regulation (EU) 2019/613 and Regulation (EU) 2019/318, and national incentives like MOVES, in Spain (Regulations (EU) 2019/813; Regulation (EU) 2019/631). Although fossil fuel cars would decrease too, other alternatives would follow the same pattern and, indeed, by 2030 it is estimated that almost all alternatives would have similar prices. However, it is important to note, that hydrogen fuel cell cars are an exception. It will have an important decrease in cost but considering the investment in budget and time to build the new infrastructure, it is understandable that in ten years it will not reach the same price range as the other alternatives.

Moreover, regarding charging points, there are programmes (like Hydrogen Mobility Europe Programme H2ME1 and H2EM2) that intend to facilitate their mobility, by increasing the number of stations to recharge an electric or hydrogen car. Apart from raising the fleet of hydrogen cars in Europe, they have already set over 40 hydrogen station on Germany, France, United Kingdom, Denmark and Sweden (Hydrogen Mobility Europe, 2021). For the electric car, it already exists a network of charging points. However, in Spain, the Plan Nacional Integrado de Energía y Clima (PNIEC) has set the objective to have five million electric vehicles in circulation by 2030;

<sup>15</sup> TCO (Total Cost of Ownership) is the general cost of a product or service through a period of time, considering direct and indirect costs (EPA, 2020).

therefore, there are not enough charging points to supply such a demand (Resolución de 30 de diciembre).

### 7.4.3. Environmental impact

The environmental impact expressed in g CO<sub>2</sub> eq/MJ for the use in circulation (fuel impact in grey) and, the production of the fuel (WTT in black) is plotted in Figure 7.12. According to it, green ammonia and hydrogen produce less CO<sub>2</sub> through their production and use. When renewable sources are used for its production, there is only an emission due to the compression of hydrogen and the Haber-Bosch process for the ammonia because it has been considered the use of electricity with a European mix.

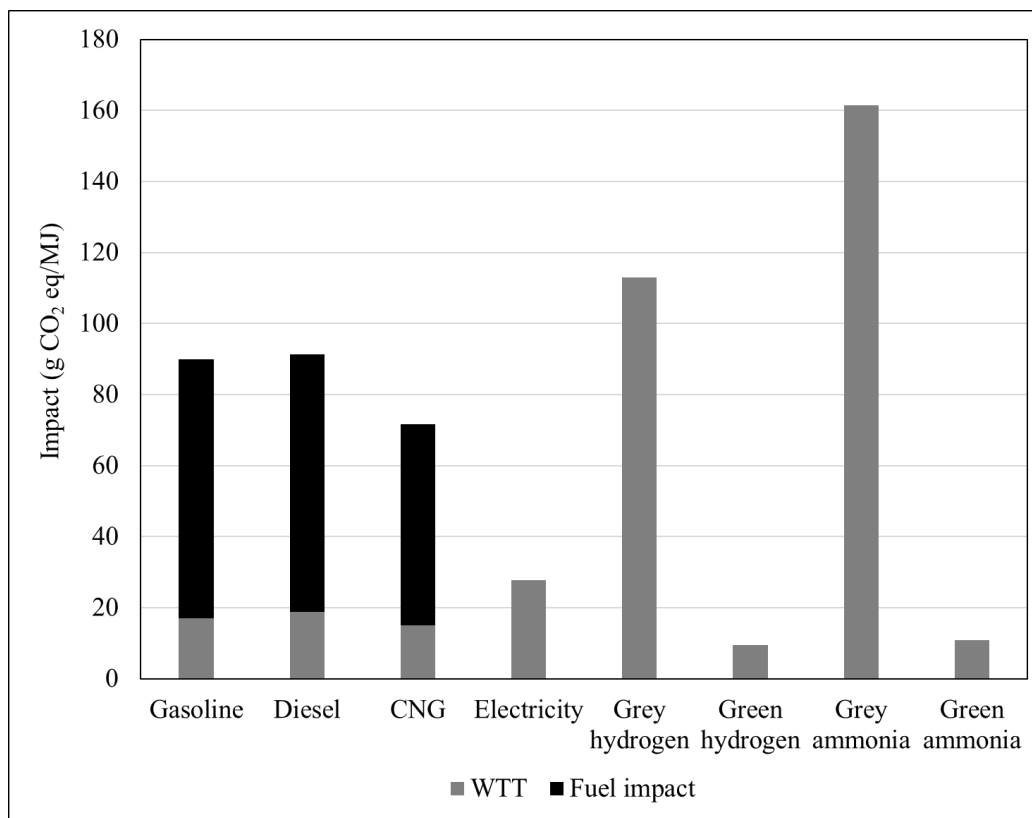


Figure 7.12. Comparison of the environmental impact (g CO<sub>2</sub> eq/MJ) for each fuel explained (Data extracted from: (Ngene *et al.*, 2016; Bicer *et al.*, 2017; Zijlema, 2018; EIA, 2020b; Prussi *et al.*, 2020; Prussi, M., Yugo, M., De Prada, L., Padella, M. and Edwards, 2020; REE, 2020; Smith, Hill and Torrente-Murciano, 2020)).

Following them, electricity is the third option in terms of less CO<sub>2</sub> emissions. It has been considered the use of the Spanish mix; thus, the impact is low because it has an almost equal ratio between renewables and no-renewables. Furthermore, within the PNIEC, there are set objectives to further increase the use of wind, solar power and other renewables.

It is well known that fossil fuel options have the biggest impact in terms of emissions in circulation. However, the refining process is not the most harmful out of the options presented. The largest impact is for the production by steam reforming of ammonia and hydrogen. This

demonstrates that producing them by this method does not solve any environmental problem, but further worsens it.

In addition, the direct and indirect emissions of CO<sub>2</sub> are always associated to the emission of air pollutants, due to the use of fossil fuels. That is why CO<sub>2</sub> and pollution follow the same trend.

Any large industry, like refineries or ammonia production are considered within IED. Their objective is to control any emission (air, water or soil) to prevent any harm to the environment or human health. Several policies are included, and the limit of the emissions is set by BAT, gathered in BREFs by IPCC. With this, industries assure that their emissions are as low as the current technology allows. Moreover, there are IED policies concerning petrol storage and transport because of their VOC (Directive 94/63/EC; Directive 2010/75/EU).

Unfortunately, these policies are not enough, and it will be always emission of pollutants and CO<sub>2</sub> as long as there are fossil fuels involved. Thus, the best choice of energy would be a renewable source, whether it would be green ammonia, green hydrogen or electricity.

Apart from the emissions into the atmosphere, there are other issues that have to be considered to fully describe the possible environmental impact of the fuels. The alternative options use a different mechanism in order to obtain energy. For the electricity is the Li-ion battery and for the hydrogen and ammonia are the catalysts used in the fuel cell and for the conversion on board. The use of lithium, platinum or other metals are scarce. Their production could become a problem if the demand of this kind of vehicles rises, because if they are not well-disposed, they could leach and contaminate the soil and the nearby waters. Therefore, as any of these metals can be extracted, they can be recycled.

#### 7.4.4. Storage and power

In theory, the optimal fuel has to be high energy density and high specific energy. These characteristics allow to have a small tank, filled with enough fuel, to power the vehicle to the established range. It is remarkable that the efficiency of the process to obtain the energy determines the size of the tank.

Figure 7.13 presents the fuels discussed by their energy density and specific energy. In this graph it can be seen that diesel and gasoline present the characteristics of an optimal fuel. Ideally, that would mean that internal combustion engines would require a small amount of fuel. However, because of the inefficiency of the process (around 25%), much more quantity of fuel is needed. Currently, their tank's capacity is about 45 L for 500 km range, which allows 35-40 kg of gasoline or diesel. With regard to natural gas, it has high specific energy, but low energy density due to its state. Considering a similar capacity and weight as for diesel and gasoline, the range obtained would be about 100-200 km. Knowing that the common range chosen for a car is about 350 to



500 km, CNG vehicles are not as competitive (Office of Energy Efficiency and Renewable Energy, 2020).

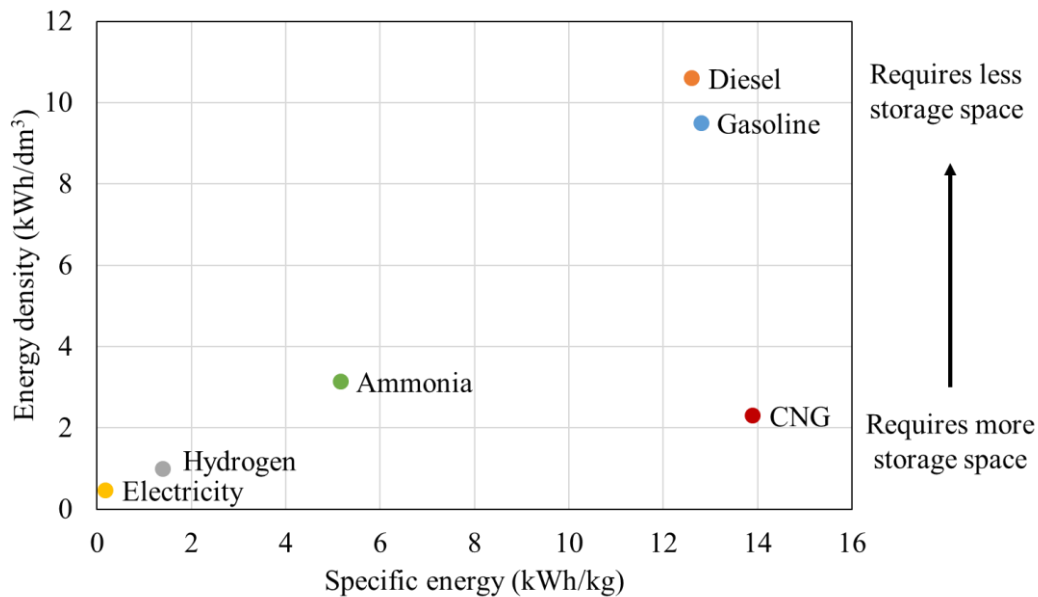


Figure 7.13. Representation of the energy density against the specific energy, for the different fuels explained (Data extracted from: (Nave, 2001; Cook, 2002; Kolb, 2017; U.S. DRIVE Partnership, 2017; Wilberforce *et al.*, 2017; Shen *et al.*, 2018; Ding *et al.*, 2019; Edwards *et al.*, 2020; Lazard, 2020)).

Within Figure 7.13, hydrogen (considering storage capacity) and electricity (considering Li-ion batteries) have the lowest energy density and specific energy. They require more storage space than gasoline and diesel and, to produce the same power as these fuels, they should weight more, as it is exemplified in Figure 7.14. Indeed, to assure that the vehicle would not need to be refuel until 500 km, the storage for hydrogen would weight 125 kg, for only 5 kg to 13 kg of hydrogen, as stated. For an electric battery (120 Wh/kg) it would need to be 830 kg, due to that the amount of energy stored depends on the mass of the battery (Wilberforce *et al.*, 2017).

Light-duty cars weight between 1300 kg and 1500 kg. For the hydrogen, 125 kg might not suppose radical changes for the vehicle. However, is almost three times heavier than the tanks for gasoline or diesel. With respect to electric batteries, as 830 kg is more than half the weight range, the structure should be modified. That is why, both options might not become the most suitable and competitive alternatives against fossil fuels (Bell and Torrente-Murciano, 2016; Wilberforce *et al.*, 2017).



Figure 7.14. Scheme of the comparison of weight and volume for diesel, hydrogen and an electric battery, to obtain an autonomy of 500 km (Wilberforce *et al.*, 2017).

One of the characteristics that allow the gasoline and diesel to be more feasible options is its liquid state. Then, if there were a hydrogen carrier that would be in this same phase, the problem of the weight might be solved. Ammonia has higher energy density and specific energy than hydrogen (stored) and batteries, but less than fossil fuels. Its network already exists, and the way to store it is by liquifying it. Moreover, it is a carbon-free compound, with one of the highest hydrogen contents. As ammonia can be liquefied, the similar structure of Liquefied Petroleum Gas (LPG) cars be used, in addition they have the same capacity as a gasoline tank (Jackson *et al.*, 2020).

For instance, assuming a tank capacity of 46 L, and a density of ammonia (in a liquified state) around  $650 \text{ kg}\cdot\text{m}^{-3}$  (7.5 bar and 20 °C), there will be 30 kg of ammonia, approximately. If the process of ammonia cracking is close to 100% efficiency (assuming that the process occurs at temperatures higher than 600 °C), 5.4 kg hydrogen could be extracted. This falls within the range of hydrogen to have an autonomy of 500 km. Thus, ammonia could be a feasible energy carrier and an alternative to other fuels. In addition, this calculation starts with a capacity of 46 L, but most common cars can have larger volumes, which allows to store more ammonia and, as a result, more hydrogen could be extracted (Jackson *et al.*, 2020).

#### 7.4.5. Criticism and conclusions

Once each comparison has been made, an overall conclusion must be extracted. To choose which of the fuels stated might be the best, all the indicators ought to be considered.

In general, in terms of price (fuel and car) the most affordable options are the internal combustion engines. However, policies and future projections, show how this could change in favour of cleaner options such as hydrogen or electric cars. The latter will become as affordable as fossil fuel options. The former will be unfeasible due to the recent start of this technology and its

infrastructure (compared to the electric cars). Hence, hydrogen needs more investments and time to become as used as electricity.

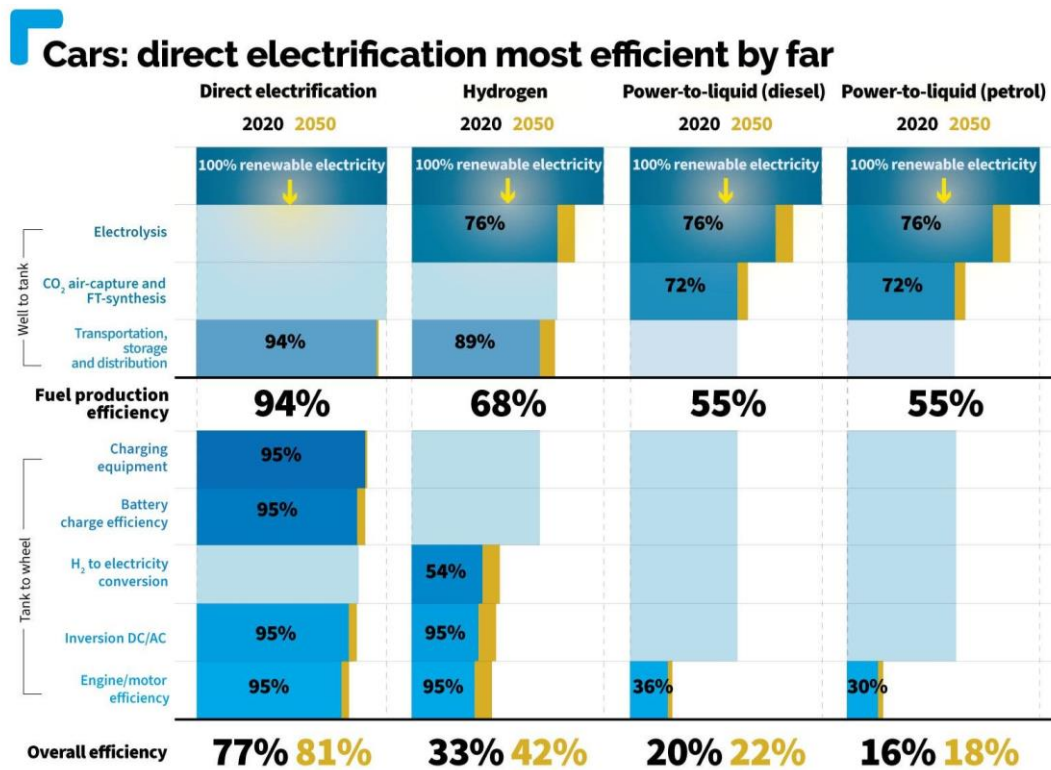
Regarding the environmental impact it is clear that using electricity or a green fuel (ammonia or hydrogen) is the best alternative to not emit pollutants or greenhouse gases. However, the disposal of fuel cells and batteries could be a concerning issue. In fact, in a near future, their demand would increase. Therefore, at the end of their life, the treatment has to be studied in order to diminish its possible impact and try to recycle its scarce components.

In terms of power and storage, the finest options are the liquid fossil fuels because their state and their high energy density. It is noteworthy, hydrogen or ammonia fuel cell cars can be as competitive as the internal combustion engines and, they achieve similar autonomies without having to create a heavier vehicle. For electric cars, their range is smaller than these options, because to be able to store more power, a heavier battery is needed. Thus, they could be a more suitable option for urban use, where the capacity range does not need to be so large. Similarly, fuel cell cars can be used in this same environment, but as they allow more autonomy, they are suitable for longer distances, too.

In conclusion, considering future changes, electric and fuel cell cars are the best option and might help into transforming a fossil fuel-based society into a cleaner energy production. Nonetheless, there are some opinions from renowned figures of the vehicle industry that have stated its disagreement with hydrogen as a fuel. They are justified by the fact that the overall production of hydrogen as a fuel (from power plant to wheel), is far less efficient than electricity.

The Chief Executive Officer of Tesla, Elon Musk, has shown his disagreement in different occasions on his Twitter account. He declares that fuel cells are “mind-bogglingly stupid” (Ivanenko, 2020) and that “fuel cells = fool sells” (see **Annex 10**) (Musk, 2020). Slightly less polar is Dr Rudolf Krebs, the Group Chief Officer of the Volkswagen *Aktiengesellschaft* for Electric Traction and General Manager. He believes that “no matter how excellent you make the cars themselves, the laws of physics hinder their overall efficiency. The most efficient way to convert energy to mobility is electricity.” (Blanco, 2013). He stated that a mighty alternative could be an electric car based on batteries with a hydrogen tank as a backup option.

As shown in Figure 7.15, both of them are right. As it has been previously stated, the use of electricity to power a car is far more efficient than hydrogen or ammonia. The reason is because of the multiple chemical transformations hydrogen and ammonia undergo to obtain energy.



Notes: To be understood as approximate mean values taking into account different production methods. Hydrogen includes onboard fuel compression. Excluding mechanical losses.

Figure 7.15. Scheme of the efficiencies of the different processes from WTW, for direct electrification, hydrogen and liquid fossil fuels (Transport & Environment, 2021).

Nevertheless, as also seen in Figure 7.15, the efficiency for gasoline or diesel is even smaller, although they are two of the most currently used fuels. That shows that even with such productivity, it does not mean that they cannot be used. Moreover, hydrogen or ammonia, appear to be easily incorporated in a vehicle structure, without too many modifications. In addition, they can produce the same power to be as competitive as fossil fuels. In the case of ammonia is even better because already existent structures, like LPG cars, can be used. For electric cars, although they might be more efficient, larger vehicles or increasing the range of light-duty vehicles would be problematic.

To sum up, hydrogen (or ammonia) and electricity have their advantages and disadvantages, and as seen in Figure 7.15, there is also room for improvements in this novel technology. Both options could be suitable as replacements of fossil fuel engines. Even though it seems that there are two sides, there is no need to choose whether to produce one or other. The cornerstone of the change relies on the use of green alternatives, no matters whether it is ammonia, hydrogen or electricity.

## 8. Conclusions

Bimetallic catalysts constitute a potential feasible solution to ensure a high conversion of ammonia at a competitive price. It has been exhibited that compared to Ni-based catalysts, the bimetallic combination performed better (Ni-Ru-b and Ni10-Ru5-b), as the conversion values were roughly 30% higher, at 450 °C. Nevertheless, no improvement could be recorded, at the same temperature, in comparison with Ru-based catalysts. The latter did achieve higher values than the bimetallic option, around 15%. Thus, the combinations studied in this work did not succeed in finding a substitute for Ru-based catalysts. It has been suggested that different combinations have to be analysed, like reducing Ru content, while increasing Ni content.

Other parameters have been analysed as well, like the support and the preparation methods used. Compared to the existent literature, it has been verified that ceria as a support improved the catalysts, regardless they were Ni-, Ru- or bimetallic based catalysts. In addition, the preparation did play an important role, thus catalysts prepared by BM did result in a more efficient ammonia conversion.

Through this work, apart from the initial objectives, some other outcomes have been found. By synthesising catalysts with BM, it did not only improve the conversion, but the order of addition when preparing the bimetallic catalysts did significantly change their performance. Therefore, when Ni was added first, followed by Ru (Ni-Ru-b and Ni10-Ru5-b), they had the best conversion values out of the three combinations studied. When further analysed, they showed a heterogeneous composition, in addition to some species that were not recorded yet in literature. So far, publications did show homogeneous compositions, highlighting the increasing presence of defects, when adding the metals. In this work, the same behaviour was recorded, but also other areas of the sample did not present the same spectrum, showing the oxidised species of the metals but not the band of defects. It was hypothesised that the heterogeneity did allow better values of ammonia conversion, where defects had a key role. In addition, it was suggested that this behaviour was enhanced by adding Ni first. More studies have to be made regarding this issue to identify the reason why the order did improve the conversion of ammonia and whether the heterogeneity does have a significant contribution.

Moreover, although the main topic was the bimetallic catalysts by BM, other conclusions have been extracted from monometallic Ni- and Ru-based catalyst. Regarding Ni-based catalysts, the wet samples showed little or no upgrade with respect with the dry ones. Furthermore, when the liquid of choice was ethanol, it worsened their ammonia conversion values over time. It is believed that by characterising these samples, it could be detected if there were carbon bonds on the surface and if so, whether their presence could decrease over time.

This has been a complex subject to tackle, as multiple parameters have to be taken into account and all of them could potentially contribute to the decomposition of ammonia. There is room for improvement and other studies isolating different parameters are needed to determine their role into the precise structure to obtain efficient catalysts.

Despite the outcomes on these catalysts, if the use of ammonia as an energy vector could not be suitable, the aim of this work would be in vain. Consequently, a whole discussion on this topic has been made, only to find that ammonia could be, indeed, a competitive option, along with hydrogen and electricity. It has been seen that there are polarised opinions on which option is better, but neither hydrogen, electricity nor ammonia are. Any of those should be welcomed to carry the change into a new society, where energy comes from green sources, friendly and respectful with the environment.

## 9. Bibliography

- ACEA (2020) *Fuel types of new cars: petrol 51.9%, diesel 29.4%, electric 7.2% market share second quarter 2020*. [online]. Available at: <https://www.acea.be/press-releases/article/fuel-types-of-new-cars-petrol-51.9-diesel-29.4-electric-7.2-market-share-se> (Accessed: 6 February 2021).
- Álvarez M, A., Centeno, M. Á. and Odriozola, J. A. (2016) ‘Ru-Ni Catalyst in the Combined Dry-Steam Reforming of Methane: The Importance in the Metal Order Addition’, *Topics in Catalysis*, 59(2–4), pp. 303–313. doi: 10.1007/s11244-015-0426-5.
- ARPA-E (2017) *Funding Opportunity Announcement Advanced Research Projects Agency – Energy ( Arpa-E ) Macroalgae Research Inspiring Novel Energy*.
- Ash, N. and Scarbrough, T. (2019) ‘Sailing on Solar. Could green ammonia decarbonise international shipping?’, *Ricardo Energy & Environment*, 53(2), p. 4.
- Australian Academy of Science (2020) *How has climate changed?*. [online]. Available at: <https://www.science.org.au/learning/general-audience/science-climate-change/2-how-has-climate-changed> (Accessed: 21 November 2020).
- Baede, A. P. M. *et al.* (2001) *The Climate System : an Overview*.
- Barrio, L. *et al.* (2010) ‘Unusual Physical and Chemical Properties of Ni in Ce<sub>1-x</sub>Ni<sub>x</sub>O<sub>2-y</sub> oxides: Structural characterization and catalytic activity for the water gas shift reaction’, *Journal of Physical Chemistry C*, 114(29), pp. 12689–12697. doi: 10.1021/jp103958u.
- Bell, T. E. and Torrente-Murciano, L. (2016) ‘H<sub>2</sub> Production via Ammonia Decomposition Using Non-Noble Metal Catalysts : A Review’, *Topics in Catalysis*. Springer US, 59(15), pp. 1438–1457. doi: 10.1007/s11244-016-0653-4.
- BEUC (2016) *Future fuel efficient cars set to boost consumer savings, study shows*. [online]. Available at: <https://www.beuc.eu/publications/future-fuel-efficient-cars-set-boost-consumer-savings-study-shows/html> (Accessed: 1 April 2021).
- Bicer, Y. *et al.* (2017) ‘Impact Assessment and Environmental Evaluation of Various Ammonia Production Processes’, *Environmental Management*. Springer US, 59(5), pp. 842–855. doi: 10.1007/s00267-017-0831-6.
- Blanco, S. (2013) *VW’s Krebs talks hydrogen, says ‘most efficient way to convert energy to mobility is electricity’*, *Autoblog*. [online]. Available at: <https://www.autoblog.com/2013/11/20/vws-krebs-talks-hydrogen-says-most-efficient-way-to-convert/> (Accessed: 5 April 2021).
- Boulamanti, A. and Moya, J. A. (2017) ‘Production costs of the chemical industry in the EU and other countries: Ammonia, methanol and light olefins’, *Renewable and Sustainable Energy Reviews*, 68, pp. 1205–1212. doi: 10.1016/j.rser.2016.02.021.
- BP (2020) ‘Statistical Review of World Energy globally consistent data on world energy markets . and authoritative publications in the field of energy The Statistical Review world of World Energy and data on world energy markets from is The Review has been providing’, p. 66.
- Brown, T. (2017) *Round-trip Efficiency of Ammonia as a Renewable Energy Transportation*

- Media, Ammonia Energy Association.* [online]. Available at: <https://www.ammoniaenergy.org/articles/round-trip-efficiency-of-ammonia-as-a-renewable-energy-transportation-media/> (Accessed: 5 April 2021).
- Butler, K. T., Frost, J. M. and Walsh, A. (2015) ‘Ferroelectric materials for solar energy conversion: Photoferroics revisited’, *Energy and Environmental Science*, 8(3), pp. 838–848. doi: 10.1039/c4ee03523b.
- CAPP (2020) *Oil extraction.* [online]. Available at: <https://www.capp.ca/oil/extraction/> (Accessed: 8 February 2021).
- Chellappa, A. S., Fischer, C. M. and Thomson, W. J. (2002) ‘Ammonia decomposition kinetics over Ni-Pt/Al<sub>2</sub>O<sub>3</sub> for PEM fuel cell applications’, *Applied Catalysis A: General*, 227(1–2), pp. 231–240. doi: 10.1016/S0926-860X(01)00941-3.
- Chen, J. *et al.* (1999) ‘Nickel Hydroxide as an Active Material for the Positive Electrode in Rechargeable Alkaline Batteries’, *Journal of The Electrochemical Society*, 146(10), pp. 3606–3612. doi: 10.1149/1.1392522.
- Choudhary, T. V., Sivadinarayana, C. and Goodman, D. W. (2009) ‘Catalytic ammonia decomposition: CO<sub>x</sub>-free hydrogen production for fuel cell applications’, *Catalysis Letters*, 72(3), pp. 193–194.
- Chung, D. B. *et al.* (2017) ‘Enhanced ammonia dehydrogenation over Ru/La<sub>(x)</sub>-Al<sub>2</sub>O<sub>3</sub> (x = 0–50 mol%): Structural and electronic effects of La doping’, *International Journal of Hydrogen Energy*. Elsevier Ltd, 42(3), pp. 1639–1647. doi: 10.1016/j.ijhydene.2016.08.020.
- CLARS (2021) *Urban Acces Regulations in Europe.* [online]. Available at: <https://urbanaccessregulations.eu/userhome/map> (Accessed: 1 June 2021).
- Climate Action Tracker (2020) *Addressing global warming.* [online]. Available at: <https://climateactiontracker.org/global/temperatures/> <https://climateactiontracker.org/global/temperatures/> (Accessed: 21 November 2020).
- Climate Watch (2020) *Global Historical Emissions.* [online]. Available at: [https://www.climatewatchdata.org/ghg-emissions?breakBy=sector&chartType=percentage&end\\_year=2016&source=CAIT&start\\_year=1990](https://www.climatewatchdata.org/ghg-emissions?breakBy=sector&chartType=percentage&end_year=2016&source=CAIT&start_year=1990) (Accessed: 21 November 2020).
- Conselleria d’Agricultura, Desenvolupament Rural (2015) *La contaminación atmosférica, Generalitat Valenciana.* [online]. Available at: <http://www.agroambient.gva.es/en/web/calidad-ambiental/la-contaminacion-atmosferica> (Accessed: 25 October 2019).
- Cook, B. (2002) ‘Introduction to fuel cells and hydrogen technology’, (December), pp. 205–216.
- Daly, A. and Zannetti, P. (2007) ‘An Introduction to Air Pollution – Definitions, Classifications, and History’, in *Ambient Air Pollution*, pp. 1–14.
- Dieselnet (2019) *EU: Cars and Light-Trucks.* [online]. Available at: <https://dieselnet.com/standards/eu/ld.php> (Accessed: 24 April 2021).
- Ding, Y. *et al.* (2019) ‘Automotive Li-Ion Batteries: Current Status and Future Perspectives’, *Electrochemical Energy Reviews*. Springer Singapore, 2(1), pp. 1–28. doi: 10.1007/s41918-018-0022-z.



- Dujim, N. J., Markert, F. and Paulsen, J. L. (2005) *Safety assessment of ammonia as a transport fuel*. Denmark. [online]. Available at: [www.risoe.dk](http://www.risoe.dk).
- Edwards, P. P. *et al.* (2020) ‘Hydrogen and fuel cells : Towards a sustainable energy future’, *Energy Policy*, 36(2008), pp. 4356–4362. doi: 10.1016/j.enpol.2008.09.036.
- EEA (2016) *Some common air pollutants*, European Environment Agency. [online]. Available at: <https://www.eea.europa.eu/publications/2599XXX/page008.html> (Accessed: 27 October 2020).
- EEA (2019) *Exceedance of air quality standards in Europe*. [online]. Available at: <https://www.eea.europa.eu/data-and-maps/indicators/exceedance-of-air-quality-limit-2/assessment> (Accessed: 24 April 2021).
- EEA (2021) *Transport fuel prices and taxes in Europe* [online]. Available at: <https://www.eea.europa.eu/data-and-maps/indicators/fuel-prices-and-taxes/assessment-5> (Accessed: 24 April 2021).
- EEA (2020a) *Air pollution*. [online]. Available at: <https://www.eea.europa.eu/themes/air> (Accessed: 13 April 2021).
- EEA (2020b) *Air quality in Europe - 2020 report*, EEA Report. [online]. Available at: <https://www.eea.europa.eu/publications/air-quality-in-europe-2020-report>.
- Eftekhari, A. (2019) ‘Lithium Batteries for Electric Vehicles: From Economy to Research Strategy’, *ACS Sustainable Chemistry and Engineering*, 7(6), pp. 5602–5613. doi: 10.1021/acssuschemeng.8b01494.
- EIA (2020a) *Diesel fuel explained*. [online]. Available at: <https://www.eia.gov/energyexplained/diesel-fuel/diesel-and-the-environment.php> (Accessed: 29 March 2021).
- EIA (2020b) *Natural gas explained*. [online]. Available at: <https://www.eia.gov/energyexplained/natural-gas/> (Accessed: 8 February 2021).
- EIA (2020c) *Oil and petroleum products explained*. [online]. Available at: <https://www.eia.gov/energyexplained/oil-and-petroleum-products/refining-crude-oil-the-refining-process.php> (Accessed: 6 February 2021).
- Electromaps (2021) *Punt de càrrega a Espanya*. [online]. Available at: <https://www.electromaps.com/ca/punts-de-recarrega/espana> (Accessed: 19 February 2021).
- EPA (1991) ‘Synthetic Ammonia’, 93, pp. 1–6. Available at: <https://www3.epa.gov/ttnchie1/ap42/ch08/final/c08s01.pdf> (Accessed: 19 February 2021).
- EPA (2006) ‘How Air Pollution Affets the View’, (April).
- EPA (2019) *Air Topics*, EPA. [online]. Available at: <https://www.epa.gov/environmental-topics/air-topics> (Accessed: 27 October 2019).
- EPA (2020) *TCO, EPA*. [online]. Available at: <https://www.epa.gov/sites/production/files/documents/costofown.pdf> (Accessed: 3 June 2021).
- EU Science Hub (2020) *Global CO<sub>2</sub> emissions continue to rise but EU bucks globa trend*. [online]. Available at: <https://ec.europa.eu/jrc/en/news/global-co2-emissions-continue-rise-eu-bucks-global-trend> (Accessed: 23 November 2020).

European Commission (2013) 'A Clean Air Program for Europe', *Com*, 918, p. 11. Available at: <https://eur-lex.europa.eu/legal-content/EN/TXT/PDF/?uri=CELEX:52013DC0918&from=EN%0Ahttp://eur-lex.europa.eu/legal-content/EN/TXT/PDF/?uri=CELEX:52013DC0918&from=EN>.

European Commission (2014a) *Cleaner air for all, European Commission*. [online]. Available at: [https://ec.europa.eu/environment/air/cleaner\\_air/#toolbox](https://ec.europa.eu/environment/air/cleaner_air/#toolbox) (Accessed: 27 October 2019).

European Commission (2018) 'A Clean Planet for all. A European strategic long-term vision for a prosperous, modern, competitive and climate neutral economy'. Brussels, p. 25.

European Commission (2019a) *Cleaner air for all*. [online]. Available at: [https://ec.europa.eu/environment/air/cleaner\\_air/](https://ec.europa.eu/environment/air/cleaner_air/) (Accessed: 13 April 2021).

European Commission (2019) *Clean air for all*. [online]. Available at: [https://ec.europa.eu/environment/air/cleaner\\_air/](https://ec.europa.eu/environment/air/cleaner_air/) (Accessed: 24 April 2021).

Eurostat Statistics Explained (2017) *Glossary: Carbon dioxide equivalent*. [online]. Available at: [https://ec.europa.eu/eurostat/statistics-explained/index.php/Glossary:Carbon\\_dioxide\\_equivalent](https://ec.europa.eu/eurostat/statistics-explained/index.php/Glossary:Carbon_dioxide_equivalent) (Accessed: 6 February 2021).

Fiat (2021) *Tipo Cross MCA*. [online]. Available at: <https://www.fiat.es/tipo/tipo-cross-hatchback> (Accessed: 19 February 2021).

Fischer, J. M. (2013) 'Handbook of Molded Part Shrinkage and Warpage'. 2nd ed. Oxford: William Andrew.

Gan, Y. *et al.* (2020) 'Carbon footprint of global natural gas supplies to China', *Nature Communications*. Springer US, 11(1), pp. 1–9. doi: 10.1038/s41467-020-14606-4.

García-bordejé, E. *et al.* (2014) 'Toward Practical Application Of H<sub>2</sub> Generation From Ammonia Decomposition Guided by Rational Catalyst Design', *Catalysis Reviews: Science and Engineering*. Taylor & Francis, 56(2), pp. 220–237. doi: 10.1080/01614940.2014.903637.

García-García, F. R. *et al.* (2010) 'The use of carbon nanotubes with and without nitrogen doping as support for ruthenium catalysts in the ammonia decomposition reaction', *Carbon*, 48(1), pp. 267–276. doi: 10.1016/j.carbon.2009.09.015.

Geng, P. *et al.* (2017) 'Effects of alternative fuels on the combustion characteristics and emission products from diesel engines: A review', *Renewable and Sustainable Energy Reviews*. Elsevier Ltd, 71(December 2016), pp. 523–534. doi: 10.1016/j.rser.2016.12.080.

*Geoportal* (2021). [online]. Available at: <https://geoportalgasolineras.es/#/Inicio> (Accessed: 10 February 2021).

Giovannini, S. (2020) *50 shades of (grey and blue and green) hydrogen*. [online]. Available at: <https://energy-cities.eu/50-shades-of-grey-and-blue-and-green-hydrogen/> (Accessed: 29 March 2021).

González, C. (2019) *¿Cuántos puntos de recarga de vehículos eléctricos hay en España?*, *BBVA*. [online]. Available at: <https://www.bbva.com/es/cuantos-puntos-de-recarga-de-vehiculos-electricos-hay-en-espana/> (Accessed: 29 March 2021).

H2 (2021) *Filling up with Hydrogen, H2*. [online]. Available at: <https://h2.live/en> (Accessed: 29 March 2021).

- Han, X. *et al.* (2007) ‘Promoting effects of iridium on nickel based catalyst in ammonia decomposition’, *Journal of Fuel Chemistry and Technology*, 35(6), pp. 691–695. doi: 10.1016/S1872-5813(08)60004-3.
- Harrison, K. W. *et al.* (2010) ‘Hydrogen Production: Fundamentals and Case Study Summaries e Preprint’, *18th World Hydrogen Energy Conference*, (January). Available at: <http://www.osti.gov/bridge>.
- He, L. *et al.* (2019) ‘Morphology-dependent catalytic activity of Ru/CeO<sub>2</sub> in dry reforming of methane’, *Molecules*, 24(3), pp. 13–15. doi: 10.3390/molecules24030526.
- Hoekstra, A. (2020) *Producing gasoline and diesel emits more CO<sub>2</sub> than we thought*, *Innovation Origins*. [online]. Available at: <https://innovationorigins.com/producing-gasoline-and-diesel-emits-more-co2-than-we-thought/> (Accessed: 6 February 2021).
- House, S. D. *et al.* (2015) ‘Effect of ball-milling duration and dehydrogenation on the morphology, microstructure and catalyst dispersion in Ni-catalyzed MgH<sub>2</sub> hydrogen storage materials’, *Acta Materialia*. Acta Materialia Inc., 86, pp. 55–68. doi: 10.1016/j.actamat.2014.11.047.
- Huang, Y. S. and Liao, P. C. (1998) ‘Preparation and characterization of RuO<sub>2</sub> thin films’, *Solar Energy Materials and Solar Cells*, 55(1–2), pp. 179–197. doi: 10.1016/S0927-0248(98)00057-9.
- Hydrogen Council (2020) *Path to hydrogen competitiveness: a cost perspective*. [online] Available at: [www.hydrogencouncil.com](http://www.hydrogencouncil.com) (Accessed: 29 March 2021).
- Hydrogen Mobility Europe (2021) ‘About’. [online]. Available at: <https://h2me.eu/about/> (Accessed: 29 March 2021).
- Hyundai (2021a) *Hyundai NEXO*. [online]. Available at: <https://www.hyundai.com/es/modelos/nexo.html> (Accessed: 6 March 2021).
- Hyundai (2021b) *Nuevo Hyundai i10*. [online]. Available at: <https://www.hyundai.com/es/modelos/nuevo-i10/configuracion.html#/trims> (Accessed: 11 February 2021).
- Iberdrola (2020) *Planta de Hidrógeno Verde de Puertollano*. [online]. Available at: <https://www.iberdrola.com/conocenos/lineas-negocio/proyectos-emblematicos/puertollano-planta-hidrogeno-verde> (Accessed: 29 March 2021).
- IPCC (1990) *CLIMATE CHANGE, The IPCC Scientific Assessment*. Bracknell.
- IUPAC (2019) *Catalyst, Gold Book*. [online]. Available at: <http://goldbook.iupac.org/terms/view/C00876> (Accessed: 24 October 2020).
- Ivanenko, A. (2020) ‘It’s Time For Elon Musk to Admit The Significance of Hydrogen Fuel Cells’, *Forbes*. [online]. Available at: <https://www.forbes.com/sites/forbestechcouncil/2020/11/02/its-time-for-elon-musk-to-admit-the-significance-of-hydrogen-fuel-cells/?sh=75314c8c20f6>.
- Jackson, C. *et al.* (2020) *Ammonia to green hydrogen project. Feasibility study*.
- Jacques, P.-A. (2011) *Hydrogen fuel Quality requirements for transportation and other energy applications*, *TRIMS*. [online]. Available at: <https://trimis.ec.europa.eu/project/hydrogen-fuel-quality-requirements-transportation-and-other-energy-applications#tab-results> (Accessed: 5 November 2020).

- Jaskula, B. W. (2015) 'Minerals Yearbooks: Lithium, 1994-2015', (November). Available at: <https://minerals.usgs.gov/minerals/pubs/commodity/lithium/myb1-2015-lithi.pdf>.
- Jones, R. R. *et al.* (2019) 'Raman Techniques: Fundamentals and Frontiers', *Nanoscale Research Letters*. *Nanoscale Research Letters*, 14(1). doi: 10.1186/s11671-019-3039-2.
- Kang, I. C. *et al.* (2008) 'Preparation of a visible sensitive carbon doped TiO<sub>2</sub> photo-catalyst by grinding TiO<sub>2</sub> with ethanol and heating treatment', *Applied Catalysis B: Environmental*, 80(1–2), pp. 81–87. doi: 10.1016/j.apcatb.2007.11.005.
- Karim, W. *et al.* (2017) 'Catalyst support effects on hydrogen spillover', *Nature Publishing Group*. *Nature Publishing Group*, 541, pp. 68–71. doi: 10.1038/nature20782.
- Kirste, K. G. *et al.* (2021) 'CO<sub>x</sub>-free hydrogen production from ammonia – mimicking the activity of Ru catalysts with unsupported Co-Re alloys', *Applied Catalysis B: Environmental*. Elsevier, 280(August 2020), p. 119405. doi: 10.1016/j.apcatb.2020.119405.
- Kolb, O. (2017) *Deployment of Alternative Fuels Infrastructure - Fuel Price Comparison*.
- Koroneos, C. *et al.* (2004) 'Life cycle assessment of hydrogen fuel production processes', *International Journal of Hydrogen Energy*, 29(14), pp. 1443–1450. doi: 10.1016/j.ijhydene.2004.01.016.
- Kozawa, T. (2021) 'Combined wet milling and heat treatment in water vapor for producing amorphous to crystalline ultrafine Li<sub>1.3</sub>Al<sub>0.3</sub>Ti<sub>1.7</sub>(PO<sub>4</sub>)<sub>3</sub> solid electrolyte particles', *RSC Advances*. Royal Society of Chemistry, 11(24), pp. 14796–14804. doi: 10.1039/d1ra02039k.
- Lamb, K. E., Dolan, M. D. and Kennedy, D. F. (2018) 'Ammonia for hydrogen storage: A review of catalytic ammonia decomposition and hydrogen separation and purification', *International Journal of Hydrogen Energy*. Elsevier Ltd, 44(7), pp. 3580–3593. doi: 10.1016/j.ijhydene.2018.12.024.
- Lazard (2020) *Levelized Cost of Energy and Levelized Cost of Storage-2020*. [online]. Available at: <https://www.lazard.com/perspective/levelized-cost-of-energy-and-levelized-cost-of-storage-2020/> (Accessed: 27 November 2020).
- Li, G. *et al.* (2019) 'Raman spectroscopy evidence for dimerization and Mott collapse in  $\alpha$ -RuCl<sub>3</sub> under pressures', *Physical Review Materials*. American Physical Society, 3(2), pp. 51–54. doi: 10.1103/PhysRevMaterials.3.023601.
- Li, X. K. *et al.* (2005) 'Ammonia decomposition over Ru and Ni catalysts supported on fumed SiO<sub>2</sub>, MCM-41, and SBA-15', *Journal of Catalysis*, 236(2), pp. 181–189. doi: 10.1016/j.jcat.2005.09.030.
- Lindsey, R. (2020) *Climate Change: Atmospheric Carbon Dioxide*, NOAA. [online]. Available at: <https://www.climate.gov/news-features/understanding-climate/climate-change-atmospheric-carbon-dioxide> (Accessed: 21 November 2020).
- Liu, H. *et al.* (2008) 'Preparation, characterization and activities of the nano-sized Ni/SBA-15 catalyst for producing CO<sub>x</sub>-free hydrogen from ammonia', *Applied Catalysis A: General*, 337(2), pp. 138–147. doi: 10.1016/j.apcata.2007.12.006.
- Llorca, J. (2010) *El hidrógeno y nuestro futuro energético*. Barcelona: Edicions UPC.
- Loridant, S. (2020) 'Raman spectroscopy as a powerful tool to characterize ceria-based catalysts',

- Catalysis Today*. Elsevier, (November 2019), pp. 1–14. doi: 10.1016/j.cattod.2020.03.044.
- Lucentini, I. *et al.* (2021a) ‘Catalytic ammonia decomposition over Ni-Ru supported on CeO<sub>2</sub> for hydrogen production: Effect of metal loading and kinetic analysis’, *Applied Catalysis B: Environmental*, 286(December 2020). doi: 10.1016/j.apcatb.2021.119896.
- Lucentini, I. *et al.* (2021b) ‘Review of the Decomposition of Ammonia to Generate Hydrogen’, *Industrial & Engineering Chemistry Research*, **Article ASAP**. doi: 10.1021/acs.iecr.1c00843.
- Lucentini, I., Casanovas, A. and Llorca, J. (2019) ‘Catalytic ammonia decomposition for hydrogen production on Ni, Ru and Ni-Ru supported on CeO<sub>2</sub>’, *International Journal of Hydrogen Energy*, 44(25), pp. 12693–12707. doi: 10.1016/j.ijhydene.2019.01.154.
- Lv, C. *et al.* (2020) ‘Triple Functions of Ni(OH)<sub>2</sub> on the Surface of WN Nanowires Remarkably Promoting Electrocatalytic Activity in Full Water Splitting’, *ACS Catalysis*, 10(22), pp. 13323–13333. doi: 10.1021/acscatal.0c02891.
- Makepeace, J. W. *et al.* (2015) ‘Ammonia decomposition catalysis using non-stoichiometric lithium imide’, *Chemical Science*. Royal Society of Chemistry, 6(7), pp. 3805–3815. doi: 10.1039/c5sc00205b.
- Marin, E. (2020) ‘Síntesis Mecanoquímica de Catalizadores Ni/CeO<sub>2</sub> para la Producción de hidrógeno a partir de la reacción de descomposición de amoníaco’, p. 76.
- Masnadi, M., El-Houjeiri, H. and Schunack, D. (2018) ‘Global carbon intensity of crude oil production’, *Science*, 361(6405), p. 3.
- McCullough, K. *et al.* (2020) ‘Material discovery and high throughput exploration of Ru based catalysts for low temperature ammonia decomposition’, *Materials*, 13(8), pp. 1–19. doi: 10.3390/MA13081869.
- Ministerio para la Transición Ecológica (2016) *Gases Eutrofizantes*, *Gobierno de España*. [online]. Available at: [https://www.miteco.gob.es/gl/calidad-y-evaluacion-ambiental/temas/atmosfera-y-calidad-del-aire/emisiones/prob-amb/gases\\_eutrofizantes.aspx](https://www.miteco.gob.es/gl/calidad-y-evaluacion-ambiental/temas/atmosfera-y-calidad-del-aire/emisiones/prob-amb/gases_eutrofizantes.aspx) (Accessed: 27 October 2019).
- Ministerio para la Transición Ecológica (2019) *Gas Natural y Medio Ambiente*. Available at: <https://energia.gob.es/gas/Gas/Paginas/gasnatural.aspx> (Accessed: 10 February 2021).
- Mironova-Ulmane, N. *et al.* (2007) ‘Raman scattering in nanosized nickel oxide NiO’, *Journal of Physics: Conference Series*, 93(1), pp. 0–5. doi: 10.1088/1742-6596/93/1/012039.
- Mogensen, M., Sammes, N. M. and Tompsett, G. A. (2000) ‘Physical, chemical and electrochemical properties of pure and doped ceria’, *Solid State Ionics*, 129(1–4), pp. 63–94.
- Mukherjee, S. *et al.* (2018) ‘Low-temperature ammonia decomposition catalysts for hydrogen generation’, *Applied Catalysis B: Environmental*. Elsevier, 226(August 2017), pp. 162–181. doi: 10.1016/j.apcatb.2017.12.039.
- Murli, C. *et al.* (2001) ‘High-pressure behavior of  $\beta$ -Ni(OH)<sub>2</sub> - A Raman scattering study’, *Physica B Condensed Matter*, 307(1–4), pp. 111–116. doi: 10.1016/S0921-4526(01)00646-9.
- Musk, E. (2020) *fuel cells = fool sells*, *Twitter*. [online]. Available at: <https://twitter.com/elonmusk/status/1270991790401699841> (Accessed: 2 June 2021).

- Narins, T. P. (2017) ‘The battery business: Lithium availability and the growth of the global electric car industry’, *Extractive Industries and Society*. Elsevier Ltd., 4(2), pp. 321–328. doi: 10.1016/j.exis.2017.01.013.
- NASA (2020a) *Climate Change: How Do We Know?* [online]. Available at: <https://climate.nasa.gov/evidence/> (Accessed: 21 November 2020).
- NASA (2020b) *Global Temperature*. [online]. Available at: <https://climate.nasa.gov/vital-signs/global-temperature/> (Accessed: 21 November 2020).
- NASA (2020c) *The Causes of Climate Change*. [online]. Available at: <https://climate.nasa.gov/causes/> (Accessed: 21 November 2020).
- Nave, C. R. (2001) *Hydrogen Fuel Cell, Hyperphysics*. [online]. Available at: <http://hyperphysics.phy-astr.gsu.edu/hbase/thermo/electrol.html#c2> (Accessed: 24 October 2020).
- Ngene, S. *et al.* (2016) ‘Environmental and Economic Impacts of Crude Oil and Natural Gas Production in Developing Countries’, *International Journal of Economy, Energy and Environment*, 1(3), pp. 64–73. doi: 10.11648/j.ijeee.20160103.13.
- NH<sub>3</sub> hydrofuel (2020) *Is Ammonia the Ideal Energy Currency*. [online]. Available at: <https://www.nh3fuel.com/index.php/faqs/16-ammonia/35-is-ammonia-the-ideal-energy-currency> (Accessed: 6 March 2021).
- NOAA (2020) *Temperature Change and Carbon Dioxide Change*. [online]. Available at: <https://www.ncdc.noaa.gov/global-warming/temperature-change> (Accessed: 21 November 2020).
- OCU (2018) *La transición a los coches ecológicos*. [online]. Available at: <https://www.ocu.org/coches/gasolina-y-carburantes/noticias/informe-beuc-coste-automovil> (Accessed: 6 February 2021).
- Office of Energy Efficiency and Renewable Energy (2020) *Hydrogen storage*. [online]. Available at: <https://www.energy.gov/eere/fuelcells/hydrogen-storage> (Accessed: 6 March 2021).
- Okura, K. *et al.* (2016) ‘Ammonia Decomposition over Nickel Catalysts Supported on Rare-Earth Oxides for the On-Site Generation of Hydrogen’, *ChemCatChem*, 8(18), pp. 2988–2995. doi: 10.1002/cctc.201600610.
- Ordoñez, J., Gago, E. J. and Girard, A. (2016) ‘Processes and technologies for the recycling and recovery of spent lithium-ion batteries’, *Renewable and Sustainable Energy Reviews*. Elsevier, 60, pp. 195–205. doi: 10.1016/j.rser.2015.12.363.
- Pachauri, R. K. and Meyer, L. A. (2014) *Climate Change 2014: Synthesis Report. Contribution of Working Groups I, II and III to the Fifth Assessment Report of the Intergovernmental Panel of Climate Change*. Geneva, Switzerland.
- Peugeot (2021) *Peugeot e-208*. [online]. Available at: <https://www.peugeot.es/gama/selector-de-coches/peugeot-208/configurador/colores-y-tapiceria.html> (Accessed: 24 February 2021).
- Pinzón, M. *et al.* (2021) ‘Hydrogen production by ammonia decomposition over ruthenium supported on SiC catalyst’, *Journal of Industrial and Engineering Chemistry*, 94, pp. 326–335. doi: 10.1016/j.jiec.2020.11.003.

- Prasad, R. and Venkateswara, B. R. (2010) 'A review on Diesel Soot Emission, its Effects and Control', *Bulletin of Chemical Reaction Engineering and Catalysis*, 5(2).
- Prigent, M. (1997) 'On Board Hydrogen Generation for Fuel Cell Powered Electric Cars', *Revue De L'Institut Français Du Pétrole*, 52, pp. 349–360.
- Prussi, M., Yugo, M., De Prada, L., Padella, M. and Edwards, R. (2020) *JEC Well-to-Tank report v5*. Luxemburg. doi: 10.2760/959137.
- Prussi, M. *et al.* (2020) *JEC Well-To-Wheels report v5*. Luxemburg. doi: 10.2760/100379.
- REE (2020) *Emisiones y factor de emisión de co2 eq. De la generación*. [online]. Available at: <https://www.ree.es/es/datos/generacion/no-renovables-detalle-emisiones-CO2> (Accessed: 19 February 2021).
- REE (2021a) *Balance eléctrico*. [online]. Available at: <https://www.ree.es/es/datos/balance/balance-electrico> (Accessed: 19 February 2021).
- REE (2021b) *Mercados*. [online]. Available at: <https://www.ree.es/es/datos/mercados> (Accessed: 10 February 2021).
- Regalbuto, J. (2016) *Catalysts Preparation*. Edited by J. Regalbuto. Boca Ratón: CRC Press.
- Registro Estatal de Emisiones y Fuentes Contaminantes (2019) *Óxido Nitroso, Ministerio para la Transición Ecológica*. [online]. Available at: <https://www.miteco.gob.es/es/calidad-y-evaluacion-ambiental/temas/atmosfera-y-calidad-del-aire/calidad-del-aire/salud/oxidos-nitrogeno.aspx> (Accessed: 10 February 2021).
- Ritchie, H. and Roser, M. (2014) *Energy, Our World in Data*. [online]. Available at: <https://ourworldindata.org/energy#citation> (Accessed: 19 February 2021).
- Sadykov, V. A. *et al.* (2019) 'Advanced Materials for Solid Oxide Fuel Cells and Membrane Catalytic Reactors', in *Advanced Nanomaterials for Catalysis and Energy*. Elsevier Inc., pp. 435–514. doi: 10.1016/B978-0-12-814807-5.00012-7.
- Sartoretti, E. *et al.* (2019) 'In situ Raman analyses of the soot oxidation reaction over nanostructured ceria-based catalysts', *Scientific Reports*. Springer US, 9(1), pp. 9–13. doi: 10.1038/s41598-019-39105-5.
- Sassykova, L. R. *et al.* (2019) 'The Main Components of Vehicle Exhaust Gases and Their Effective Catalytic Neutralization', *Oriental Journal of Chemistry*, 35(1), pp. 110–127. doi: 10.13005/ojc/350112.
- Sayyah, M. *et al.* (2013) 'Mechanical activation of CaO-based adsorbents for CO<sub>2</sub> capture', *ChemSusChem*, 6(1), pp. 193–198. doi: 10.1002/cssc.201200454.
- Seinfeld, J. H. and Pandis, S. N. (1998) *Atmospheric Chemistry and Physics. From Air Pollution to Climate Change*. John Wiley&Sons.
- Service, R. F. (2018) *Ammonia - a renewable fuel made from sun, air, and water - could power the globe without carbon*, *Science*. [online]. Available at: <https://www.sciencemag.org/news/2018/07/ammonia-renewable-fuel-made-sun-air-and-water-could-power-globe-without-carbon> (Accessed: 5 December 2020).
- Shen, X. *et al.* (2018) 'Beyond lithium ion batteries: Higher energy density battery systems based

on lithium metal anodes', *Energy Storage Materials*. Elsevier B.V., 12(November 2017), pp. 161–175. doi: 10.1016/j.ensm.2017.12.002.

Sherman, P. (2019) *Fluorite structure*. [online]. Available at: [https://www.wpclipart.com/rocks\\_minerals/F/Fluorite\\_structure.png.html](https://www.wpclipart.com/rocks_minerals/F/Fluorite_structure.png.html) (Accessed: 9 November 2020).

Shiozawa, B. (2020) *The Cost of CO<sub>2</sub>-free Ammonia*, *Ammonia Energy Association*. [online]. Available at: <https://www.ammoniaenergy.org/articles/the-cost-of-co2-free-ammonia/>.

Simonsen, S. B. *et al.* (2012) 'Alloyed Ni-Fe nanoparticles as catalysts for NH<sub>3</sub> decomposition', *Applied Catalysis A: General*. Elsevier B.V., 447–448, pp. 22–31. doi: 10.1016/j.apcata.2012.08.045.

Skoda (2021) *Skoda Octavia*. [online]. Available at: <https://www.skoda.es/modelos/nuevo-octavia/nuevo-octavia> (Accessed: 29 March 2021).

Smith, C., Hill, A. K. and Torrente-Murciano, L. (2020) 'Current and future role of Haber-Bosch ammonia in a carbon-free energy landscape', *Energy and Environmental Science*. Royal Society of Chemistry, 13(2), pp. 331–344. doi: 10.1039/c9ee02873k.

Stern, L. A. and Hu, X. (2014) 'Enhanced oxygen evolution activity by NiO<sub>x</sub> and Ni(OH)<sub>2</sub> nanoparticles', *Faraday Discussions*. Royal Society of Chemistry, 176, pp. 363–379. doi: 10.1039/c4fd00120f.

Stojmenović, M. *et al.* (2016) 'Structural, morphological and electrical properties of Ce<sub>1-x</sub>Ru<sub>x</sub>O<sub>2-δ</sub> (x=0.005–0.02) solid solutions', *Ceramics International*, 42(12), pp. 14011–14020. doi: 10.1016/j.ceramint.2016.06.007.

Transport & Environment (2019) *Low-Emission Zones are a success - but they must now move to zero-emission mobility*. [online]. Available at: <https://www.transportenvironment.org/publications/low-emission-zones-are-success-%E2%80%93-they-must-now-move-zero-emission-mobility> (Accessed: 5 April 2021).

Transport & Environment (2021) *Cars: direct electrification most efficient by far*. [online]. Available at: <https://cleantechnica.com/files/2021/02/Why-Battery-Electric-Vehicles-Beat-Hydrogen-Electric-Vehicles.jpeg> (Accessed: 5 April 2021).

U.S. Department of Energy (2020) *About Hydrogen Programme*. [online]. Available at: <https://www.hydrogen.energy.gov/about.html> (Accessed: 29 March 2021).

U.S. Department of Transportation (2020) *Fact Sheet: Natural Gas Processing Plants*. [online]. Available at: <https://primis.phmsa.dot.gov/comm/FactSheets/FSNaturalGasProcessingPlants.htm> (Accessed: 8 February 2021).

U.S. DRIVE Partnership (2017) *Target Explanation Document: Onboard Hydrogen Storage for Light-Duty Fuel Cell Vehicles*.

United Nations Framework Convention on Climate Change (2020) *The Paris Agreement*.

Urban Acces Regulations (2021) *Urban Acces Regulations in Europe*. [online]. Available at: <https://eur-lex.europa.eu/legal-content/ES/TXT/?uri=celex%3A32007R0715> (Accessed: 24 April 2021).

Vasilchenko, D. *et al.* (2020) 'Cerium(III) Nitrate Derived CeO<sub>2</sub> Support Stabilising PtO<sub>x</sub> Active



- Species for Room Temperature CO Oxidation', *ChemCatChem*, 12(5), pp. 1413–1428. doi: 10.1002/cctc.201902146.
- Wilberforce, T. *et al.* (2017) 'Developments of electric cars and fuel cell hydrogen electric cars', *International Journal of Hydrogen Energy*. Elsevier Ltd, 42(40), pp. 25695–25734. doi: 10.1016/j.ijhydene.2017.07.054.
- Wilkinson, I., Nayak-luke, R. and Ban, R. (2018) "'Green" Ammonia: Impact of Renewable Energy Intermittency on Plant Sizing and Levelized Cost of Ammonia', *Industrial & Engineering Chemistry Research*, 57(43), pp. 14607–14616. doi: 10.1021/acs.iecr.8b02447.
- World Health Organisation (2018) *WHO Global Ambient Air Quality Database (update 2018)*. [online]. Available at: <https://www.who.int/airpollution/data/cities/en/> (Accessed: 30 November 2019).
- World Resources Institute (2020) *World Greenhouse Gas Emissions: 2016*. [online]. Available at: <https://www.wri.org/resources/data-visualizations/world-greenhouse-gas-emissions-2016> (Accessed: 21 November 2020).
- Yang, J., Gu, F. and Guo, J. (2020) 'Environmental feasibility of secondary use of electric vehicle lithium-ion batteries in communication base stations', *Resources, Conservation and Recycling*, 156(January). doi: 10.1016/j.resconrec.2020.104713.
- Yin, S. F. *et al.* (2004a) 'A mini-review on ammonia decomposition catalysts for on-site generation of hydrogen for fuel cell applications', 277, pp. 1–9. doi: 10.1016/j.apcata.2004.09.020.
- Yin, S. F. *et al.* (2004b) 'Investigation on the catalysis of CO<sub>x</sub>-free hydrogen generation from ammonia', *Journal of Catalysis*, 224(2), pp. 384–396. doi: 10.1016/j.jcat.2004.03.008.
- Yu, P. *et al.* (2016) 'Effects of Alkaline Earth Metal Amides on Ru in Catalytic Ammonia Decomposition', *Journal of Physical Chemistry C*, 120(5), pp. 2822–2828. doi: 10.1021/acs.jpcc.5b11768.
- Zamel, N. and Ñ, X. L. (2008) 'Transient analysis of carbon monoxide poisoning and oxygen bleeding in a PEM fuel cell anode catalyst layer', 33, pp. 1335–1344. doi: 10.1016/j.ijhydene.2007.12.060.
- Zamfirescu, C. and Dincer, I. (2009) 'Ammonia as a green fuel and hydrogen source for vehicular applications', *Fuel Processing Technology*, 90(5), pp. 729–737. doi: 10.1016/j.fuproc.2009.02.004.
- Zhang, C. *et al.* (2014) 'Synthesis of stable Ni-CeO<sub>2</sub> catalysts via ball-milling for ethanol steam reforming', *Catalysis Today*. Elsevier B.V., 233, pp. 53–60. doi: 10.1016/j.cattod.2013.08.013.
- Zhang, H. *et al.* (2020) 'Techno-economic comparison of green ammonia production processes', *Applied Energy*. Elsevier, 259(August 2019), p. 114135. doi: 10.1016/j.apenergy.2019.114135.
- Zijlema, P. J. (2018) *The Netherlands: list of fuels and standard CO<sub>2</sub> emission factors version of January 2019*. Netherlands. [online]. Available at: [https://english.rvo.nl/sites/default/files/2019/05/The Netherlands list of fuels version January 2019.pdf](https://english.rvo.nl/sites/default/files/2019/05/The_Netherlands_list_of_fuels_version_January_2019.pdf).

---

## Legislation

España. ‘Ley 34/2007, de 15 de noviembre, de calidad del aire y protección de la atmósfera’, *Boletín Oficial del Estado*, 17 noviembre 2007, núm. 275, pp. 46962–46987.

España. ‘Real Decreto-ley 17/2019, de 22 de noviembre, por el que se adoptan medidas urgentes para la necesaria adaptación de parámetros retributivos que afectan al sistema eléctrico y por el que se da respuesta al proceso de cese de actividad de centrales térmica’, *Boletín Oficial del Estado*, 28 febrero 2014, núm. 51, pp. 18987–19106.

España. ‘Resolución de 30 de diciembre de 2020, de la Dirección General de Calidad y Evaluación Ambiental, por la que se formula la declaración ambiental estratégica’, *Boletín Oficial del Estado*, 11 enero 2021, núm. 9, pp. 61561–61567.

España. ‘Real Decreto 266/2021, de 13 de abril, por el que se aprueba la concesión directa de ayudas a las comunidades autónomas y a las ciudades de Ceuta y Melilla para la ejecución de programas de incentivos ligados a la movilidad eléctrica (MOVES III) en el mar’, *Boletín Oficial del Estado*, 24 abril de 2021, núm. 89, pp. 26798–26800.

European Commission. ‘Council Directive 91/441/EEC of 26 June 1991 amending Directive 70/220/EEC on the approximation of the laws of the Member States relating to measures to be taken against air pollution by emissions from motor vehicles’, *Official Journal of the European Communities*, 30th August 1991, num. 21, pp. 1–106.

European Commission. ‘Council Directive 93/59/EEC of 28 June 1993 on the Approximation of the Laws of the Member States on Measures to be Taken Against Air Pollution by Emissions from Motor Vehicles’, *Official Journal of the European Communities*, 8th July 1993, num. 13, pp. 21–27.

European Commission. ‘Directive 94/12/EC relating to measures to be taken against air pollution by emissions from motor vehicles and amending Directive 70/220/EEC’, *Official Journal of the European Commission*, 9th May 1994, num. 26, pp. 42–52.

European Commission. ‘Directive 94/63/EC of 20 December 1994 on the control of volatile organic compounds (VOC) emissions resulting from the storage petrol and its distribution from terminals to service stations’, *Official journal of the European Communities*, 31st December 1994, num. 2, pp. 24–33.

European Commission. ‘Directive 96/69/EC of the European Parliament and of the council of 8 October 1996 amending Directive 70/220/EEC on the approximation of the laws of the Member States relating to measures to be taken against air pollution by emissions from motor vehicle’, *Analytical Proceedings*, 21st November 1996, num. 21, pp. 196.

European Commission. ‘Directive 98/69/EC of the European Parliament and of the Council of 13 October 1998 relating to measures to be taken against air pollution by emissions from motor vehicles and amending Council Directive 70/220/EEC’, *Official Journal of the European Communities*, 28th December 1998, num. 350, pp. 1–56.

European Commission. ‘Commission Directive 2002/80/EC of 3 October 2002 - adapting to technical progress Council Directive 70/220/EEC relating to measures to be taken against air pollution by emissions from motor vehicles’, *Official Journal of the European Communities*, 28th October 2002, num. 291, pp. 20–56.

European Commission. ‘Directive 2004/107/EC of the European Parliament and of the Council of 15/12/2004 relating to arsenic, cadmium, mercury, nickel and polycyclic aromatic hydrocarbons in ambient air’, *Official Journal of the European Union*, 15th February 2005, num. 23, pp. 3–16.

European Commission. ‘Regulation (EC) no. 715/2007 of the European Parliament and of the Council of 20 June 2007 on type approval of motor vehicles with respect to emissions from light passenger and commercial vehicles (Euro 5 and Euro 6) and on access to vehicle repair and maintenance’, *Official Journal of the European Union*, 29th June 2007, num. 171, pp. 1–16.

European Commission. ‘Directive 2008/50/EC of the European Parliament and of the Council of 21 May 2008 on ambient air quality and cleaner air for Europe’, *Official Journal of the European Union*, 11th June 2008, num. 152, pp. 169–212.

European Commission. ‘Directive 2010/75/EU of the European Parliament and of the Council of 24 November 2010 on industrial emissions (integrated pollution prevention and control)’, *Official Journal of the European Union*, 17th December 2010, num. 334, pp. 17–119.

European Commission. ‘Commission Implementing Decision of 12 December 2011 laying down rules for Directives 2004/107/EC and 2008/50/EC of the European Parliament and of the Council as regards the reciprocal exchange of information and reporting on ambient air quality (notified under document C(2011) 9068)’, 17th December 2011, num. 335, pp. 86–106.

European Commission. ‘Amending, for the purposes of its adaptation to technical progress, Directive 2009/126/EC on Stage II petrol vapour recovery during refuelling of motor vehicles at service stations’, 23th October 2014, num. 304, pp. 2013–2014.

European Commission. ‘Directive (EU) 2015/1480 of 28 August 2015 amending several annexes to Directives 2004/107/EC and 2008/50/EC of the European Parliament and of the Council laying down the rules concerning reference methods, data validation and location of sampling points for the assessment of ambient air quality’ *Official Journal of the European Union*, 29th August 2015, num. 226, pp. 1–71.

European Commission. ‘Directive (EU) 2015/2193 of the European Parliament and of the Council on the limitation of emissions of certain pollutants into the air from medium combustion plants’, *Official Journal of the European Union*, 28th November 2015, num. 451, pp. 134–23.

European Commission. ‘Directive (EU) 2016/2284 of the European Parliament and of the Council of 14 December 2016 on the reduction of national emissions of certain atmospheric pollutants, amending Directive 2003/35/EC and repealing Directive 2001/81/EC’, *Official Journal of the European Union*, 17th December 2016, num. 344, pp. 1–31.

European Commission. ‘Commission regulations (EU) 2019/318 of February 2019 amending Regulation (EU) 2017/2400 and Directive 2007/46/EC of the European Parliament and of the Council as regards the determination of the CO<sub>2</sub> emission and fuel consumption of heavy-duty’, *Official Journal of the European Union*, 26th February 2019, num. 58, pp. 20–30.

European Commission. ‘Regulation (EU) 2019/631 of the European Parliament and of the Council of 17 April 2019 setting CO<sub>2</sub> emission performance standards for new passenger cars and for new light commercial vehicles, and repealing Regulations (EC) No 443/2009 and (EU) No 510/20’, *Official Journal of the European Union*, 25th April 2019, num. 10, pp. 1–21.

## 10. Annex

### 10.1. Annex 1

Table 10.1 presents the planned reduction of the levels of pollution for each European State Member (referred to the 2005 levels), gathered in NECD. There are two objectives: the levels from 2020 to 2029 and the levels for further than 2050. The limits are set for NH<sub>3</sub>, PM<sub>2.5</sub>, SO<sub>2</sub>, NO<sub>x</sub> and NMVOC (Directive (EU) 20/2284).

*Table 10.1. Reduction level objective for each European State Member for SO<sub>2</sub>, NO<sub>x</sub>, NMVOC, NH<sub>3</sub> and PM<sub>2.5</sub> (Directive (EU) 2016/2284).*

Member State	SO <sub>2</sub> reduction compared with 2005		NO <sub>x</sub> reduction compared with 2005		NMVOC reduction compared with 2005	
	For any year from 2020 to 2029	For any year from 2030	For any year from 2020 to 2029	For any year from 2030	For any year from 2020 to 2029	For any year from 2030
Belgium	43 %	66 %	41 %	59 %	21 %	35 %
Bulgaria	78 %	88 %	41 %	58 %	21 %	42 %
Czech Republic	45 %	66 %	35 %	64 %	18 %	50 %
Denmark	35 %	59 %	56 %	68 %	35 %	37 %
Germany	21 %	58 %	39 %	65 %	13 %	28 %
Estonia	32 %	68 %	18 %	30 %	10 %	28 %
Greece	74 %	88 %	31 %	55 %	54 %	62 %
Spain	67 %	88 %	41 %	62 %	22 %	39 %
France	55 %	77 %	50 %	69 %	43 %	52 %
Croatia	55 %	83 %	31 %	57 %	34 %	48 %
Ireland	65 %	85 %	49 %	69 %	25 %	32 %
Italy	35 %	71 %	40 %	65 %	35 %	46 %
Cyprus	83 %	93 %	44 %	55 %	45 %	50 %
Latvia	8 %	46 %	32 %	34 %	27 %	38 %
Lithuania	55 %	60 %	48 %	51 %	32 %	47 %
Luxembourg	34 %	50 %	43 %	83 %	29 %	42 %
Hungary	46 %	73 %	34 %	66 %	30 %	58 %
Malta	77 %	95 %	42 %	79 %	23 %	27 %
Netherlands	28 %	53 %	45 %	61 %	8 %	15 %
Austria	26 %	41 %	37 %	69 %	21 %	36 %

Austria	26 %		41 %	37 %		69 %	21 %		36 %
Poland	59 %		70 %	30 %		39 %	25 %		26 %
Portugal	63 %		83 %	36 %		63 %	18 %		38 %
Romania	77 %		88 %	45 %		60 %	25 %		45 %
Slovenia	63 %		92 %	39 %		65 %	23 %		53 %
Slovakia	57 %		82 %	36 %		50 %	18 %		32 %
Finland	30 %		34 %	35 %		47 %	35 %		48 %
Sweden	22 %		22 %	36 %		66 %	25 %		36 %
United Kingdom	59 %		88 %	55 %		73 %	32 %		39 %
EU 28	59 %		79 %	42 %		63 %	28 %		40 %

Member State	NH <sub>3</sub> reduction compared with 2005			PM <sub>2.5</sub> reduction compared with 2005		
	For any year from 2020 to 2029		For any year from 2030	For any year from 2020 to 2029		For any year from 2030
Belgium	2 %		13 %	20 %		39 %
Bulgaria	3 %		12 %	20 %		41 %
Czech Republic	7 %		22 %	17 %		60 %
Denmark	24 %		24 %	33 %		55 %
Germany	5 %		29 %	26 %		43 %
Estonia	1 %		1 %	15 %		41 %
Greece	7 %		10 %	35 %		50 %
Spain	3 %		16 %	15 %		50 %
France	4 %		13 %	27 %		57 %
Croatia	1 %		25 %	18 %		55 %
Ireland	1 %		5 %	18 %		41 %
Italy	5 %		16 %	10 %		40 %
Cyprus	10 %		20 %	46 %		70 %
Latvia	1 %		1 %	16 %		43 %
Lithuania	10 %		10 %	20 %		36 %
Luxembourg	1 %		22 %	15 %		40 %
Hungary	10 %		32 %	13 %		55 %
Malta	4 %		24 %	25 %		50 %

Netherlands	13 %		21 %	37 %		45 %
Austria	1 %		12 %	20 %		46 %
Poland	1 %		17 %	16 %		58 %
Portugal	7 %		15 %	15 %		53 %
Romania	13 %		25 %	28 %		58 %
Slovenia	1 %		15 %	25 %		60 %
Slovakia	15 %		30 %	36 %		49 %
Finland	20 %		20 %	30 %		34 %
Sweden	15 %		17 %	19 %		19 %
United Kingdom	8 %		16 %	30 %		46 %
EU 28	6 %		19 %	22 %		49 %

## 10.2. Annex 2

Most of the car restrictions in the European LEZ are based on the Euronorms. These are a set of regulations established and re-evaluated since 1991, where they classify light-duty vehicles regarding their tested emissions. Currently, the applicable regulation is the Euro 5/6 (European Commission, 2007), but the formers were (in chronological order):

- Euro 1 standards (Council Directive 91/441/EEC; Council Directive 93/59/EEC).
- Euro 2 standards (Directive 94/12/EC; Directive 96/69/EC).
- Euro 3 and 4 (Directive 98/69/EC; Directive 2002/80/EC).

It is worth to note a change in the testing method, from the NEDC (New European Driving Cycle) to the WLTC (The Worldwide harmonized Light vehicles Test Procedure). The reason lays in the lax conditions of the former. Therefore, with this replacement, the values obtained are more realistic and cars undergo a strict examination (European Commission, 2007).

Table 10.2. EU emission standards for passenger cars (Dieselnet, 2019).

Stage	Date	CO	HC	HC+NOx	NOx	PM	PN
		g/km					
<b>Positive Ignition (Gasoline)</b>							
Euro 1†	1992.07	2.72 (3.16)	-	0.97 (1.13)	-	-	-
Euro 2	1996.01	2.2	-	0.5	-	-	-
Euro 3	2000.01	2.30	0.20	-	0.15	-	-
Euro 4	2005.01	1.0	0.10	-	0.08	-	-
Euro 5	2009.09 <sup>b</sup>	1.0	0.10 <sup>d</sup>	-	0.06	0.005 <sup>e,f</sup>	-
Euro 6	2014.09	1.0	0.10 <sup>d</sup>	-	0.06	0.005 <sup>e,f</sup>	6.0×10 <sup>11</sup> e,g
<b>Compression Ignition (Diesel)</b>							
Euro 1†	1992.07	2.72 (3.16)	-	0.97 (1.13)	-	0.14 (0.18)	-
Euro 2, IDI	1996.01	1.0	-	0.7	-	0.08	-
Euro 2, DI	1996.01 <sup>a</sup>	1.0	-	0.9	-	0.10	-
Euro 3	2000.01	0.64	-	0.56	0.50	0.05	-
Euro 4	2005.01	0.50	-	0.30	0.25	0.025	-
Euro 5a	2009.09 <sup>b</sup>	0.50	-	0.23	0.18	0.005 <sup>f</sup>	-
Euro 5b	2011.09 <sup>c</sup>	0.50	-	0.23	0.18	0.005 <sup>f</sup>	6.0×10 <sup>11</sup>
Euro 6	2014.09	0.50	-	0.17	0.08	0.005 <sup>f</sup>	6.0×10 <sup>11</sup>
<p>* At the Euro 1..4 stages, passenger vehicles &gt; 2,500 kg were type approved as Category N<sub>1</sub> vehicles</p> <p>† Values in brackets are conformity of production (COP) limits</p> <p>a. until 1999.09.30 (after that date DI engines must meet the IDI limits)</p> <p>b. 2011.01 for all models</p> <p>c. 2013.01 for all models</p> <p>d. and NMHC = 0.068 g/km</p> <p>e. applicable only to vehicles using DI engines</p> <p>f. 0.0045 g/km using the PMP measurement procedure</p> <p>g. 6.0×10<sup>12</sup> 1/km within first three years from Euro 6 effective dates</p>							

### 10.3. Annex 3

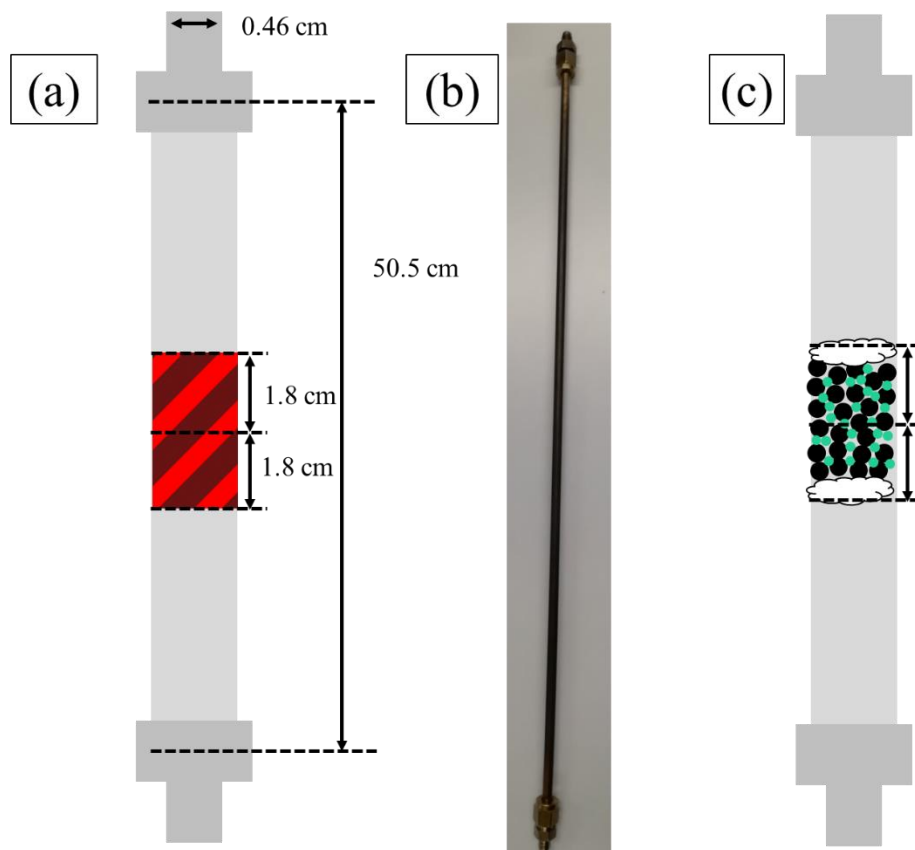


*Figure 10.1. (a) Scheme of the characteristic measurements of the reactor, (b) an image of the real reactor used and (c) the placement of the catalyst in the reactor (in white the glass wool fibre, in Black the SiC and in green the catalyst).*



## 10.4. Annex 4

### Raman spectroscopy

This characterisation technique allows to retrieve information regarding the crystallinity and the molecular composition of the analysed material. It is based on the inelastic light scattering received from sample, which has been irradiated during a short period of time by a monochromatic laser. This light excites the sample into a virtual energy state, which only exists during a short period of time. After that, the material emits a photon, which instead of returning to its original ground state, it is in a different one. Therefore, as there is a change in the energy of the molecule, the photon emitted has to balance the overall energy. Then, the light from the sample has a different frequency. This shift in the energy, called Raman shift, allows to characterise the different samples, as it is related to the bonds of the molecule. Its intensity is related to the change in the polarizability of the molecules. Then, if a molecule is already polar, which means that it is not symmetric regarding the disposition of their atoms, the possible change in its dipole moment would be low, thus its intensity peak in the Raman spectra. Contrary, a neutral molecule, which has a symmetrical disposition of its atoms, is more sensitive and returns more photons (more intense peaks). It is worth to note that the excitation of the molecule can produce two types of peaks, as it is depicted in Figure 10.2. On one hand, when the emitted photons from the sample have lower frequency than the incident light, a Stokes-Raman peak is produced. On the other hand, if the frequency of emitted photons from the sample increases, regarding the initial ones, the peak is called Anti-Stokes-Raman peak (Jones *et al.*, 2019).

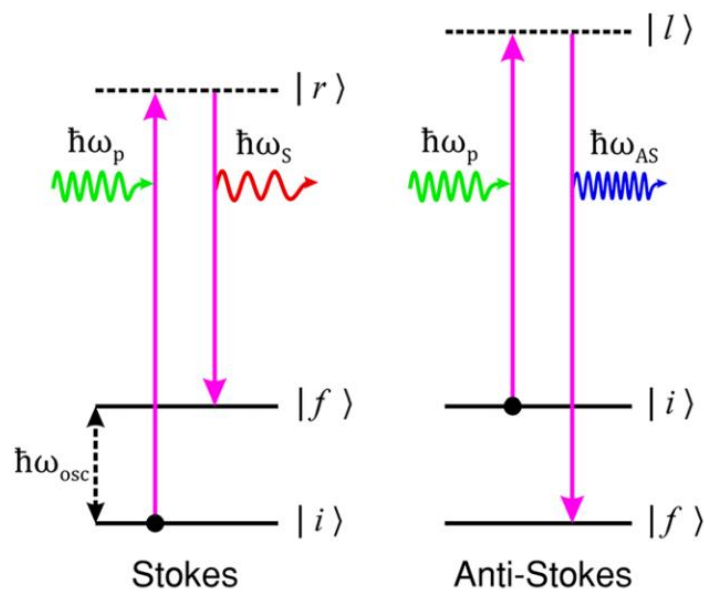


Figure 10.2. Scheme of the transitions between electronic states that produce the Stokes and Anti-Stokes peaks (Jones *et al.*, 2019).

## 10.5. Annex 5

Table 10.3. Data of the ammonia conversion for the catalysts analysed.

T (°C)	Ceria <sup>16</sup>	Empty <sup>17</sup>	Ni-D-10				IWI	Ni-W-0.5				Ni-W-1				
			Initial	Repetition (2 months)	Average	Error		Initial	Repetition (2 months)	Average	Error	Initial	Repetition (2 months)	Average	Error	
			NH <sub>3</sub> conversion (%)													
300	0	0	0,0	0,0	0,0	0,0	0,0	0,0	0,0	0,0	0,0	0,0	0,0	0,0	0,0	0,0
350	1	2	5,8	5,6	5,7	0,1	6,0	6,0	6,5	6,2	0,3	3,8	1,9	2,8	0,9	
400	4	4	23,3	19,8	21,6	1,8	21,3	24,3	22,9	23,6	0,7	15,8	15,0	15,4	0,4	
450	10	13	63,2	52,4	57,8	2,7	55,6	58,3	60,1	59,2	0,9	48,6	46,6	47,6	1,0	
500	27	34	89,8	87,6	88,7	1,1	89,5	91,4	93,5	92,5	1,1	86,6	87,5	87,1	0,4	
550	55	62	98,7	98,8	98,8	0,0	98,5	98,8	99,5	99,2	0,4	98,8	99,2	99,0	0,2	
600	90	98	98,9	99,7	99,3	0,4	99,7	99,3	99,8	99,5	0,2	99,1	99,7	99,4	0,3	

T (°C)	Ni-E-0.5		Ni-E-1		Ni-D-20	Ru-Ni-s				NiRu-b	Ru-Ni-b	Ni-Ru-b	Ni10-Ru5-b
	Initial	Repetition (2 months)	Initial	Repetition (2 months)		Initial	Repetition (2 days)	Average	Error				
	NH <sub>3</sub> conversion (%)												
300	0,0	0,0	0,0	0,0	0,0	0,0	0,0	0,0	0,0	0,0	0,0	0,0	0,0
350	7,3	4,3	6,9	1,8	4,1	6,1	5,2	5,7	0,5	4,7	4,8	8,9	8,7
400	25,2	18,1	27,4	6,6	11,7	22,2	19,5	20,9	1,4	18,6	24,1	33,1	33,9
450	60,3	51,2	66,6	22,8	35,9	67,2	63,2	65,2	2,0	65,2	73,6	80,4	82,1
500	93,1	89,4	94,9	61,2	78,0	95,5	93,2	94,4	1,1	97,4	98,8	98,9	99,8
550	98,9	99,4	99,0	93,2	98,0	99,5	99,3	99,4	0,1	99,8	100,0	99,7	99,2
600	99,7	100,0	99,7	99,6	99,7	99,8	99,8	99,8	0,0	100,0	100,0	99,8	99,8

<sup>16</sup> Data extracted from: (Lucentini, Casanovas and Llorca, 2019).

<sup>17</sup> Data extracted from: (Lucentini, Casanovas and Llorca, 2019).

T (°C)	Ru-400-10	Ru-400-30	Ru-400-5	Ru-100-5	Ru-800-5	Ru-IWI
	NH <sub>3</sub> conversion (%)					
300	0,0	0,0	0,0	0,0	0,0	0,0
350	16,2	9,0	17,2	13,2	8,6	18,4
400	60,4	31,4	59,9	46,9	30,2	56,6
450	98,1	82,8	96,8	90,7	83,2	91,6
500	99,8	99,4	99,7	99,8	99,4	99,5
550	99,9	99,8	99,7	99,8	99,8	99,8
600	99,9	99,8	99,8	99,8	99,8	99,8

### 10.6. Annex 6

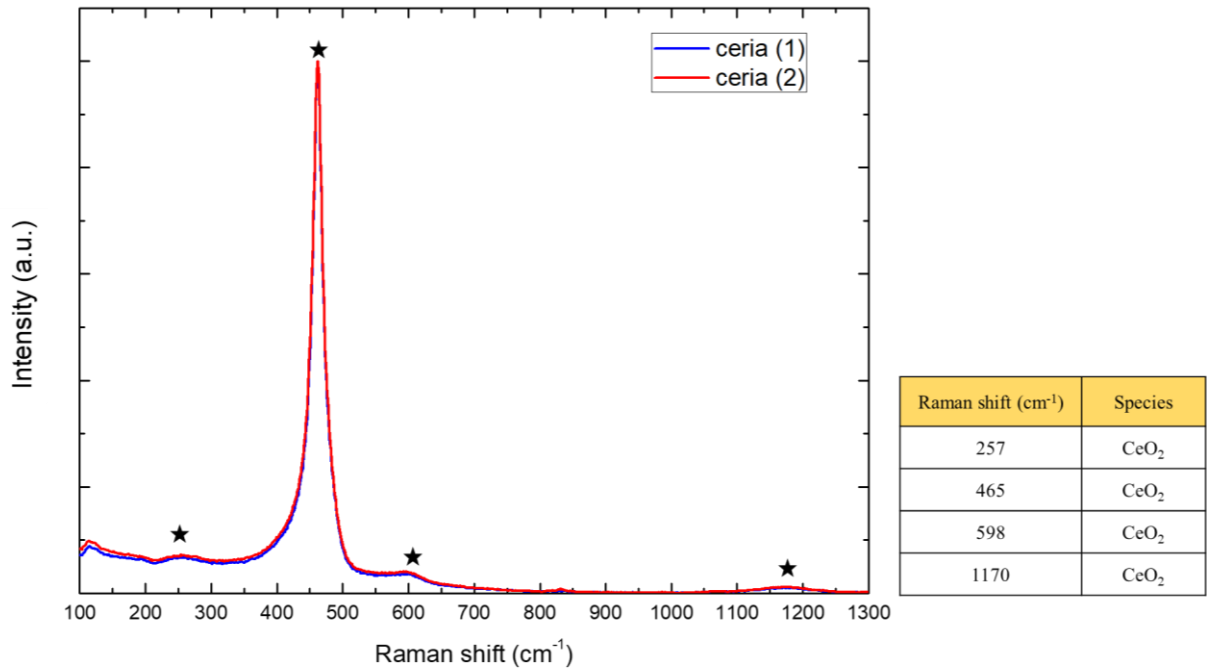


Figure 10.3. Raman spectrum of ceria with a table with the peaks specified.

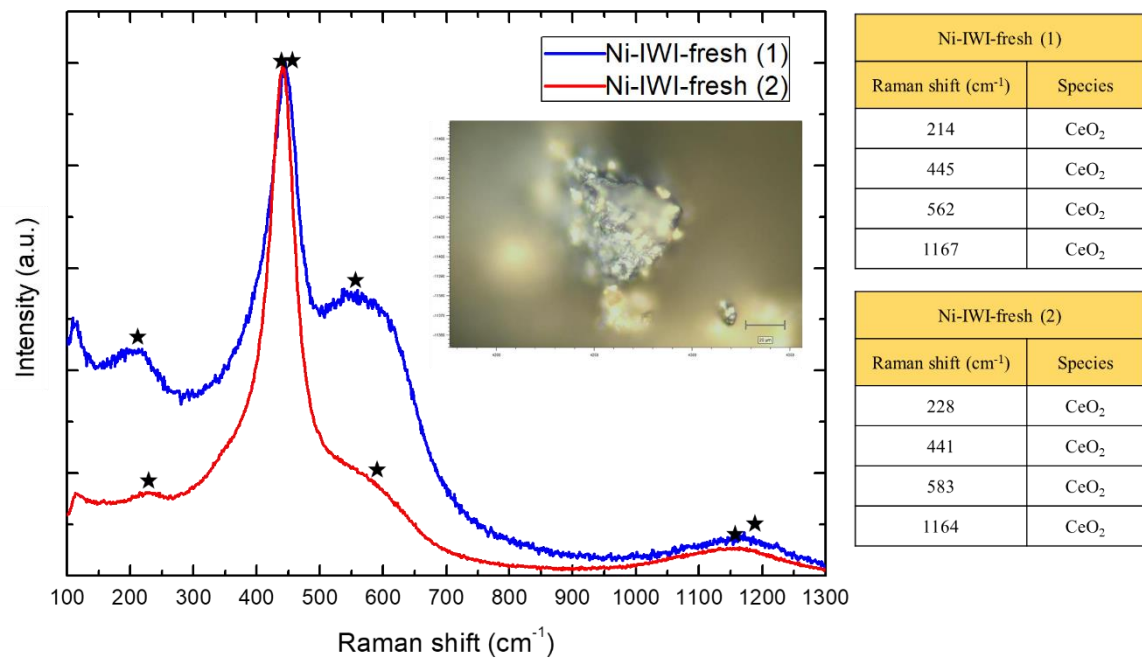


Figure 10.4. Raman spectra of Ni-IWI fresh with a table with the peaks specified and an image of its surface.

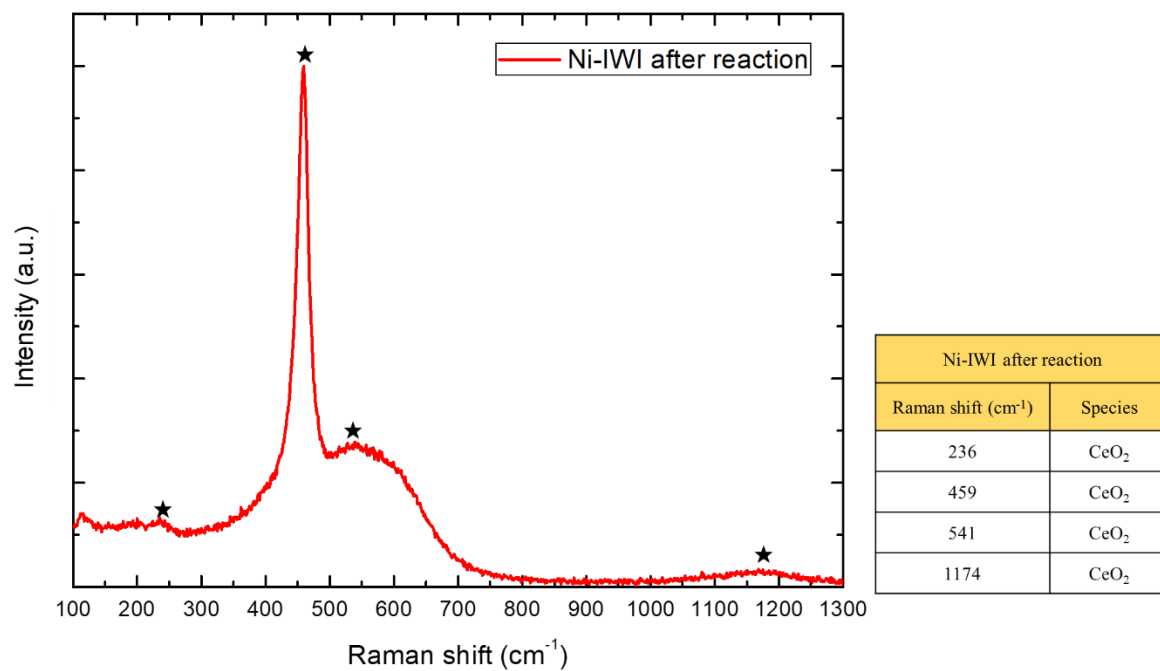


Figure 10.5. Raman spectrum of Ni-IWI after reaction with a table with the peaks specified.

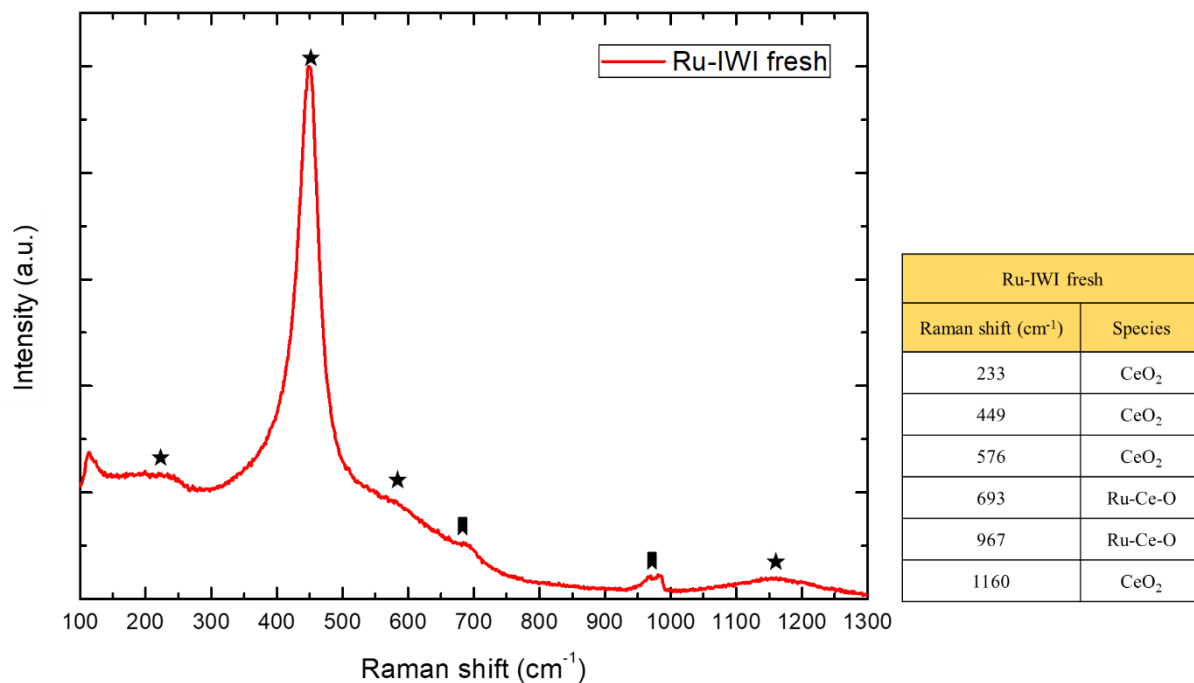


Figure 10.6. Raman spectrum of Ru-IWI fresh with a table with the peaks specified.

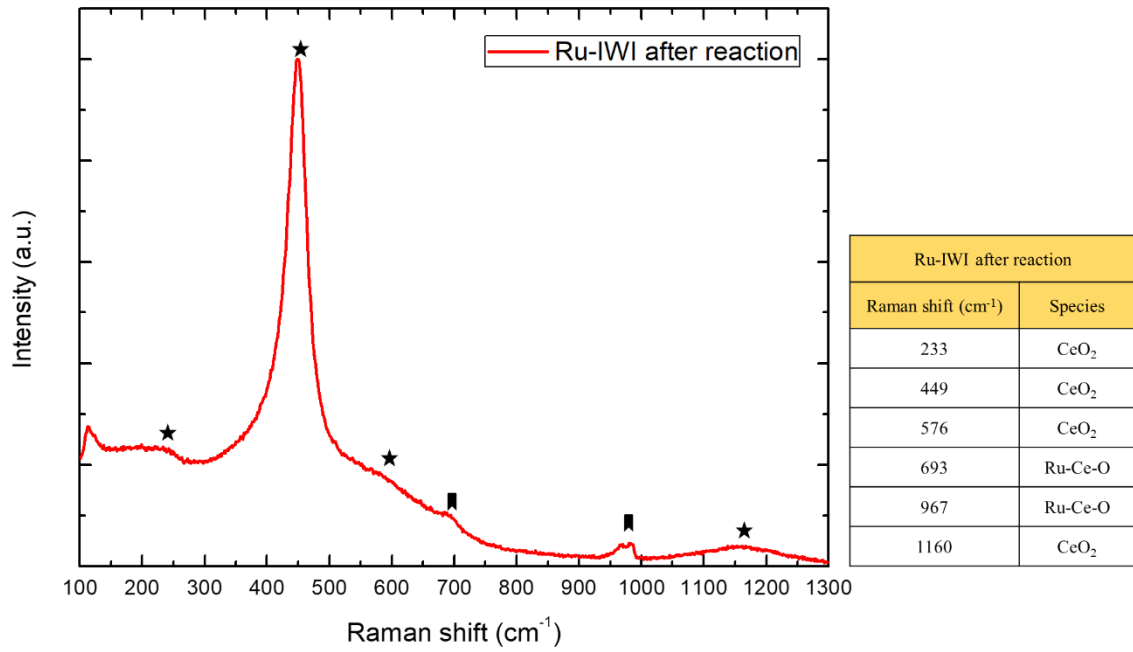


Figure 10.7. Raman spectrum of Ru-IWI after reaction with a table with the peaks specified.

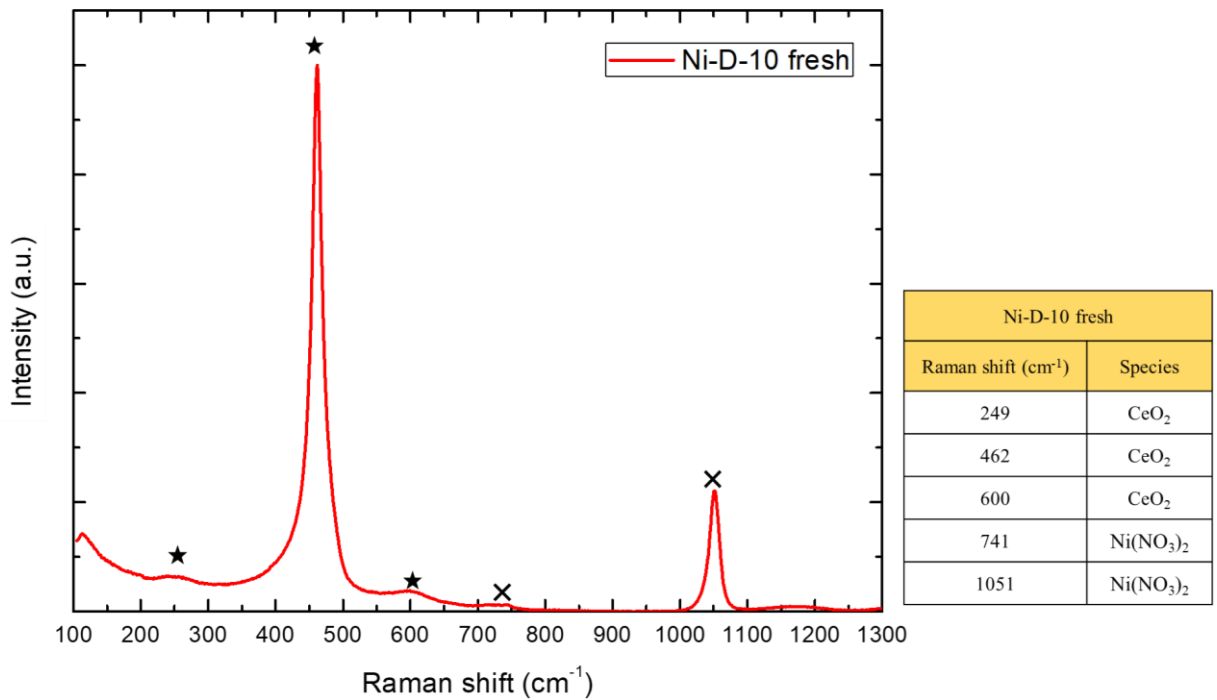


Figure 10.8. Raman spectrum of Ni-D-10 fresh with a table with the peaks specified.

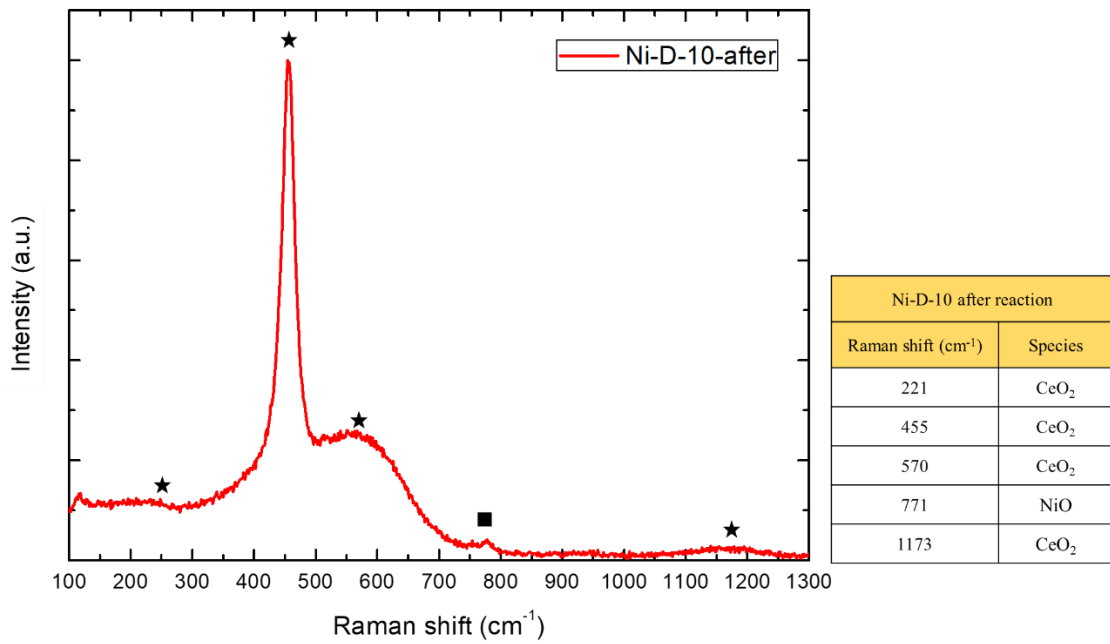


Figure 10.9. Raman spectrum of Ni-D-10 after reaction with a table with the peaks specified.

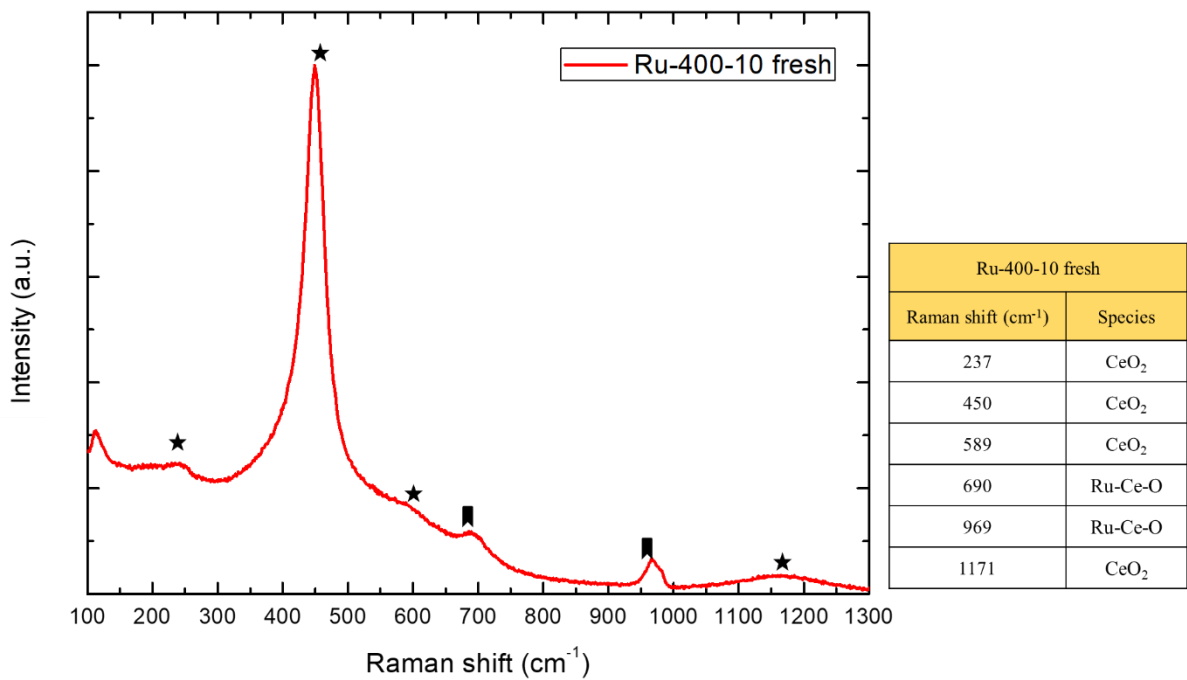


Figure 10.10. Raman spectrum of Ru-400-10 fresh with a table with the peaks specified.

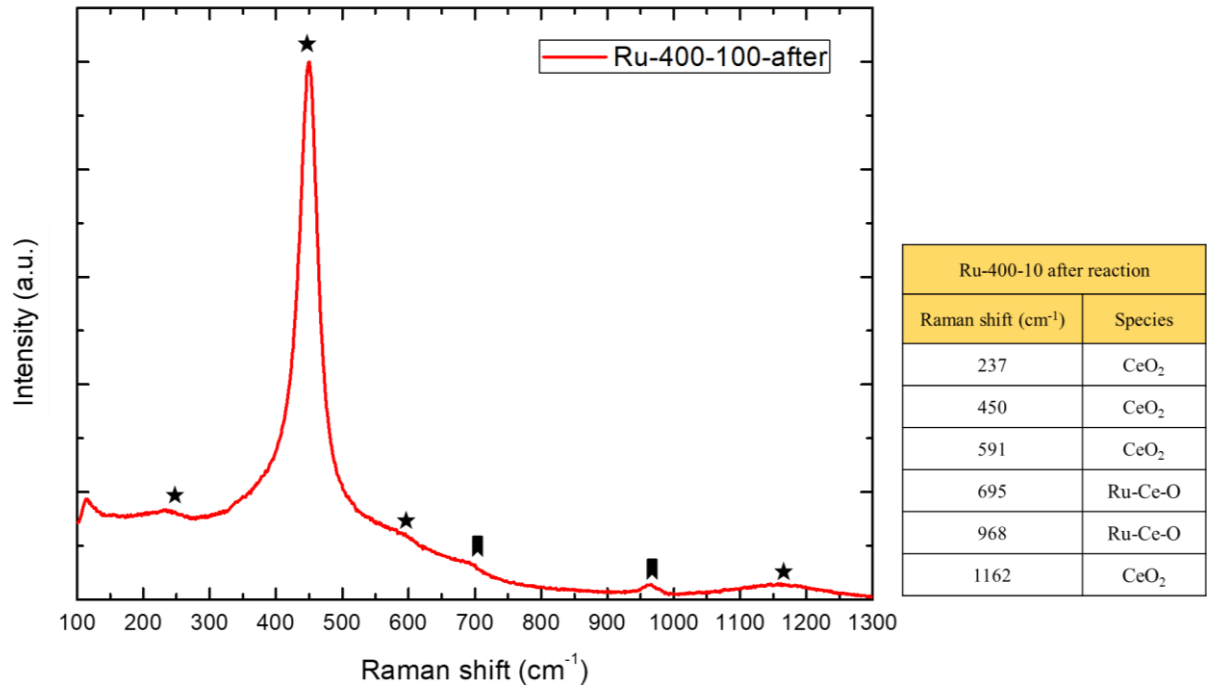


Figure 10.11. Raman spectrum of Ru-400-100 after reaction with a table with the peaks specified.

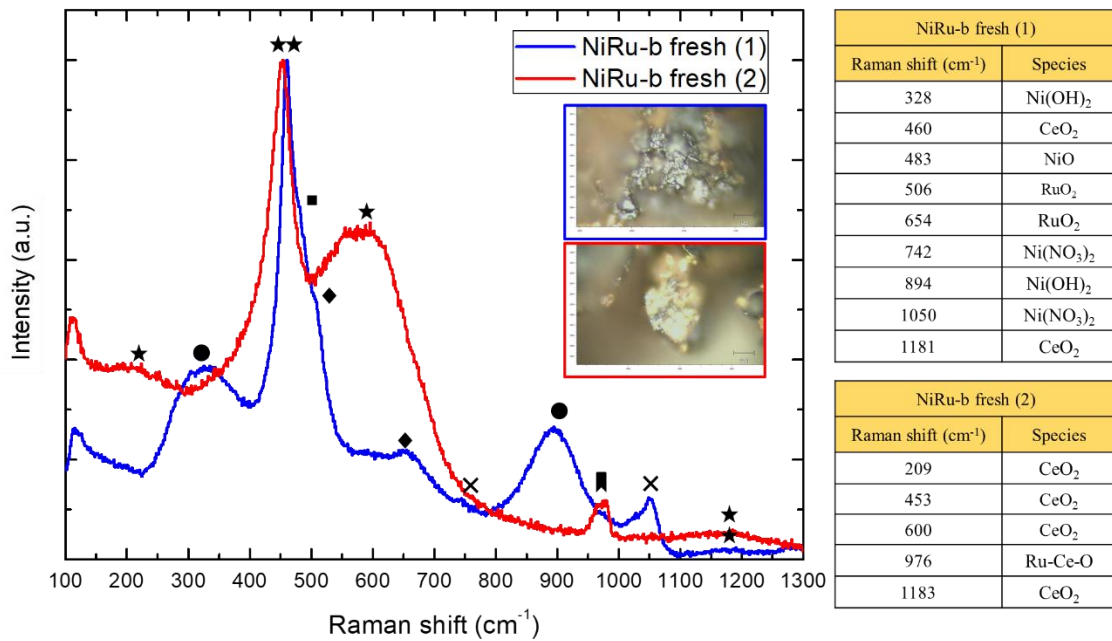


Figure 10.12. Raman spectra of NiRu-b with a table with the peaks specified.



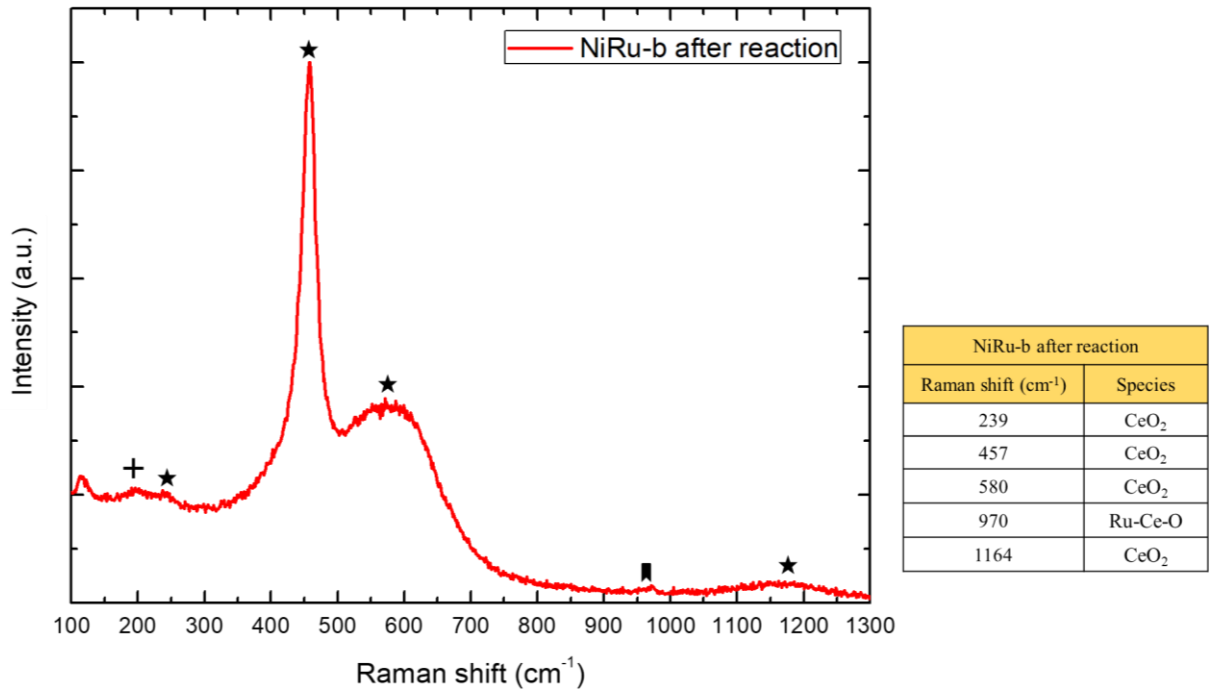


Figure 10.13. Raman spectrum of NiRu-b after reaction with a table with the peaks specified.

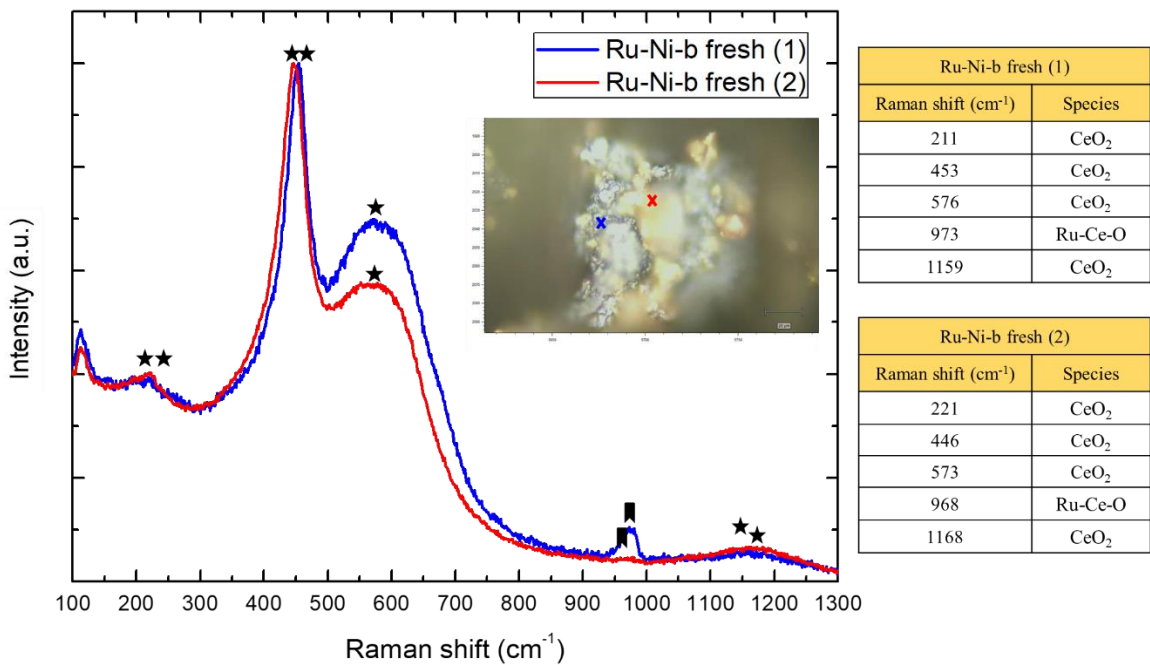


Figure 10.14. Raman spectra of Ru-Ni-b fresh with a table with the peaks specified and an image of its surface.

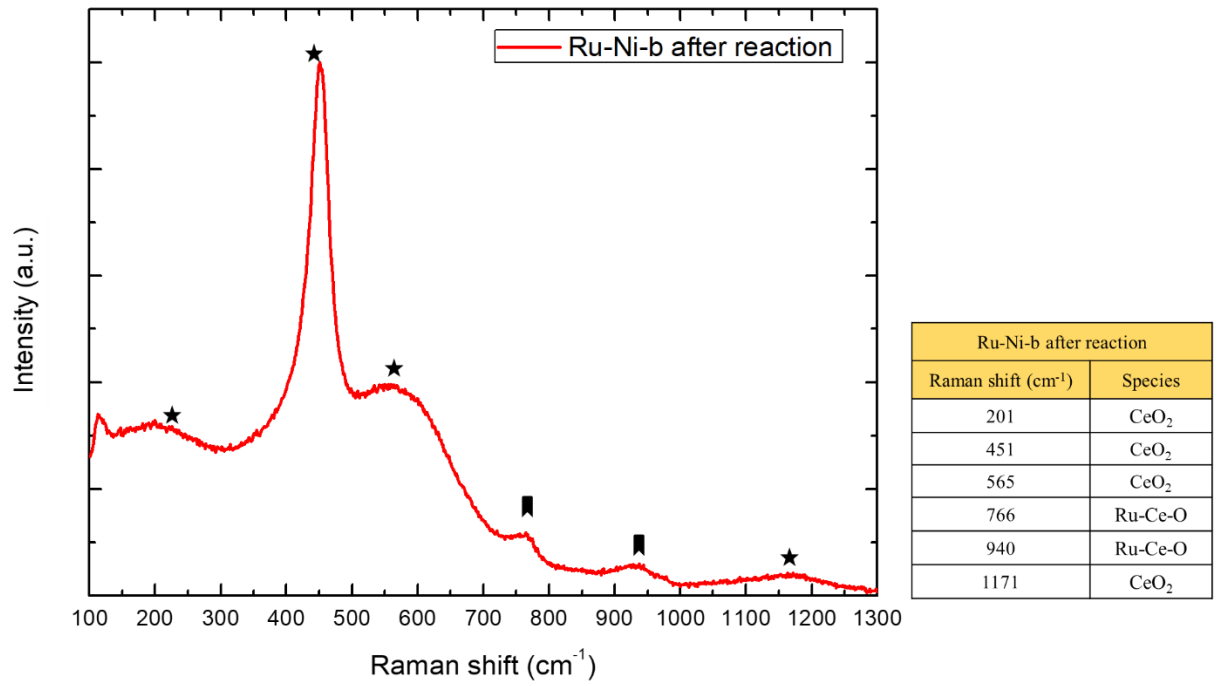
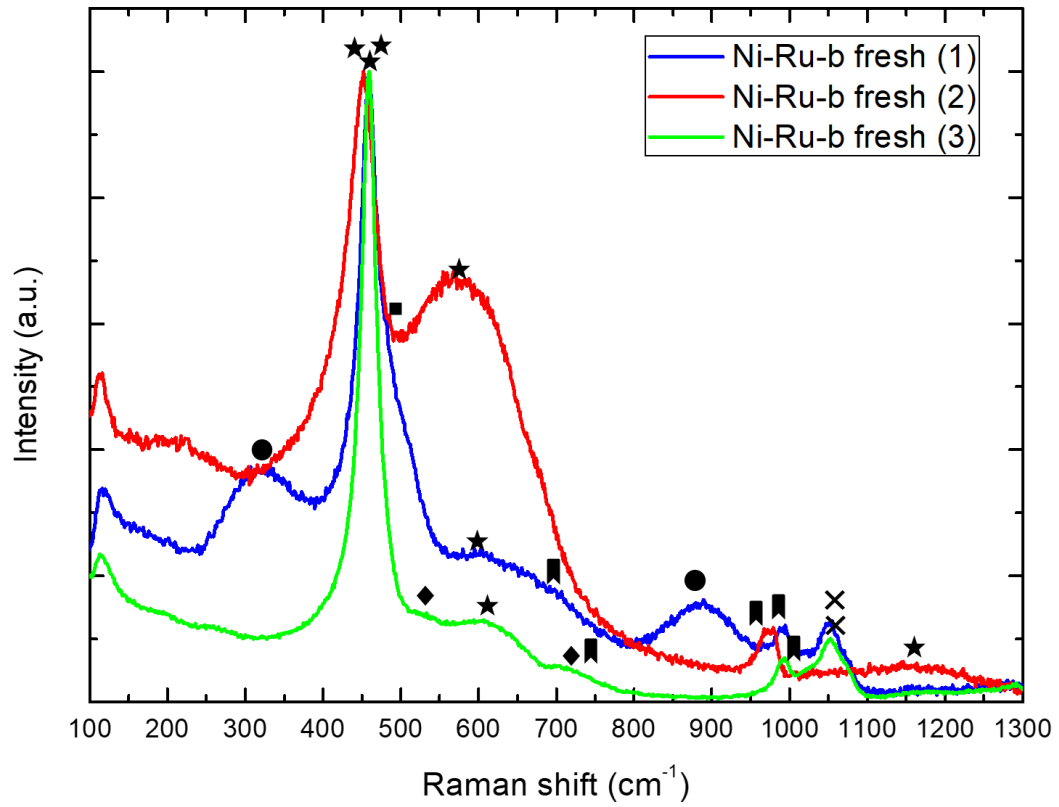


Figure 10.15. Raman spectrum of Ru-Ni-b after reaction with a table with the peaks specified.



Ni-Ru-b fresh (1)	
Raman shift (cm <sup>-1</sup> )	Species
316	Ni(OH) <sub>2</sub>
459	CeO <sub>2</sub>
480	NiO
603	CeO <sub>2</sub>
698	Ru-Ce-O
888	Ni(OH) <sub>2</sub>
991	Ru-Ce-O
1052	Ni(NO <sub>3</sub> ) <sub>2</sub>

Ni-Ru-b fresh (2)	
Raman shift (cm <sup>-1</sup> )	Species
221	CeO <sub>2</sub>
452	CeO <sub>2</sub>
572	CeO <sub>2</sub>
975	Ru-Ce-O
1160	CeO <sub>2</sub>

Ni-Ru-b fresh (3)	
Raman shift (cm <sup>-1</sup> )	Species
459	CeO <sub>2</sub>
532	RuO <sub>2</sub>
609	CeO <sub>2</sub>
707	Ru-Ce-O RuO <sub>2</sub>
992	Ru-Ce-O
1053	Ni(NO <sub>3</sub> ) <sub>2</sub>

Figure 10.16. Raman spectra of Ni-Ru-b with a table with the peaks specified.

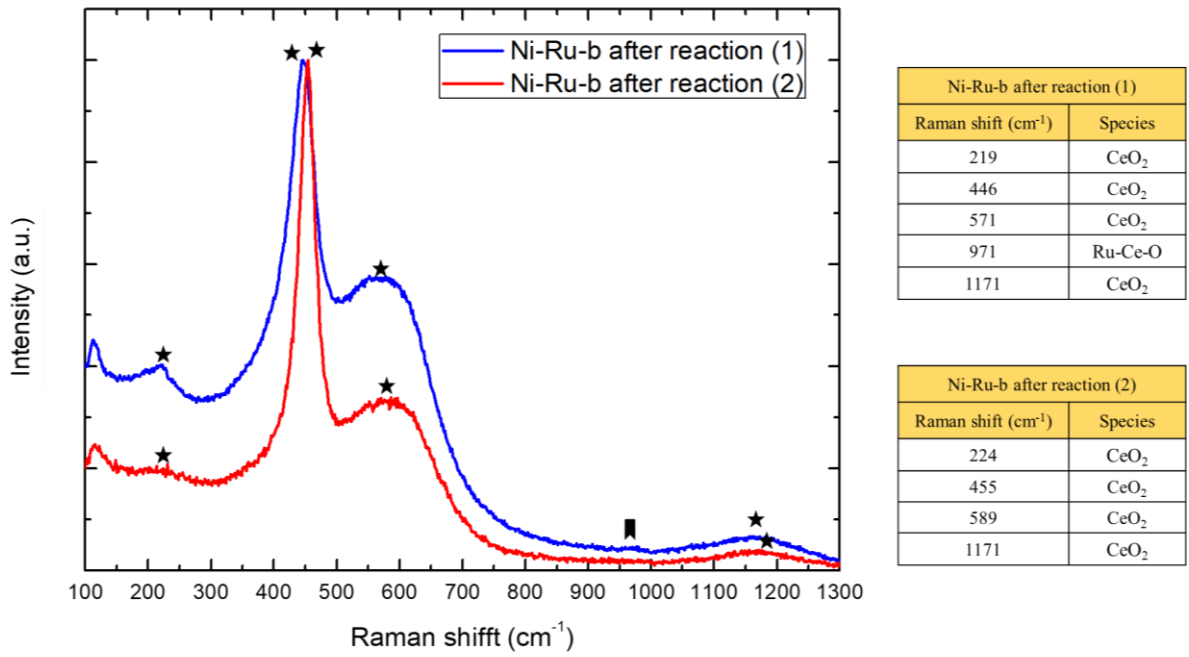


Figure 10.17. Raman spectra of Ni-Ru-b after reaction with a table with the peaks specified.

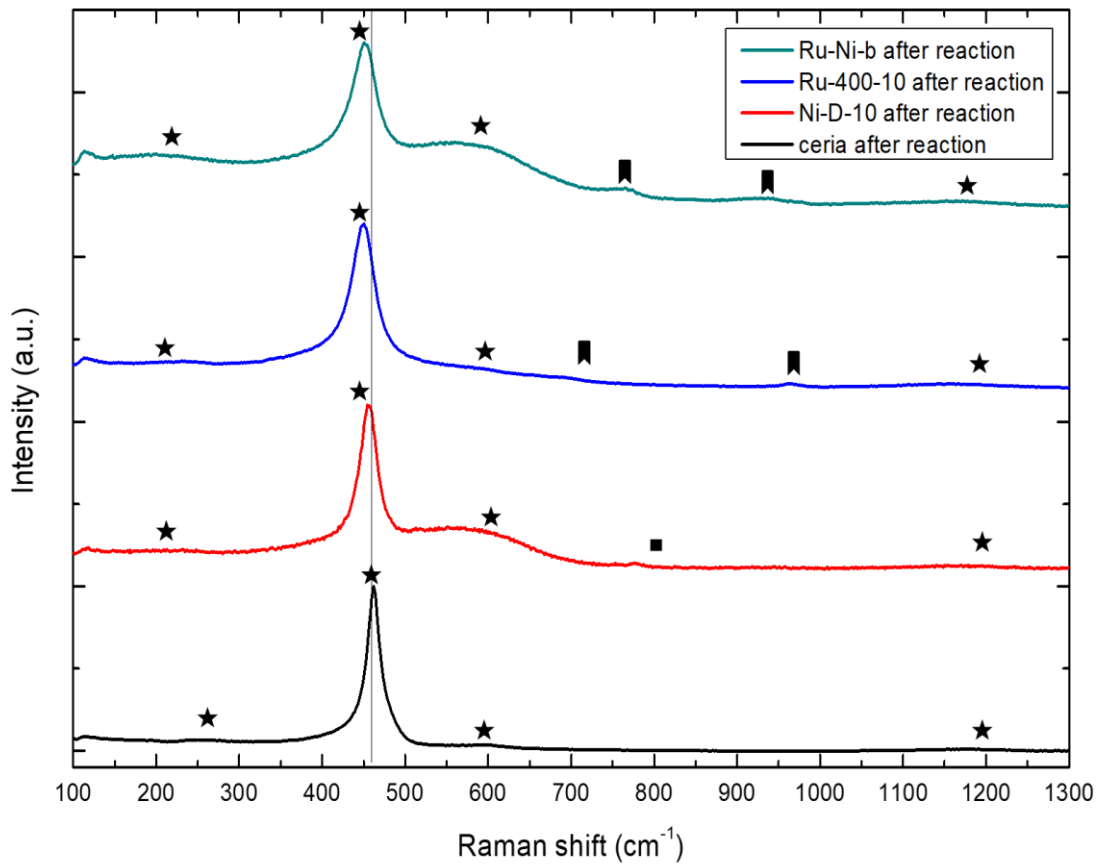


Figure 10.18. Raman spectra of ceria, Ni-D-10, Ru-400-10, and Ru-Ni-b, after reaction.

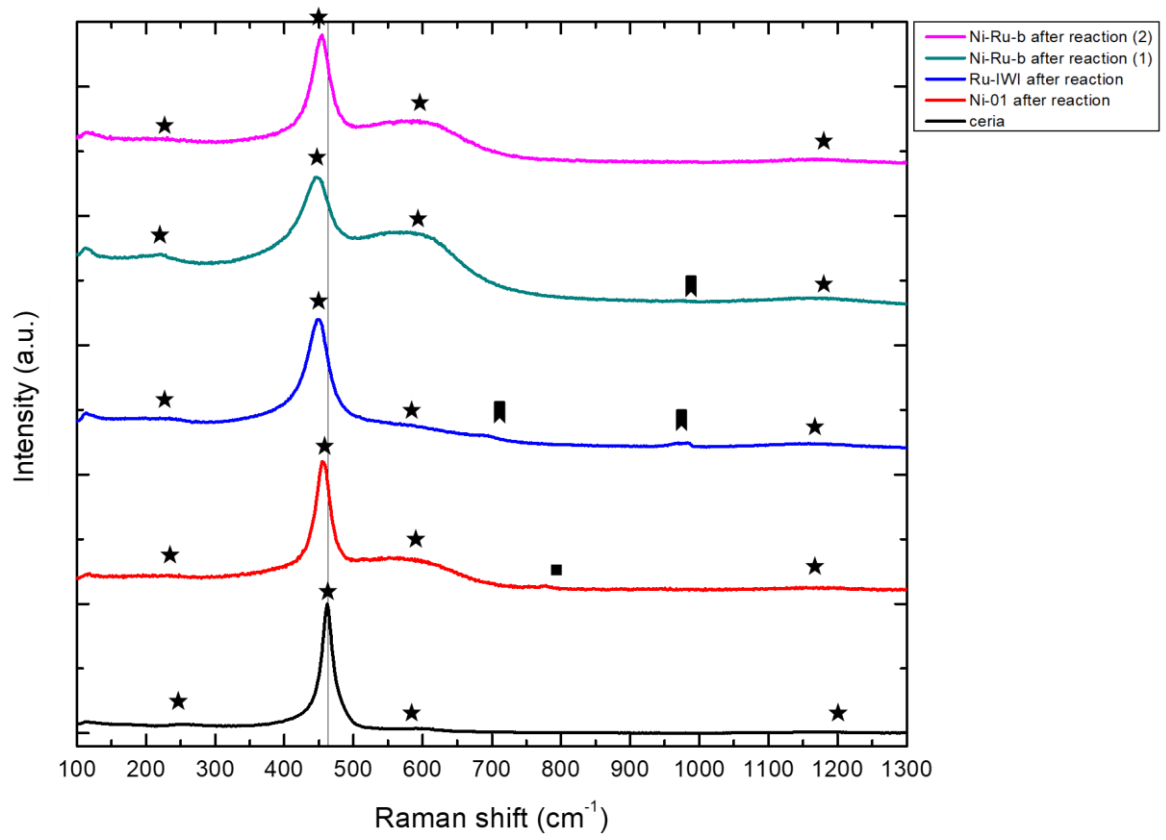


Figure 10.19. Raman spectra of ceria, Ni-D-10, Ru-400-10, and N-Ru-b, after reaction.

## 10.7. Annex 7

Table 10.4. Ni-based catalysts for ammonia decomposition.

Metal	Metal content (% wt.)	Catalyst (g)	Technique	Support (promoter)	T (K)	NH <sub>3</sub> conversion (%)	Reference			
Ni	10	0.1	IWI	SiO <sub>2</sub>	673	1.4	(Yin <i>et al.</i> , 2004a)			
					723	4.2				
					773	10.5				
					823	21.6				
					873	36.4				
					923	70.0				
	66	0.2	IWI	SiO <sub>2</sub> (Al <sub>2</sub> O <sub>3</sub> )	723	34	(Makepeace <i>et al.</i> , 2015)			
	43.4	0.1	IWI	Al <sub>2</sub> O <sub>3</sub> (CeO <sub>2</sub> )	773	71.9	(Okura <i>et al.</i> , 2016)			
	37.8	0.2	IWI	Al <sub>2</sub> O <sub>3</sub> (La)	773	62	(Choudhary, Sivadinarayana and Goodman, 2009)			
	10	0.1	IWI	SiO <sub>2</sub>	873	10.5	(Liu <i>et al.</i> , 2008)			
	65	0.1	IWI	SiO <sub>2</sub> and Al <sub>2</sub> O <sub>3</sub>	873	21.7	(Li <i>et al.</i> , 2005)			
	23.4	0.3	IWI	SBA-15	873	57	(Bell and Torrente-Murciano, 2016)			
	7.2	0.1	IWI	MCM-41	873	26.9	(Chellappa, Fischer and Thomson, 2002)			
	10	0.1	IWI	CeO <sub>2</sub>	623	5	(Lucentini, Casanovas and Llorca, 2019)			
					673	13				
					723	61				
773					97					
823					100					
10					0.1	IWI		Al <sub>2</sub> O <sub>3</sub>	623	1
									673	9
									723	30
	773	62								

## 10.8. Annex 8

Table 10.5. Ru-based catalysts for ammonia decomposition.

Metal	Metal content (% wt.)	Catalyst (g)	Technique	Support (promoter)	T (K)	NH <sub>3</sub> conversion (%)	Reference
Ru	10	0.1	IWI	SiO <sub>2</sub>	673	14	(Yin <i>et al.</i> , 2004a)
					723	36	
					773	64	
					873	97	
					923	99	
	2	0.1	IWI	CeO <sub>2</sub>	623	37	(Lucentini, Casanovas and Llorca, 2019)
					673	79	
					723	98	
					773	100	
					823	100	
	2	0.3	IWI	CNT	640	18	(García-García <i>et al.</i> , 2010)
					680	37	
					720	64	
	5	0.1	IWI	CNT	623	9	(Yin <i>et al.</i> , 2004b)
					673	19	
					723	41	
					773	85	
	5	0.1	IWI	ZrO <sub>2</sub>	623	2,5	(Yin <i>et al.</i> , 2004b)
					673	5	
723					10		
773					17		
2.5 (N <sub>2</sub> flow)	0.1	IWI	SiC	673	99.3	(Pinzón <i>et al.</i> , 2021)	
0.7	0.1	IWI	La-Al <sub>2</sub> O <sub>3</sub>	673	20	(Chung <i>et al.</i> , 2017)	
4.7	0.1	IWI	MgO	673	47	(Yu <i>et al.</i> , 2016)	
4.7	0.1	IWI	Ba(NH <sub>2</sub> ) <sub>2</sub>	673	54	(Yu <i>et al.</i> , 2016)	
1	0.1	IWI	SBA 200- $\gamma$ -Al <sub>2</sub> O <sub>3</sub>	673	99.7	(McCullough <i>et al.</i> , 2020)	

## 10.9. Annex 9

Table 10.6. Bimetallic catalysts for ammonia decomposition.

Metal	Metal content (% wt.)	Catalyst (g)	Technique	Support (promoter)	T (K)	NH <sub>3</sub> conversion (%)	Reference
Ni-Pt	5 (Ni) 1 (Pt)	0.1	IWI	Al <sub>2</sub> O <sub>3</sub>	973	78	(Choudhary, Sivadinarayana and Goodman, 2009)
Ni-Ru	10 (Ni) 2 (Ru)	0.1	IWI	CeO <sub>2</sub>	623	17	(Lucentini, Casanovas and Llorca, 2019)
					673	50	
					723	90	
					773	99	
					823	100	
Co-Re	100	0.025	Coprecipitation	unsupported	723	52	(Kirste <i>et al.</i> , 2021)
Ni-Fe	50 (Ni) 10 (Fe)	0.05	IWI	Al <sub>2</sub> O <sub>3</sub>	673	22	(Simonsen <i>et al.</i> , 2012)
					773	80	
					873	100	
Ni-Ir	10(Ni) 0.7 (Ir)	0.2	IWI	Al <sub>2</sub> O <sub>3</sub>	623	17	(Han <i>et al.</i> , 2007)
					673	42	



## 10.10. Annex 10



Figure 10.20. Screenshot of a tweet from the account @elonmusk, of 11<sup>th</sup> June 2020 (Musk, 2020).